Contextual fear learning induced changes in AMPA receptor subtypes along the proximodistal axis in dorsal hippocampus

by

Marijo Jevtić

April, 2022

A thesis submitted to the
Graduate School
of the
Institute of Science and Technology Austria
in partial fulfillment of the requirements
for the degree of
Doctor of Philosophy

Committee in charge:

Joszef Csicsvari, Thesis Defense Chair
Ryuichi Shigemoto, supervisor
Gaia Novarino, internal Committee member
Zoltan Nusser, external Committee member
Yugo Fukazawa, external Committee member

The thesis of Marijo Jevtić, titled *Contextual fear learning induced changes in AMPA receptor subtypes along the proximodistal axis in dorsal hippocampus*, is approved by:

Supervisor: Ryuichi Shigemoto, IST Austria, Klosterneuburg, Austria

Signature: _____

Committee Member: Gaia Novarino, IST Austria, Klosterneuburg, Austria

Signature: _____

Committee Member: Zoltan Nusser, Institute of Experimental Medicine (KOKI), Budapest, Hungary

Signature: _____

Committee Member: Yugo Fukazawa, Division of Brain Structure and Function, Faculty of Medical Sciences, University of Fukui, Fukui, Japan

Signature: _____

Defense Chair: Jozsef Csicsvari, IST Austria, Klosterneuburg, Austria

Signature: _____

Signed page is on file

IST Austria Thesis, ISSN: 2663-337X

I hereby declare that this thesis is my own work and that it does not contain other people's work without this being so stated; this thesis does not contain my previous work without this being stated, and the bibliography contains all the literature that I used in writing the dissertation.

I declare that this is a true copy of my thesis, including any final revisions, as approved by my thesis committee, and that this thesis has not been submitted for a higher degree to any other university or institution.

I certify that any republication of materials presented in this thesis has been approved by the relevant publishers and co-authors.

Signature: _____

Marijo Jevtić

April 2022

Signed page is on file

Abstract

AMPA receptors (AMPARs) mediate fast excitatory neurotransmission and their role is implicated in complex processes such as learning and memory and various neurological diseases. These receptors are composed of different subunits and the subunit composition can affect channel properties, receptor trafficking and interaction with other associated proteins. Using the high sensitivity SDS-digested freeze-fracture replica labeling (SDS-FRL) for electron microscopy I investigated the number, density, and localization of AMPAR subunits, GluA1, GluA2, GluA3, and GluA1-3 (panAMPA) in pyramidal cells in the CA1 area of mouse hippocampus. I have found that the immunogold labeling for all of these subunits in the postsynaptic sites was highest in stratum radiatum and lowest in stratum lacunosum-moleculare. The labeling density for the all subunits in the extrasynaptic sites showed a gradual increase from the pyramidal cell soma towards the distal part of stratum radiatum. The densities of extrasynaptic GluA1, GluA2 and panAMPA labeling reached 10-15% of synaptic densities, while the ratio of extrasynaptic labeling for GluA3 was significantly lower compared than those for other subunits. The labeling patterns for GluA1, GluA2 and GluA1-3 are similar and their densities were higher in the periphery than center of synapses. In contrast, the GluA3-containing receptors were more centrally localized compared to the GluA1- and GluA2-containing receptors.

The hippocampus plays a central role in learning and memory. Contextual learning has been shown to require the delivery of AMPA receptors to CA1 synapses in the dorsal hippocampus. However, proximodistal heterogeneity of this plasticity and particular contribution of different AMPA receptor subunits are not fully understood. By combining inhibitory avoidance task, a hippocampus-dependent contextual fear-learning paradigm, with SDS-FRL, I have revealed an increase in synaptic density specific to GluA1-containing AMPA receptors in the CA1 area. The intrasynaptic distribution of GluA1 also changed from the periphery to center-preferred pattern. Furthermore, this synaptic plasticity was evident selectively in stratum radiatum but not stratum oriens, and in the CA1 subregion proximal but not distal to CA2. These findings further contribute to our understanding of how specific hippocampal subregions and AMPA receptor subunits are involved in physiological learning.

Although the immunolabeling results above shed light on subunit-specific plasticity in AMPAR distribution, no tools to visualize and study the subunit composition at the single channel level *in situ* have been available. Electron microscopy with conventional immunogold labeling approaches has limitations in the single channel analysis because of the large size of antibodies and steric hindrance hampering multiple subunit labeling of single channels. I managed to develop a new chemical labeling system using a short peptide tag and small synthetic probes, which form specific covalent bond with a cysteine residue in the tag fused to proteins of interest (reactive tag system). I additionally made substantial progress into adapting this system for AMPA receptor subunits.

Acknowledgments

I would like to thank Professor Ryuichi Shigemoto for giving me the opportunity to join his group and pursue my PhD studies. The door to his office was always open for guidance, discussion and support.

Many thanks to other members of Shigemoto group, colleagues and friends at IST Austria, with special regards to EM Facility, and finally, to my interns and rotation students, for all the assistance and headaches they have, intentionally or otherwise, caused in the last couple of years.

Finally, I would like to express eternal gratitude to my elementary school math and physics teachers, Đuro Runić and Ljubinka Rakita, for lighting the spark of curiosity in me. To my family, especially my mother, for nourishing that spark for all coming years. And in the end, once again, to Professor Ryuichi Shigemoto, for not letting that spark to fade away.

About the Author

Marijo Jevtić completed a Bachelor of Sciences in Biology and a Master of Sciences in Experimental Biology at the University of Zagreb, Croatia. He did research work for his master thesis titled “GABRA2 polymorphism in alcoholism” at the Ruđer Bošković Institute in Zagreb, Croatia. In September 2015 he joined IST Austria for his PhD studies and affiliated with the Shigemoto group in June 2016. His main research interests include development of novel high resolution protein labeling methods for light and electron microscopy, but also how AMPA receptors are involved in basal neurotransmission and synaptic plasticity. During his PhD studies, Marijo presented his research results at the *NEURO2019,* The 42nd Annual Meeting of the *Japan Neuroscience* Society in Niigata in 2019.

List of Publications

Tabata S, Jevtic M, Kurashige N, Fuchida H, Kido M, Tani K, Zenmyo N, Uchinomiya S, Harada H, Itakura M, Hamachi I, Shigemoto R, Ojida A. Electron Microscopic Detection of Single Membrane Proteins by a Specific Chemical Labeling. iScience. 2019 Dec 20;22:256-268. doi: 10.1016/j.isci.2019.11.025. Epub 2019 Nov 16. PMID: 31786521; PMCID: PMC6906691.

Table of Contents

List of Figures

List of Tables

List of Abbreviations

AAV	Adeno-associated virus
AMPA	a-amino-3-hydroxy-5-methyl-4-isoxazolepropionic acid
ANOVA	Analysis of variance
B2R	Bradykinin receptor 2
BB	blocking buffer
CA	Cornu Ammonis
CA1	Cornu Ammonis 1 - region of hippocampus
$CaCl_2$	calcium chloride
CamKIIa	Calcium/Calmodulin Dependent Protein Kinase II Alpha
CI-AMPAR	calcium impermeable AMPA receptor
CNS	central nervous system
CP-AMPAR	calcium permeable AMPA receptor
C-terminus	carboxy terminus
DAPI	4′,6-diamidino-2-phenylindole
DMEM	Dulbecco's Modified Eagle *Medium*
DR	distal radiatum
E/S	extrasynaptic/synaptic
EDTA	Ethylenediaminetetraacetic acid
EGFP	enhanced green fluorescent protein
EM	electron microscopy
EPSC	excitatory postsynaptic current
EtOH	ethanol
FBS	fetal bovine serum
GluR	glutamate receptor
GPCR	G-protein coupled receptor
GPDQ	Gold Particle Detection and Quantification
GRIA1	gene encoding for GluA1 subunit of AMPAR
HBS	HEPES buffered saline
HBSS	Hanks' Balanced Salt Solution
hD2	helix D2

HEK293	Human Embryonic Kidney 293 cells
IA	inhibitory avoidance
IDT	Integrated DNA Technologies
iGluR	ionotropic glutamate receptor
IMP	intramembrane particle
K	potassium
kDA	kiloDalton
KS	Kolmogorov-Smirnov
LM	1. light microscopy 2. stratum lacunosum moleculare
LSF	Life Science Facility
LTD	long term depression
LTP	long term potentiation
mA	mili-Amper
MEM	modified Eagle medium
mEPSC	miniature EPSC
mM	millimolar
MR	middle radiatum
Na	sodium
NGS	Normal goat serum
NMDA	N-methyl-D-aspartate
NND	nearest neighbour distance
N-terminus	amino terminus
ORI	stratum oriens
OsO4	osmium tetroxide
P/D	proximal/distal
PB	phosphate buffer
PBS	phosphate buffered saline
PCL	pyramidal cell layer, stratum pyramidale
PFA	paraformaldehyde
pH	potential of hydrogen
PLL	poly-L-lysine
POI	protein of interest

PPi	pyrophosphate
PR	proximal radiatum
PSD	postsynaptic density
PSD-95	Postsynaptic density protein 95
RNA	Ribonucleic acid
RT	room temperature
SD	standard deviation
SDS	Sodium dodecyl sulfate
SDS-FRL	SDS-digested freeze fracture replica labeling
SEM	standard error of the mean
ssODN	single stranded oligodeoxynucleotide
TARP	Transmembrane AMPAR regulatory proteins
TBS	Tris-buffered saline
TCEP	tris(2-carboxyethyl) phosphine
TEM	transmission electron microscopy
UV	ultraviolet
vHH	Single variable domain on a heavy chain
WB	washing buffer
WT	wild type

1 INTRODUCTION

Brain is one of the largest and the most complex organ in the human body. More than 100 billion brain cells [1] communicate through trillions of connections called synapses and control all functions of the body, interpret information from the outside world and embody the essence of our body and soul. How the brain learns and stores information was and still is one of the most fascinating questions in the history of humanity.

In ancient times, it has been believed that not brain, but the heart was seat of intelligence. Greek physician Hippocrates and philosopher Plato were the first who speculated that the brain was not associated only with sensation (due to proximity of the brain and sensory organs – eyes, ears, nose and tongue) but that the rational part of the soul is also seated there [2]. This was further supported by Roman physician Galen, who observed that his patients, Roman gladiators, had problems with their mental capabilities after they had sustained damage to their brains [3]. A key idea in biology is that structure and function are tightly connected and regulated. More sophisticated studies of the brain structure (and therefore function) were only made possible by the invention of the microscope and development of staining procedure that could reveal delicate structure of individual brain cells by Italian pathologist Camillo Golgi in the late 19 century. This technique was extensively used by Spanish neuroanatomist Santiago Ramon y Cajal for detailed observations, descriptions and categorization of brain cells in all parts of the brain [4]. This work, for which they shared the Nobel Prize in Physiology and Medicine in 1906, was crucial for realization that brain is not continuous single network (as it was believed previously), but rather composed of large number of individual brain cells and led to formation of neuron doctrine - the hypothesis that the functional unit of the brain is the single brain cell or neuron [5]. It has already been known at that time that the number of neurons does not increase significantly with age or experience, so formation of new memories could not be explained by new neuron production. Ramon y Cajal was among the first to suggest that formation of new memories doesn't require involvement of new neurons, but is rather mediated by establishing new and stronger connections between existing neurons [4]. Canadian psychologist Donald Hebb introduced his theory in 1949, later known as Hebbian theory, which supported Cajal's ideas by further proposing that cells may undergo metabolic and structural synaptic changes that enhance their ability to communicate and create a neural network of experiences [6].

However, experimental evidence that neuronal connections in the mammalian brain undergo such changes came only later with the discovery of long-term potentiation (LTP) [7]. This is a phenomenon in which brief, high-frequency stimulation, typically referred to as tetanic stimulation, of hippocampal excitatory synapses produced a rapid and long-lasting increase in strength of these synapses that could persist for many days. Phenomenon of LTP, which has since been described at many different synapses throughout the brain, to this day remains one of the most attractive molecular models for learning and memory and one of the most studied topics in neuroscience. Subsequent studies revealed that the neurotransmitter involved in the excitatory neurotransmission was glutamate, that it is acting on NMDA receptors and non-NMDA receptors (later called AMPA and kainate receptors) and the modification of activity of these receptors is the way how LTP is expressed postsynaptically.

Today we know that the modulation of the AMPA receptor function and membrane trafficking is critical for many forms of synaptic plasticity and a large number of proteins have been identified that regulate this complex process. But before taking a look into the detailed role of AMPA receptors in synaptic transmission and plasticity, it is necessary to overview some important basic facts about them.

1.1 AMPA receptors

Fast synaptic neurotransmission in the mammalian central nervous system (CNS) is mediated by presynaptically secreted neurotransmitter glutamate which activates postsynaptic ionotropic transmembrane glutamate receptors (iGluR). Traditionally, they were classified as NMDA-type (named after their selective agonist *N*-Methyl-D-aspartate, NMDA) and non-NMDA-type receptors (which include AMPA and kainate receptors). Among these, AMPA receptors (AMPAR) are the most numerous, they are expressed throughout the whole brain, and therefore mediate majority of glutamatergic neurotransmission in CNS. Their name is derived from the ability to be activated by the artificial glutamate analog **α-amino-3-hydroxy-5-methyl-4-isoxazolepropionic acid** (AMPA). The receptor was first named the "quisqualate receptor" [9] after a naturally occurring agonist quisqualate and the name "AMPA receptor" was given after the selective agonist was developed [8].

1.2 Structure and subunits of AMPA receptors

The subunits forming the AMPARs are GluA1-4 (GluR1-4), and are encoded by genes Gria1-4. These subunits can be assembled in receptors as homo- or heterotetramers. All AMPAR subunit proteins have an extracellular N-terminus, an intracellular-C terminus, and four membrane-associated hydrophobic domains (M1–4), one of which (M2) forms a re-entrant loop (Figure 1A, 1B). Upon binding of glutamate, the pore opening allows the influx of Na^+ ions (along with K^+ efflux) to depolarize the postsynaptic compartment; however, depending on the subunit composition and the RNA editing, AMPARs also permit Ca^{2+} influx, which has important consequences for plasticity by engaging Ca^{2+}-dependent signaling events (Figure 1C) [11,12,13].

The four AMPAR subunits are highly homologous with around 70% amino acid residue identity and conserved transmembrane and extracellular domains [14]. The C-terminal intracellular tails are diverse amongst the subunits, and alternative splicing and RNA editing contribute to additional variants (Figure 1D). Alternative splicing at the so-called flip/flop exon produces subunit variants with distinct receptor desensitization properties [15]. Several different subtypes of AMPARs are expressed in the mammalian central nervous system, with individual neurons often expressing more than one subtype. For example, immature hippocampal neurons at early developmental stages express the GluA4 subunit, which

complexes with the GluA2 subunit [16]. However, mature hippocampal neurons express two predominant combinations of AMPAR subunits, GluA1/GluA2 or GluA2/GluA3 heterotetrameric receptors [17].

As different subunits have differences in structure and posttranslational modifications, therefore, subunit composition dictates many of the properties of AMPA receptors, such as interaction with scaffolding proteins, channel localization, conductance, open probability and ion selectivity [11,12,13]. Considerable evidence suggests that changes in the composition of AMPAR subtypes present at synapses are an important aspect of synaptic plasticity [18,19,20,21], though delineating the specific subtypes involved and the precise role that subtype switching plays has been hindered by the lack of selective tools for native receptors. The messenger RNA that encodes different AMPAR subunit types can also be posttranscriptionally modified by alternative splicing and RNA editing, which contributes even more to diversity of AMPAR types and properties. The most important RNA editing change affects the GluA2 subunit, where it switches glutamine (Q) to arginine (R) at the "Q/R site" in the M2 region lining the pore of receptor. This switch happens at nearly all (>99%) of GluA2 subunits and deeply affects the properties of AMPA receptors that contain this subunit, rendering them impermeable to calcium (calcium impermeable AMPAR, CI-AMPAR) (Figure 1C). Receptors lacking this subunit in their composition are permeable to calcium ions (calcium permeable, CP-AMPAR), they show higher single channel conductance and are blocked in a voltage dependent manner by endogenous polyamines (they show inwardly rectifying current voltage (I/V) relationship), which makes GluA2 subunit a key determinant of AMPA receptor function [11,12,13]. A precise role for CP-AMPARs in synaptic plasticity is still controversial. The properties of receptors are dictated not only by their subunit composition but also by the presence of auxiliary, non-poreforming, transmembrane AMPAR regulatory proteins (TARPs). The TARPs act as auxiliary subunits that are required for AMPAR maturation, trafficking, and channel function [22,23], but also influence their functional properties, such as single channel conductance, deactivation and desensitization, and pharmacological properties [11]. Aside from TARPs, AMPAR properties can be modulated by several other identified auxiliary subunits (Figure 1E).

Regulation of the precise localization and number of AMPARs at the cell surface membrane is critical for most excitatory synaptic transmission at the steady state and also for long-term synaptic plasticity, such as LTP and LTD [24,25]

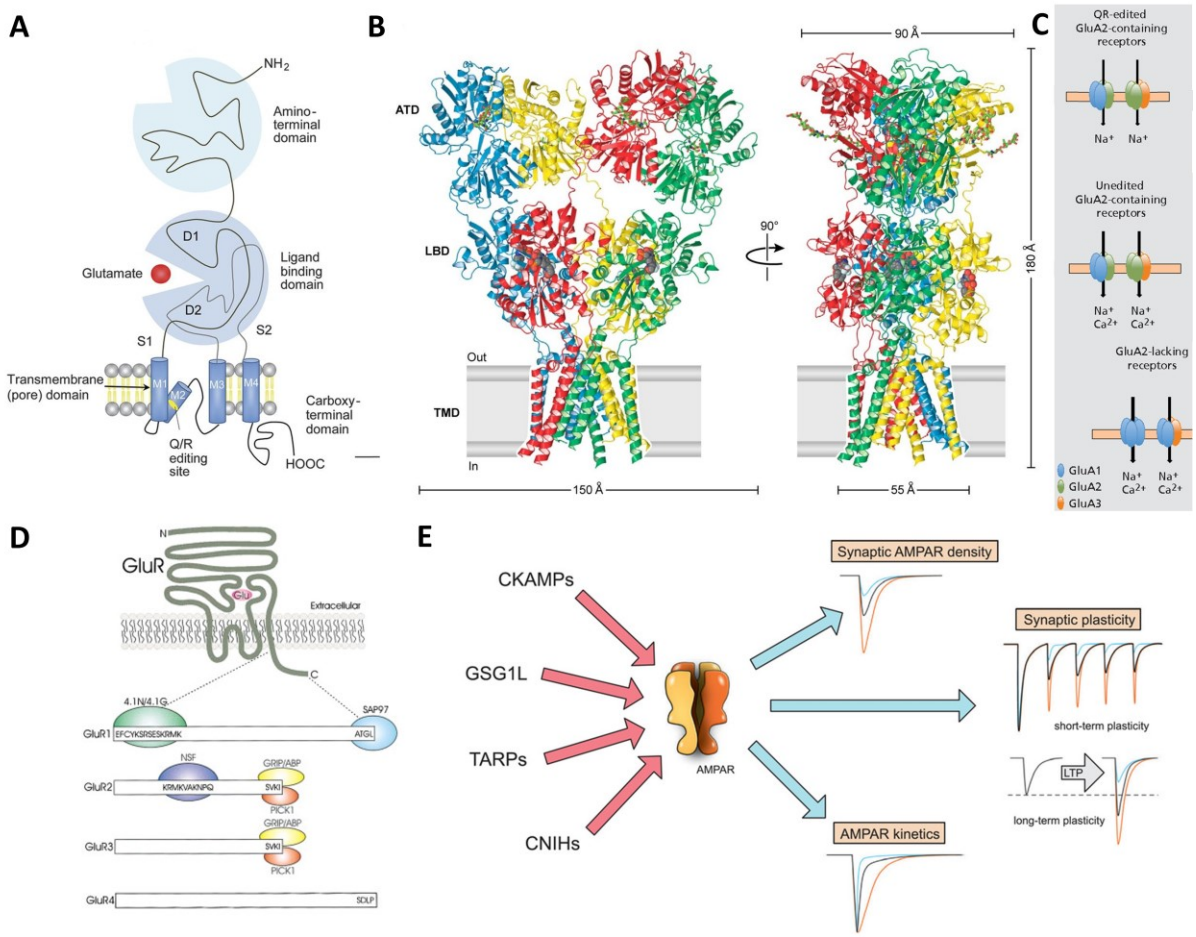

Figure 1.1. AMPA receptors Structure of the AMPAR subunits. The AMPARs are heterotetrameric cation channels that are composed of various combinations of GluA1 to GluA4 subunits, which form a pore with an approximately 4-fold symmetry. These subunits consist of 4 domains: extracellular amino-terminal domain, extracellular ligand-binding domain, transmembrane domain, and intracellular carboxy-terminal domain. The amino-terminal domain has a regulatory function. The ligand-binding domain is formed by 2 stretches of amino acids, termed S1 and S2, and forms a structure that adopts a clamshell-like conformation with 2 lobes referred to as domain (D1) and D2; the agonist-binding pocket is located between the 2 lobes of the clamshell. The transmembrane domain consists of 3 transmembrane helices (M1, M3, and M4) and a membrane reentrant loop (M2); the M2 loop lines the inner cavity of the pore. The GluA2 subunit is posttranscriptionally modified by RNA editing at the glutamine/arginine (Q/R) site located at the apex of the reentrant loop of M2. The carboxy-terminal domain is highly variable among subunits, and is the site of posttranslational modification of protein–protein interactions that influences membrane targeting, synaptic stabilization, and function of AMPARs. B) Architecture of homomeric rat GluA2 receptor. View of the 'broad' face of the receptor, perpendicular to the overall 2-fold axis of molecular symmetry. Each subunit is in the different color. C) RNA editing of the GluA2 subunit determines calcium permeability of AMPARs. AMPA receptors (AMPARs) lacking the GluA2 subunit, or an unedited GluA2 subunit are calcium permeable. However, receptors containing an edited GluA2 subunit do not gate calcium. For simplicity, and because their existence in neurons is unclear, GluA3 homomers, which are calcium permeable, and GluA2 homomers, whose calcium permeability depends on the RNA editing state of the GluA2 subunits involved, are not shown. GluA4 (not shown) behaves identically to GluA1. D) Membrane topology and cytoplasmic protein interactions of AMPA receptor subunits. E) AMPAR auxiliary subunits and their influence on synaptic AMPAR. Modified from [82, 83, 84, 85, 86]

1.3 Localization and distribution of AMPAR

Multiple studies utilizing electrophysiology, light and electron microscopy have demonstrated that AMPA receptors are localized throughout the neurons, in both synaptic and extrasynaptic membranes [26,27,28]. Electron microscopy, which provides the highest sensitivity and spatial resolution, has demonstrated presence of AMPAR on somata, dendrites, dendritic spines, within intracellular compartments and in synapses [11,27]. AMPARs are most abundant in excitatory glutamatergic synapses where they are located in the postsynaptic membrane across the presynaptic active zone where the glutamate secretion into the synaptic cleft takes place [30,31,32]. Number of AMPARs in the synapses can go from tens to hundreds and it is correlated with spine size and synaptic strength [29].

Development of super-resolution optical methods for tracking single receptors has shown that AMPAR are in constant dynamic exchange between synaptic and extrasynaptic membranes, and not static as initially believed [33,40,53]. Synaptic transmission is regulated by constant exchange of AMPARs between these different pools by lateral diffusion and recycling, while the total pool of extrasynaptic glutamate receptors available to enter into synapses would be determined by relative rates of synthesis, degradation, endocytosis, and exocytosis. Changes in AMPAR number in the synapse is one of the major ways by which the efficacy of synaptic transmission can be altered. The dynamic nanoscale organization of neurotransmitter receptors in the postsynaptic membrane has recently been suggested to play a major role in various aspects of synaptic function [33,40,53].

1.4 Synaptic organization of AMPA receptors

Precise spatial organization of postsynaptic molecular elements and their correlation with presynaptic organization and synaptic activity is a very active area of research. Presynaptic vesicles contain a limited number of glutamate molecules which create a transient local glutamate gradient upon vesicular release [34], and this gradient activates only a fraction of synaptic AMPARs [35]. The biophysical explanation for such a low efficiency of AMPAR activation comes from their relatively low affinity for glutamate and the rapid decrease in glutamate concentration from the vicinity of the release site [36]. Therefore, the precise localization of AMPARs with respect to the presynaptic terminal and glutamate release sites is crucial for fast and efficient synaptic transmission. Modeling and experimental data has

indicated that intrasynaptic AMPAR distribution may have a strong impact on synaptic transmission [33,37,38,39].

Understanding of AMPAR organization inside synapses has improved remarkably in the last decade with studies utilizing super-resolution imaging and freeze-fracture replica labeling [39]. Immunogold labeling of AMPARs for EM is currently the highest-resolution imaging technique [27,42] and post-embedding immunogold EM and replica-based labeling have revealed the existence of AMPAR clusters on the membrane [28,38,39]. The current view is that AMPAR are accumulated in subdomains of around 100 nm inside the PSD. These nano-clusters seem to be organized by local aggregates of PSD95, however, the exact molecular basis for such arrangement is still debated [40]. Since the proposition that AMPAR are organized in clusters [33,39,43], several studies have investigated the relative position of post-synaptic AMPAR domains with respect to presynaptic release sites, and the molecular basis of such co-organization. By using dual color super-resolution, a trans-synaptic organization (termed nanocolumn) was observed between the presynaptic protein RIM1 and PSD95 [44]. Modeling data also indicates that with such AMPAR organization in domains facing release sites, regulation of synaptic currents amplitude is not necessarily related to a modification in AMPAR content [45]. In addition, acute artificial increase in synaptic AMPAR content is not sufficient to increase mEPSC amplitude [41]. Modification of transsynaptic organization could be a mechanism for synaptic plasticity [40], although direct evidence is still lacking. New perspective of the nanoscale organization of AMPA receptors and the presynaptic machinery raises new possibilities to explain the modifications in synaptic transmission observed during long-term plasticity.

1.5 AMPA receptors in long term potentiation

Long-term potentiation (LTP) is one of the several forms of synaptic plasticity in the vertebrate central nervous system (CNS) and by far the most studied, driven by the widely-held view that this mechanism is critical for learning and memory processes [46]. Different areas of the brain exhibit different forms of LTP. Because of its well-known organization and easily inducible LTP, the CA1 area of the hippocampus has become the most common site of mammalian LTP study. In particular, NMDA receptor-dependent LTP has been most extensively studied at the excitatory synapses of Schaffer collateral-commissural pathway, a

monosynaptic connection between axons of CA3 pyramidal neurons and dendrites of CA1 pyramidal neurons in the hippocampus [47,48].

During LTP, specific patterns of input activity trigger a chronological series of events, which can persist for days or even weeks *in vivo* [47,48,119]. “Early phase” of LTP, which lasts up to 60 min, requires the activation of NMDA receptors for its induction, Ca^{2+} influx through activated NMDA-receptors and subsequent calcium/calmodulin-dependent protein kinase II (CaMKII) activation [48,49]. In addition, delivery of new AMPARs to the postsynaptic sites is believed to be responsible for LTP expression in its early phases. Expression of the “late phase” of LTP, which lasts days or even weeks, requires gene transcription and new protein synthesis, resulting in parallel increase in size of pre- and postsynaptic structures [50,51,52]. In the first phase of LTP, these signaling events lead to both a diffusion-trapping of surface AMPAR at synapses and an increase in their exocytosis [53]. AMPARs, particularly those lacking the GluA2 subunit (and therefore calcium permeable, CP-AMPAR), have been suggested to play an important role in LTP expression at CA1 synapses in studies using knockout mice lacking GluA1 or GluA2 and electrophysiological recordings of hippocampal slice expressing tagged GluA1 or GluA2, either as an alternative source of calcium influx for induction of LTP or as the way for enhancing postsynaptic depolarization due to their higher conductance [21,54,55,56]. The GluA1 subunit requirement for LTP has been investigated and supported by studies focusing on the cytoplasmic carboxy terminal (C-terminal) tail, which has been demonstrated to be involved in intracellular signaling through phosphorylation, palmitoylation or protein interactions, indicating that the CP-AMPAR involved in LTP are primarily GluA1 homomers [21,54,55,56]. However, the GluA1 C-terminal tail requirement for LTP was challenged by a report showing that LTP requires AMPAR trafficking, independent of subunit type [57]. In addition to that, other studies found no evidence for a role of CP-AMPARs in LTP at CA1 synapses [58,59]. Involvement of GluA1-homomeric AMPAR in the initial phases of LTP still remains unclear and controversial. Recent studies have also demonstrated that the extracellular amino-terminal domain (NTD) of AMPARs governs their trafficking for synaptic plasticity dependent on the AMPAR subunit type [55,60].

Another controversial question regarding initial phases of LTP is whether the AMPARs are delivered into the synapse for LTP through exocytosis directly from the intracellular pool to synaptic sites or through lateral mobility from the extrasynaptic plasma membrane or a

combination of both. Although direct AMPAR exocytosis can occur at spines, it has usually been visualized all over the dendrite [40,53]. This led to the suggestion that the contribution of perisynaptically exocytosed AMPAR to increase synaptic AMPAR content only occurs several minutes after LTP induction and requires their diffusion to the synapse. Experiments where AMPAR exocytosis was prevented usually did not block the very first phase of synaptic potentiation, indicating that an alternative mechanism such as diffusion trapping or receptor nanoscale re-organization is at play in the first minutes of potentiation [40].

1.6 AMPA receptors in hippocampus mediated learning

Hippocampus became the primary focus of research to explain learning and memory formation after the case of patient H.M. [61] who was unable to form long term memory after he underwent the medial temporal lobectomy in the attempt to cure his epilepsy. This indicated that some of the removed brain structures (including hippocampus) were crucial in memory formation.

The phenomenon of LTP, which was also discovered in the hippocampus [7] has attracted huge attention and many studies have been published on hippocampal LTP [47,48], all based on the assumption that LTP reveals an important mechanism for memory in the brain. However, directly demonstrating that hippocampal LTP is actually induced by learning and identifying changes in molecular structure and function of the synapses after physiological learning can be challenging because of difficulty identifying precise subregion and subpopulation of synapses affected by this learning, and the effect can be too subtle to be firmly confirmed. Inherent technical variability of currently using methods also adds another layer of complexity for successful detection of the changes and interpretation of the results.

There are several reasons why learning-induced LTP has been difficult to demonstrate in the hippocampus [62,63]. Many hippocampus-dependent learning tasks require multiple training trials for memory formation and due to differences in learning rates between animals the subtle markers of LTP might be obscured and difficult to detect. The changes in individual synapses might be sparse and distributed across larger area, and therefore difficult to detect when surrounded by many unmodified synapses. Also, since learning can induce long-term depression (LTD) as well as LTP simultaneously at different synapses the effect might mask each other when looking for changes on the population level [62,63].

The use of the inhibitory avoidance (IA) behavioral task provides us with solutions for some of the mentioned problems. IA training creates a stable memory trace in a single trial and causes substantial changes in gene expression in area CA1 of the dorsal hippocampus, which suggests that this is a site of robust synaptic plasticity [62,64].

The dorsal hippocampus is a key structure for acquiring and memorizing contextual aspects of fear memories [62,65] and these processes have been tied to AMPAR trafficking and synaptic potentiation *in vivo* [19,62,66]. Although many studies have shown that there are prominent functional differences along the proximodistal axis of the CA1 region [67,68,69,70,71], synaptic plasticity along the proximo-distal axis was unknown. Mitsushima and colleagues [72,73,74] have shown in their work based on behavior and electrophysiology how the AMPA receptor currents increase after inhibitory avoidance task in trained animals compared to the untrained control, most prominently in hippocampal region of CA1 proximal to CA2 and less so in distal part of CA1. I chose this approach on one hand because I was interested in AMPA receptor changes after learning induced plasticity in the hippocampus, one of the most studied areas of the brain in the research area of synaptic plasticity. On the other hand, it was chosen based on its simplicity and noninvasiveness over some alternative approaches which are more refined but at the same time, more invasive and artificial, while being technically more complicated to perform. The results from Mitsushima et al. [72,73] indicated increase in the AMPA/NMDA ratio driven only by increase in the AMPA receptor currents, which can be caused by several factors: increased number of AMPA receptors in the affected synapses or increased conductance driven by either subunit composition changes or (taking into account low affinity of AMPA receptors for glutamate) more precise alignment of the AMPA receptor with the presynaptic neurotransmitter release machinery, or combination of these factors. In this study I aimed to investigate some of these possibilities using a combination of IA behavior with protein labeling and detection *in situ* approaches for electron microscopy.

1.7 Limitations of electron microscopy

Electron microscopy (EM) with its nanometer scale resolution is currently the most powerful technique that can be used for detection of localization and distribution of AMPA receptors in fixed mouse brain tissue (and other proteins of interest (POI) in biological

samples). Conventional immunolabeling approach in electron microscopy, where protein of interest is detected by antibody raised against specific epitope (such as AMPA receptor subunit), which is subsequently visualized by secondary antibody conjugated with metal nanoparticle (raised against Fc region of primary antibody), suffers from two major problems for the precise localization of protein of interest. These problems do not come from the limitation of the electron microscope, since the power and magnification provided by transmission electron microscope (TEM) are more than enough to resolve distances between different subunits of AMPA receptors, or any other protein complex, but rather from the antibody labeling itself. First problem is the size of primary and secondary antibodies (*about 8nm in length or* 150 kDa) which makes gold particles appear up to 20–30 nm away from POI [75], making it difficult to precisely visualize protein localization in biological samples. Size of the antibodies also prevents simultaneous labeling of different subunits in protein complexes, such as the tetrameric AMPA receptors, or even detection of receptors very close to each other in high density environments (such as synapses). Numerous proteins are assembled into permanent or transient functional protein complexes in living cells and inability to detect individual components of these complexes prevents us from utilizing the full potential of EM in protein localization analysis. Large size of antibodies also prevents deeper penetration into biological tissue during sample preparation which further complicates precise protein distribution analyses [28,77]. Another antibody related problem is the fact that the development of high-quality antibodies with high efficiency and low nonspecific labeling can be technically difficult and costly.

Possibly the best approach to overcome these limitations is usage of smaller probes for labeling and detection of the protein of interest (POI). In my work I have explored several options that can overcome some of these limitations, but at the same time they introduce different kinds of difficulties for successful labeling, detection and analysis of AMPA receptor subtypes in different systems. All these approaches rely on the interaction of short peptide tag and small probe which can improve labeling efficiency and spatial resolution but genetical engineering required to insert short peptide tag at desired location within the protein of interest is a potential source of problems for proper folding, trafficking and function of the tagged protein.

Chemical protein labeling methods using small molecular probe are potential ways overcome above-described problems with immunolabeling. The method for covalent labeling of proteins with a synthetic chemical probe enables analyses of POI under biological

conditions. Multiple covalent protein labeling methods with synthetic chemical probes have been developed recently and mainly used for fluorescence imaging of POI under live cell conditions. Among them, specific cysteine conjugation using reactive peptide tag-probe pair has attracted considerable attention [76,77,78]. Since then, several peptide tag-based approaches have been devised for specific protein labeling. These chemical labeling methods using the tag-probe pair can tolerate a wide range of labeling conditions (different pH, solvent composition, chemical fixation) and small molecular size of the tag and the probe allows for more precise localization of POI due to closer distance between probe and POI. All these properties make chemical labeling method suitable for high-resolution protein analysis by EM, where chemically fixed tissues and cells are used.

In this research work I attempted to utilize a newly developed peptide tag-probe pair for specific protein labeling for EM detection of membrane proteins at single-molecular level [77,79]. We [77] demonstrated EM detection of the labeled G protein-coupled receptor (GPCR) in cell membrane freeze-fracture replicas and ultrathin sections. The efficiency and resolution obtained by the chemical labeling was significantly higher than those obtained by the immunogold labeling. The chemical labeling method also revealed high-density clusters of molecules closer than a few nanometers to each other, also demonstrating its utility in single protein detection by EM.

Another potential improvement of the immunolabeling approach is the usage of nanobodies. Nanobodies as a tool for protein labeling are attracting a lot of interest in recent years, since they have been developed for an increasing number of different targets and their production simplicity and low cost. However, for my work the main point of interest is their size and potential higher labeling efficiency and spatial resolution that they can provide for the electron microscopy. Nanobodies are purified variable (VHH) fragments of a heavy chain of camelid antibodies. Animals from this family naturally have antibodies different from the antibodies derived from other animals used so far (rabbits or guinea pigs for example) in that they have only two heavy chains with constant and variable regions, unlike other animals whose antibodies contain two heavy and two light chains. Variable region of both of these chains is what provides epitope specificity. Multiple nanobodies have been developed against specific proteins of interest, however, for this study I was more interested in the nanobodies which were specific for short epitope tags. This approach was introduced in 2019 with the introduction of nanobodies specific for ALFA- and Spot-tag [80,81] and during the course of

my PhD studies I attempted to implement this approach to overcome the limitations of EM and achieve my goal.

1.8 Open questions

In addition to being the major component of basal synaptic transmission, AMPA receptors are also one of the main mediators of synaptic plasticity. One of the most studied phenomena of synaptic plasticity and the one that is considered to be the molecular basis of more complex processes, such as learning and memory, is long term potentiation (LTP). Long history of studying this process has revealed to us that increase in synaptic transmission followed by high frequency stimulation is mediated by increase in the synapse size and subsequent increase in number and density of AMPA receptors in the potentiated synapses [11,47,48]. There is some evidence that specific subtypes of AMPA receptors, Ca-permeable GluA1 homomers play a particularly important role in the initial stages of LTP but their exact contribution is not yet fully understood. In addition to that, there remains a question about the rules of exact AMPA receptor positioning within the synapse, how it affects the basal transmission and how this positioning, and possibly involvement of different subtypes changes and affects plasticity. This is also one of the main questions and aims of this study.

Majority of the work done on the AMPA receptor functionality, subunit composition and involvement in plasticity so far has been done using electrophysiological, biochemical or super-resolution microscopy approaches. However, in terms of resolution and precision, electron microscopy is an indispensable tool and the only one that can potentially reveal to us accurate subsynaptic localization of AMPA receptors and possible very fine changes in their arrangement that happen in response to plasticity inducing stimulus. Changes in subunit composition are another very important aspect of synaptic plasticity study which can be revealed by resolution provided by electron microscopy. Not much is known about single channel subunit composition *in situ* because the highly specific methods for detection and visualization of protein complexes are still missing. Conventional immunolabeling methods for electron microscopy, although providing the best resolution at the moment, still suffer from few key limitations that prevent us to successfully detect and visualize subunit composition of a specific channel, most notably lack of specific antibodies for selected protein of interest, inaccurate representation of actual receptor location due to 2-step approach (location of gold particle can be more than 20 nm away from actual location of POI) and size of the antibodies,

which prevents successful analysis of different subunits within one receptor due to steric hindrance and inability to bind two different antibodies to two spatially close epitopes. Therefore, successful labeling and detection of individual subunits with the same protein complex remains a challenge even for the electron microscopy. It is necessary to establish new methods for labeling and analysis of single channels using smaller probes which will provide us with better spatial resolution and ability to resolve specific subtypes of different receptors and subunit composition of single channels.

1.9 Aims

- In this study I investigated detailed distribution of AMPA receptor subunits and subtypes in mouse CA1 pyramidal cells of hippocampus with special emphasis on CA3-CA1 synapses by utilizing high specificity antibodies against AMPA receptor subunits and high resolution SDS-FRL technique for electron microscopy to potentially reveal special rules of AMPA receptor distribution and synaptic organization that might have effects on synaptic transmission.
- Next thing was to investigate how AMPA receptor subunit distribution and synaptic organization might change during learning-induced plasticity by combining inhibitory avoidance behavioral task with SDS-FRL and investigating synaptic AMPAR labeling across a wider CA1 area.
- Because of the limitations of immunolabeling with regards to spatial resolution and labeling efficiency that precludes the investigation of exact AMPAR subunit composition *in situ*, an ultimate goal of this study was to develop novel EM labeling approach by utilizing short peptide tag and chemical probe/nanobody approach and obtain the final full picture of how the AMPAR distribution, arrangement and subunit composition changes during learning-induced plasticity.

2 MATERIALS AND METHODS

2.1 Animals

For this study, wild type male C57BL/6J, 8-10 weeks old mice were used. Before experiments, animals were kept on a 12:12 light-dark cycle with ad libitum access to food and water in the Preclinical Facility of IST Austria. All experiments were performed in accordance with the license approved by the Austrian Federal Ministry of Science and Research (Animal license number: BMWFW-66.018/0012-WF/V/3b/2016, approved on 19.06.2014) and the Austrian and EU animal laws.

2.2 Labeling reagents

Table 1. Labeling reagents used in this study:

Reagent	Concentration	Reference/Source
Anti GluA1 rabbit antibody	4 µg/ml	Antal et al, 2008 [87]
Anti-GluA2 rabbit antibody	2 µg/ml	Tabata et al, 2019 [77]
Anti-GluA3 rabbit antibody	10 µg/ml	Rubio et al, 2017 [88]
Anti-panAMPA rabbit antibody	4 µg/ml	Eguchi et al, 2020 [89]
Reactive zinc complex chemical probe, nanogold conjugated	3 µM	Tabata et al, 2019 [77]
Anti-ALFA nanobody, biotinylated	1 µg/ml	Nanotag Biotechnologies
Anti-Spot nanobody, ATTO594 conjugated	1 µg/ml	Chromotek
Anti-rabbit antibody, 5 nm gold conjugated	1:30 dilution	British Biocell International
Streptavidin, Alexa488 conjugated	1 µg/ml	ThermoFisher
Anti-FLAG mouse antibody	5 µg/ml	Sigma-Aldrich
Anti-mouse antibody, 5 nm conjugated	1:30 dilution	British Biocell International
Anti-rabbit antibody, 10nm conjugated	1:30 dilution	British Biocell International
Anti-mouse antibody, Alexa488 conjugated	1 µg/ml	

2.3 Inhibitory avoidance task

Inhibitory avoidance is a commonly used behavioral task to investigate learning and memory processes in rodents [91,92]. Inhibitory avoidance training was designed as previously described [72,73]. The training apparatus (Ugo Basile, Gemonio, Italy) consists of two chambers separated by computer operated and programmable door between chambers. Animals were placed in the light chamber of the apparatus for habituation for 5 minutes a day before the actual experiment. On the day of the experiment, animal was placed in the light compartment of the apparatus and 5s later the door to the dark compartment was open so the animal could

freely pass. Time from opening the door until the animal entered the dark compartment was measured as 1st latency before entering. Upon entering the dark compartment, 3s later the door was closed and electric foot shock (1s, 0.5mA) was applied via electrified steel rods in the floor of the apparatus. Animal was kept in the dark compartment for 10s and then returned to the home cage. After 30 min, the animal was exposed again to the light compartment of the apparatus and the time to enter the dark compartment was measured as 2nd latency and taken as a measure of successful learning. Briefly after that, animals were anesthetized and perfused. Control animals were kept in their cages before perfusion, without exposure to IA training.

2.4 SDS digested freeze-fracture replica labeling (SDS-FRL) – mouse brain tissue

SDS-FRL technique was described previously [95,96] Animals were anesthetized with pentobarbital (100 µl of 60 mg/ml solution) and brains were fixed via transcardial perfusion with either 2% (figure 3.1 to 3.6) or 0.5% paraformaldehyde (PFA), 15% picric acid in 0.1M phosphate buffer (PB). Mouse brains were sliced into coronal sections at thickness of 80 µm (Figure 3.7-3.9) or 120 µm using vibratome (Linear Slicer Pro, Dosaka). Brain slices were cryoprotected with 30% glycerol in 0.1M PB and CA1 area from the dorsal hippocampus was trimmed out, and then high-pressure frozen using the Baltec HPM010. Frozen tissue samples were fractured using the Baltec BAF060 (Figure 3.1-3.9) and Jeol JFDV and a thin layer of carbon (5nm) was deposited on top of fractured tissue, followed by 2nm platinum layer and additional 20nm of carbon. Tissue was then dissolved in SDS solution (2.5% sodium dodecyl sulphate solution (SDS), 20% sucrose, 0.05% sodium azide in 15mM Tris) in a shaking incubator at 80°C and 50 RPM (Fig 3.1 to 3.9) or 30 RPM. For the labeling, replicas were washed once in SDS solution, then once in washing buffer (WB, 0.1% Tween-20, 0.05% BSA (bovine serum albumin), 0.05% NaN_3 in TBS (Tris-buffered saline), twice in TBS and then incubated in blocking buffer (BB, WB with 5% BSA) for 30-60 min. After blocking, replicas were incubated in primary antibody solution (antibody diluted in BB) for 24-72h at 15°C, and washed again 1xWB, 2xTBS before again incubating in BB and secondary antibody solution (gold conjugated secondary antibody diluted in BB). After this, replicas were washed again once with WB, 2xTBS and flattened on the surface of MilliQ water before mounting them on copper grids with parallel bars for EM observation.

2.4.1 Grid glued replica

Some of the analyzed replicas were prepared using the grid glued replica method [90]. After fracturing the samples but before tissue digestion with SDS-solution, samples (tissue + carbon replica) were glued tissue side up to the nickel finder grids with UV (ultraviolet) glue. Tissue digestion and replica labeling was done the same as described in the previous paragraph. In case of grid glued replica, glue removal is necessary before EM observation. To protect gold particle labeling, samples were coated with a 20nm carbon layer before treating the samples with glue removing agent (Dynasolve) for 2x45 min at 60°C and 50 RPM in a shaking incubator.

2.5 EM imaging

Only replicas containing complete areas of CA1 were selected and imaged. Images were taken using the Tecnai10 or Tecnai12 (FEI) transmission electron microscopes. For figures 3.1-3.6, pyramidal cell dendrites and synapses were identified and randomly sampled from every layer in the CA1 area (s.oriens, pyramidal cell layer, s.radiatum and s.lacunosum-moleculare). For figures 3.6 to 3.9, synapses were randomly sampled from middle one third of stratum radiatum (middle radiatum). For figures 3.10-3.20, synapses were sampled from CA1 area proximal and distal to CA2 in the middle one third of stratum radiatum and stratum oriens.

2.6 Image analysis, visualization and statistics

For image analysis and visualization GPDQ or Darea software (Darea is the advanced version of GPDQ) was used [98,99]. First, manual demarcation of areas of interest (PSD and gold particles in the images obtained by SDS-FRL, and subsequent analysis of gold particle density within demarcated area and outer rim of synapses, quantification of distances between particles and center or gravity and edge of demarcated area, gold particle clustering, as well as running a random simulation of gold particle placement for comparison with real data. In addition to that, all example EM images with annotated synapse areas, outer rims, gold particles and scale bars were prepared by Darea. Statistical analysis of data was performed by GraphPad Prism 6 (San Diego, CA, USA). Graphs were also prepared with GraphPad Prism. Error bars indicate

standard error of the mean. To indicate p-value in graphs, * $p<0.05$, ** $p<0.01$, *** $p<0.001$ was used. Detailed statistics can be found in Appendix.

2.7 Cell Culture and B2R Expression in HEK293 Cells.

HEK293 cells were cultured in high glucose DMEM supplemented with 10% fetal bovine serum (FBS), penicillin (100 units/mL), streptomycin (100 µg/mL) and amphotericin B (250 ng/mL). Cells were maintained at 37 ºC in a humidified atmosphere of 5% CO2 in air. Subculture was performed every 3-4 days from subconfluent (< 80%) cultures using trypsin-EDTA solution. Transfection of the expression vector for B2R was carried out in a 35 mm glass-bottomed dish (Iwaki) using Lipofectamine LTX (Invitrogen) according to the general procedure. The cells were subjected to labeling experiment after 48 h of the transfection.

2.8 EM Detection of B2R in Freeze-fracture Replicas.

HEK293T cells (ca. $2x10^7$ cells) transiently expressing helixD2-B2R-EGFP, GluA2 (for negative control) or co-expressing helixD2-B2R-EGFP and GluA2 were washed with HEPES-buffered saline (HBS), and treated with 2 mM TCEP in HBS (1 mL) for 10 min at 37 °C. After removal of TCEP solution, the cells were treated with 3 µM 1.4 nm gold conjugated-chemical probe solution (reactive zinc complex) in HBS for 2 h at 37 °C. For estimation of chemical labeling density in unfixed cells, cells were fixed after chemical labeling (after washing out the chemical probe with PPi) and for estimation of chemical labeling density in fixed cells, fixation was performed before chemical labeling (before HBS washing). Fixation was done with 2% paraformaldehyde (PFA) in phosphate-buffered saline (PBS) for 15 min at RT. The cells were harvested by scraping, collected by centrifugation (100g, 5 min), and the cell pellet was sandwiched between gold carriers for high-pressure freezing (HPM010, Bal-Tec). The frozen pellet was then fractured into two parts at –120 °C and replicated by depositions of a 30 nm carbon layer using a freeze-fracture replica machine (BAF 060, Bal-Tec). After thawing, the replicas were washed with 2.5% SDS, 20% sucrose, and 15 mM Tris-HCl (pH 8.3) for 48 h at 60 °C

For immunolabeling, the replicas were treated with mouse anti-FLAG (Sigma-Aldrich) or rabbit anti-GluA2 antibodies for 48 h at 15 °C, followed by staining with anti-mouse secondary

antibody conjugated with 5-nm gold particles or anti-rabbit secondary antibody conjugated with 10-nm gold particles (British Biocell International). Replicas were analyzed by JEM-2800 scanning transmission electron microscope (JEOL) in dark field mode. For quantitative analysis of particle distribution, I used GPDQ software [98] to calculate the density and NND of particles, particle number per cluster, and cluster area. For the definition of clusters of particles, we used 3 particles as a minimum number and mean + 2SD [107,98] of fitted peaks of NND (Figure 5I) as a maximum distance allowed (6 + 3×2 = 12 nm for chemical labeling, 22 + 10×2 = 42 nm for immunolabeling).

2.9 EM Detection of B2R in Embedded Ultrathin Sections.

HEK293 cells (*ca.* $2x10^7$ cells) transiently expressing helixD2-B2R-EGFP cultured on a coverslip were treated with 2 mM TCEP in HBS for 10 min at 37 °C. After removal of the solution, the cells were treated with 3 μM gold conjugated-chemical probe solution (reactive zinc complex) for 2 h at 37 °C, and washed with 2 mM PPi in HBS. The cells were then fixed in PBS containing 4% paraformaldehyde and 0.05% glutaraldehyde for 10 min at RT. After 3-6 min silver intensification, the cells were treated with 0.2% OsO4 in PBS for 20 min, counterstained with 0.25% uranyl acetate overnight at 4 °C, dehydrated in ascending series of EtOH and propylene oxide, and embedded in Durcupan (Sigma-Aldrich). Ultrathin sections (70-nm thick) prepared using ultramicrotome (Leica Ultracut UCT, Leica) were counterstained with lead citrate and uranyl acetate, and analyzed by Tecnai 10 transmission electron microscope (FEI). For immunolabeling of the FLAG tag, HEK293 cells were fixed by 4% paraformaldehyde and 0.05% glutaraldehyde in PBS for 10 min at rt. After blocking with 10% normal goat serum and 2% bovine serum albumin in Tris-buffered saline (TBS), the cells were treated with anti-FLAG antibody (Sigma-Aldrich) followed by anti-mouse secondary antibody conjugated with 1.4-nm gold particles (Nanoprobes). After 3-6 min silver intensification, the cells were treated, sectioned and observed in the same way as described above. To measure the distance between gold particles and cell membrane, we first tilted the ultrathin sections to obtain perpendicular views of lipid bilayer. We discarded the particles if it was not possible to obtain perpendicular views. Then, the distance between the center of silver-intensified gold particles and the midpoint of plasma membrane was determined by ImageJ v1.51 software (National Institutes of Health).

2.10 Construction of expression vectors for tagged GluA subunits

Fragments of DNA encoding sequence for GluA1 and GluA2 were amplified from plasmids encoding respective subunits [100]. Signal peptides and peptide tags (hD2 (KKCPYSAADAAADAAADAAAD), Spot (PDRVRAVSHWSS) [81] and ALFA (SRLEEELRRRLTE)) [80] were inserted into N-terminus of GluA1 and GluA2 via overlap extension polymerase chain reaction or (depending on the length) purchased separately as oligonucleotides from IDT (Integrated DNA Technologies). Plasmid backbones were obtained from pCIneo plasmid encoding α7-D4-B2R vector [101] or pAAV-GFP (donation from Yoav Ben Simon) either by PCR amplification or restriction enzyme reaction. All fragments were then joined together with Gibson assembly [102] to produce vectors encoding tagged AMPAR subunits in pCI-Neo backbone (for expression in HEK cells) or pAAV backbone (for further generation of AAV virus encoding tagged AMPAR subunits). Final sequences used are shown in Figure 3.28. All DNA sequences were confirmed by LGC Genomics (Berlin, Germany) or Microsynth (Vienna, Austria). Virus particles were synthesized by the Lab Support Facility (LSF) at IST Austria.

2.11 Stereotaxic AAV injection

Animals were anesthetized with Ketamine/Xylazine mixture intraperitoneally and head fixed in a stereotaxic setup. Hole was then drilled into the skull and 500 nl of AAVDJ-CAG-Spot-GluA1 or AAVDJ-CAG-Spot-GluA2 was injected into right CA1 at coordinates (AP: -2.0mm; ML:1.7mm; DV: -1.4mm) using a microinjector (Nanoliter 2010, World Precision Instruments, Sarasota, FL, USA). Skin was closed with tissue glue after surgery and animals were treated with Meloxicam (5mg/kg BM, subcutaneous). After 2 weeks, animals were perfused, fixed brains were sliced at 50 µm thickness and slices were used for fluorescence immunolabeling.

2.12 Hippocampal neuron cultures

Hippocampal neuron cultures were obtained from dissociated hippocampi of newly born mice (P0-P4) [103]. Pups were sacrificed by decapitation and brains were extracted from the skulls. Brains were placed in ice cold HBSS (Hank's Balanced Salt Solution, Gibco) and hippocampi were extracted under a dissection microscope in a sterile laminar flow hood. Hippocampi were then transferred into fresh cold HBSS, chopped with a razor blade and all pieces were transferred and incubated for 1h at 37°C in enzyme solution (10 ml DMEM, 2 mg cysteine, 100 mM CaCl2, 50 mM EDTA, and 25 U papain, equilibrated with carbogen for 10 min, and sterile filtered). After this, cells were incubated for 5 min in inactivation solution (25mg bovine serum albumin (BSA) in 10ml of FBS (fetal bovine serum)-containing MEM medium. Coverslips were sterilized with ethanol and coated for 1h with 1mg/ml PLL (poly-L-lysin, Gibco). After washing with MilliQ water, they were placed in a 24 well plate with 1ml plating medium (MEM supplemented with 10% horse serum, 3.3 mM glucose, and 2 mM glutamine. Neurons were plated at concentration of 50000 cells per well and left for 1-2h to adhere. Plating medium was then replaced with Neurobasal-A culture medium (Gibco) containing 1:50 dilution of B27 supplement (Gibco) and 1:100 Glutamax (Gibco). Cultures were kept in the incubator at 37°C and 5% CO_2 for 14 days before use.

2.13 Confocal imaging of cell cultures and tissue sections

Cultured cells grown on coverslips or brain tissue sections were washed with PBS before incubating in primary antibody. For labeling of living cells, antibody was diluted in warm PBS and applied for 1h at 37°C. Cells were washed then 3x10 min in warm PBS and fixed with 4% PFA in PBS. For fixed brain slices, blocking of nonspecific binding was performed for 30 min at RT with 10% normal goat serum (NGS) in PBS, followed in incubation in primary antibody solution overnight at 4°C. Both fixed cells and brain slices were incubated in fluorescence conjugated secondary antibody solution for 1h at RT. After washing out the secondary antibody, cell nuclei were stained with DAPI and coverslips with cells/brain slices were mounted on slide glasses using Mowiol. Light microscopy images were taken with LSM800 (Zeiss, Germany) confocal microscope and example images were prepared with ImageJ v1.51 software (National Institutes of Health).

2.14 Generation of knock-in animals

Guide RNA and ssODN for CRISPR/Cas9 were designed using the SnapGene software and online tool Crispor. Peptide tags were inserted in the same loci as described in 3.4. High quality CRISPR reagents, which includes Cas9 protein or mRNA, guide-RNA and repair templates are either generated in-house or sourced commercially (IDT, EU) for efficient knock-in. Microinjection procedure, animal genotyping and maintenance was performed by PCF at IST Austria.

3 RESULTS

Results presented here are separated into three parts based on the different project aims stated previously and different methodology and approach which was utilized to achieve those aims.

First part includes detailed EM analysis of AMPAR subunits distribution in hippocampal CA1 area of wild type C57BL/6 mice in the basal state, with focus on synaptic and extrasynaptic membranes of pyramidal neurons in different layers, strata oriens, pyramidale, radiatum and lacunosum moleculare. This is followed by intrasynaptic distribution analysis with the aim to reveal possible rules of AMPAR subunit two-dimensional arrangement within the synaptic area.

Second part includes synaptic plasticity induction by physiological learning in the form of inhibitory avoidance memory task and subsequent EM analysis of changes in density and distribution of individual subunit-containing AMPAR within synaptic sites. Additional emphasis was placed on investigating possible differences in nature of synaptic plasticity induction in different layers and subregions of CA1 area.

Third part describes progress in development of novel high-resolution techniques for EM analysis of single channels *in situ* and its application on AMPAR subunits. Results from this part were published as Tabata et al (Electron microscopic detection of single membrane proteins by a specific chemical labeling, 2019), [77].

3.1 Distribution of AMPAR labeling in pyramidal neurons of hippocampal CA1 area

Single labeling for individual AMPAR subunits (GluA1, GluA2, GluA3 or panAMPA antibody labeling for GluA1-3 containing AMPAR) was performed on replicas prepared from tissue of CA1 hippocampal area (Figure 3.1). Specificity of the antibodies has been confirmed using knockout animals and reported earlier (GluA1 [87], GluA2 [77], GluA3 [88], panAMPA (GluA1-3), [89]. Only replicas containing all substrata (stratum oriens (**ORI**), stratum pyramidale (**PCL**), stratum radiatum and stratum lacunosum-moleculare (**LM**)) were selected and analyzed. For the purposes of analysis, stratum radiatum was further divided into three layers of similar width (one third closest to pyramidal cell layer – proximal radiatum (**PR**), middle third – middle radiatum (**MR**) and one third furthest away from pyramidal cell layer – distal radiatum (**DR**)).

3.1.1 Subunit- and layer-dependent differences in synaptic and extrasynaptic labeling for AMPAR

Synaptic sites were identified as tightly packed clusters of IMPs (intramembrane particles) on the E-face of dendritic spines representing postsynaptic membrane specializations (PSDs). Majority of synapses found on dendritic spines in the stratum oriens and stratum radiatum of CA1 area have their origin in CA3 area, while synapses found on dendritic spines in stratum lacunosum-moleculare have their origin mainly from entorhinal cortex [133]. In contrast, interneuron synapses are usually found on the dendritic shafts of the interneurons which can be distinguished by their cylindrical, tubular shape and absence of spine necks. Images from pyramidal cell layer were taken from E-face of pyramidal cell somata, each image representing different cell. In all other layers, extrasynaptic images were samples from E-face of dendritic shafts after confirming that the observed dendrite belongs to the CA1 pyramidal cells (by presence of spine necks). From each layer, 20-30 synaptic sites were imaged and analyzed per replica. Extrasynaptic sites were imaged from the same replicas. For extrasynaptic sites, number of sampled images was 10-15 in pyramidal cell layer (one image per cell) and 10-15 for dendrites in every other layer. Each replica included in the analysis corresponded to individual animal and total number of animals included in the study was 4. Absolute values of observed densities for synaptic and extrasynaptic (cell bodies and dendrites) membranes are

shown in Table 2. and Figures 3.2 and 3.3. Density of AMPAR labeling in all four types of labeling was highest in stratum radiatum. In extrasynaptic sites, observed values have shown gradient of AMPAR density increasing from PCL and peaking in middle and/or distal radiatum, which was common for all four types of labeling (Figure 3.3). No significant density gradient could be observed for synaptic labeling, possibly due to variable size and density in sampled synapses or because some PSDs were included only partially.

Table 2. Absolute values for AMPAR subunit labeling in individual CA1 strata in synaptic and extrasynaptic sites (mean±sem)

Synaptic	s.oriens	s.pyramidale	s.radiatum (proximal)	s.radiatum (middle)	s.radiatum (distal)	s.lacunosum-moleculare
GluA1	334.9±67.7	N/A	462.4±64.9	443.3±53.7	508.3±75.8	314.1±60.9
GluA2	616.1±101.5		881.2±204.5	787.4±166.6	831.5±184.9	532.3±99.7
GluA3	333.3±65.4		492.1±149.7	426.7±54.9	479.6±119.7	279.9±59.8
panAMPA(GluA1-3)	564.7±201.9		554.7±202.9	637.8±245.3	660.9±241.7	489.6±183.9
Extrasynaptic	s.oriens	s.pyramidale	s.radiatum (proximal)	s.radiatum (middle)	s.radiatum (distal)	s.lacunosum-moleculare
GluA1	54.6±15.3	34.7±6.5	46±13.3	64.6±14.2	69.7±17	51±10.5
GluA2	97.2±17.1	60.5±13.2	85.7±19.6	131.1±30.7	118.3±27.5	76.4±14.2
GluA3	36.7±9.2	20.4±7.8	25.3±10	34.6±8.7	36.3±8.6	27.7±8.5
panAMPA(GluA1-3)	113.6±50	60.7±25.7	102.6±48.2	119.5±54.9	106.4±57.5	92.1±44.2

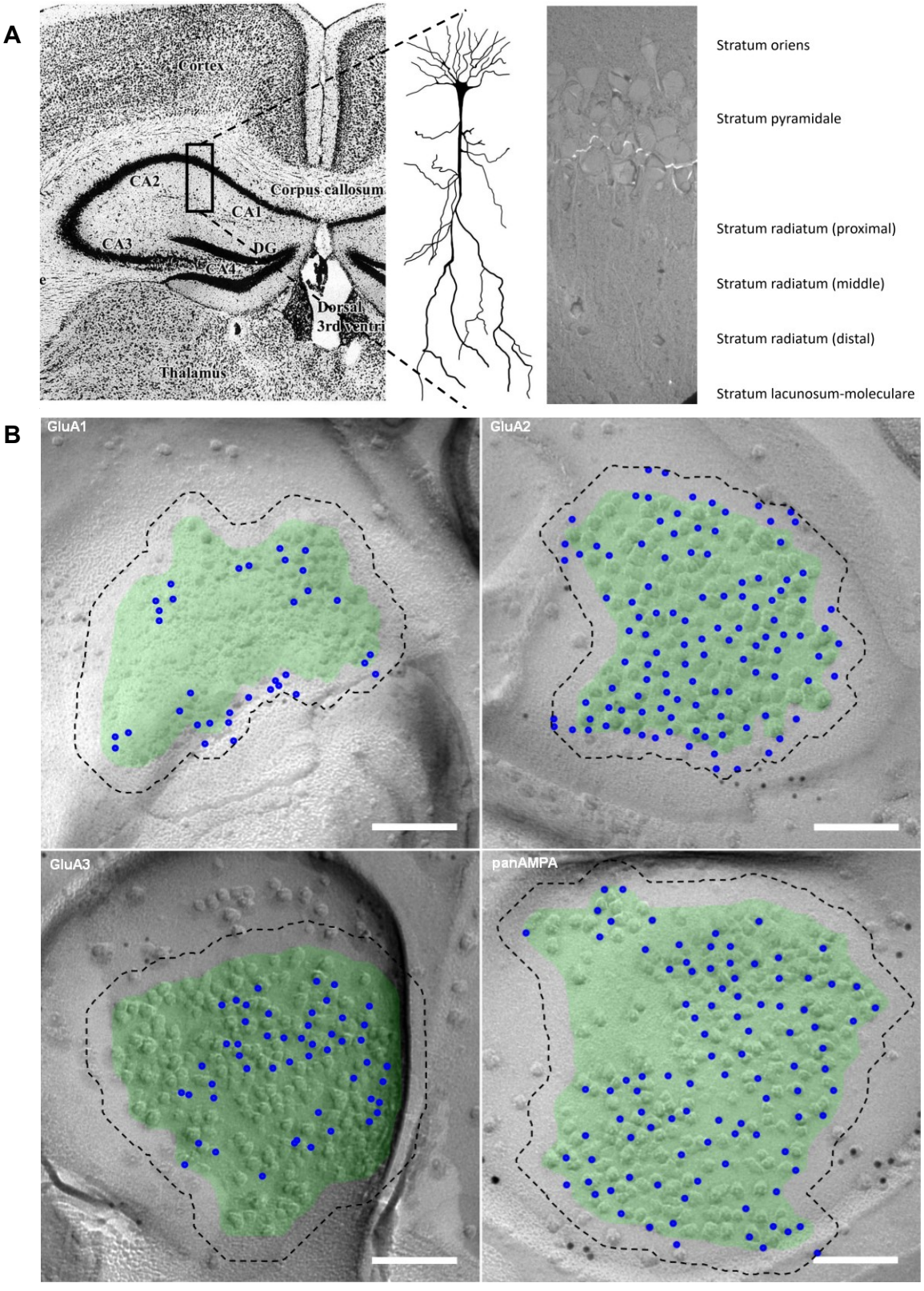
A
Cortex
CA2
Corpus callosum
CA1
CA3
DG
CA4
Dorsal 3rd ventri
Thalamus
Stratum oriens
Stratum pyramidale
Stratum radiatum (proximal)
Stratum radiatum (middle)
Stratum radiatum (distal)
Stratum lacunosum-moleculare
B
GluA1
GluA2
GluA3
panAMPA

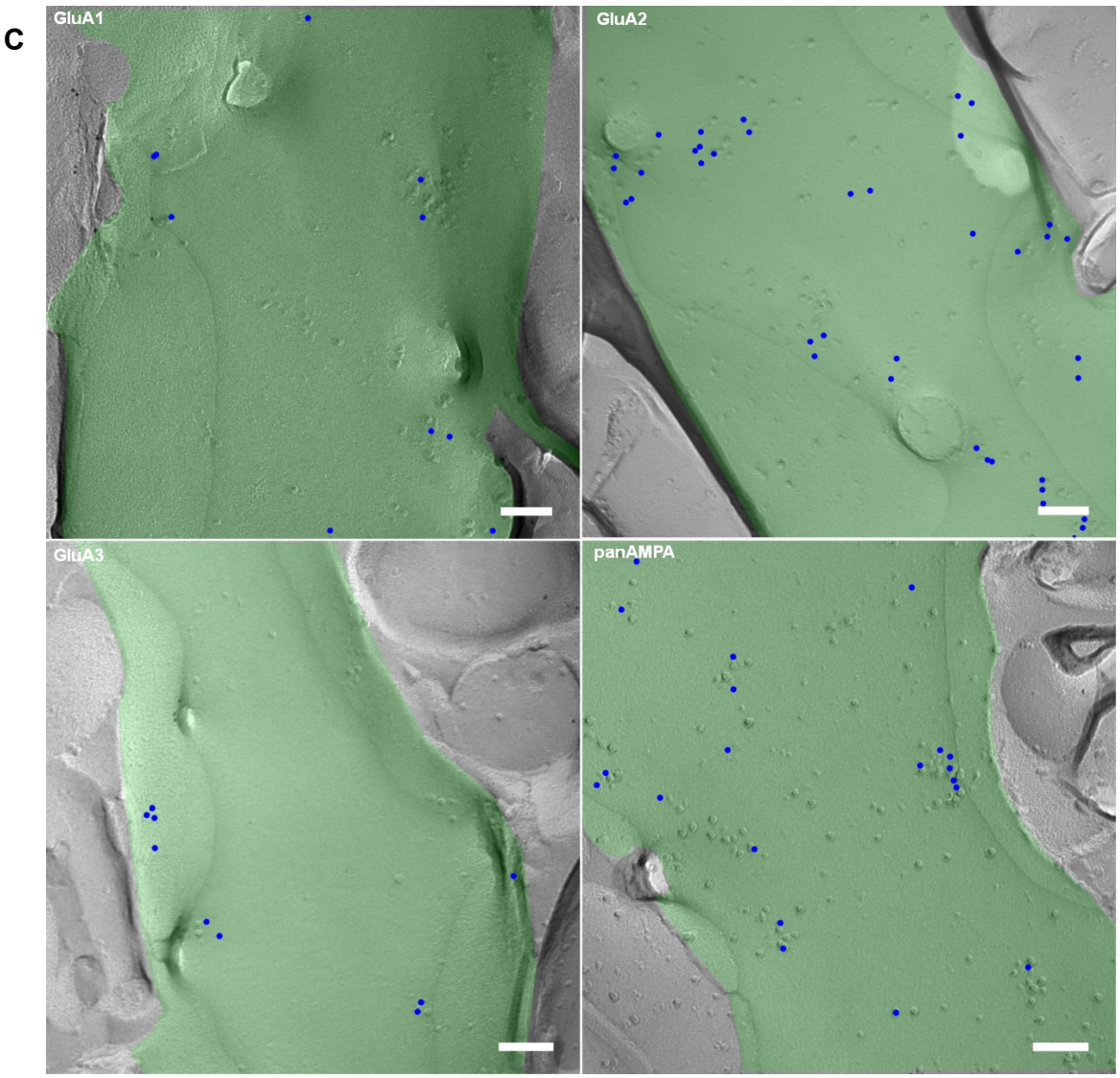

Figure 3.1. Overview of mouse hippocampus and example images A) indicated area of analysis and corresponding low magnification EM image from replica with layers indicated. Scale bar: 500nm (adapted from [104]) B) example images of synaptic labeling C) example images for dendritic labeling. Scale bar: 100 nm

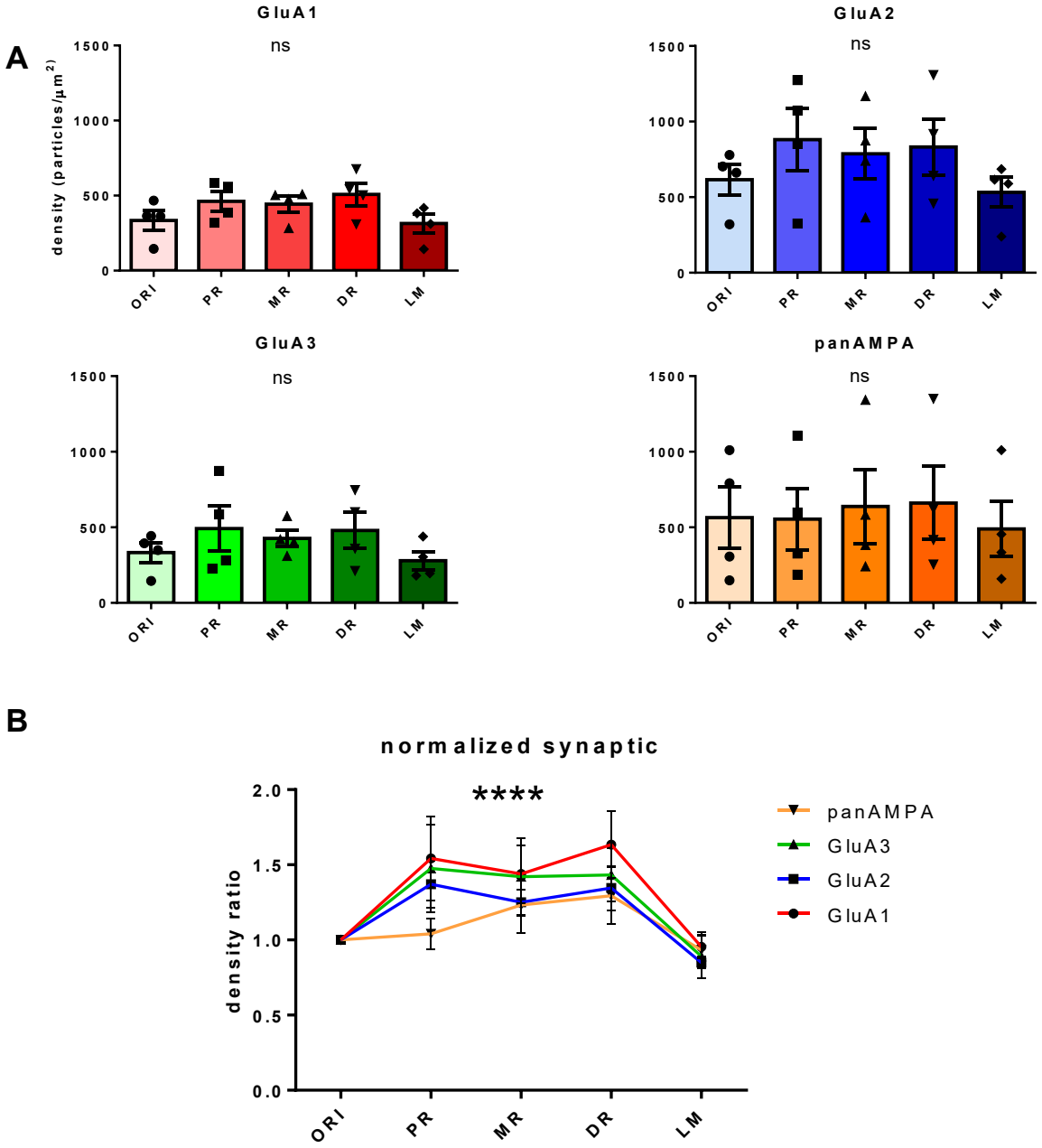

Figure 3.2. Labeling density for AMPAR subunits in synapses. (A) Absolute values of labeling density (one-way ANOVA, ns) (B) Normalized densities for each subunit in synaptic sites (2-way ANOVA, layers $F(4, 60) = 8.43$, $p<0.0001$; subunits $F(3, 60) = 1.66$, $p=0.18$; interaction $F(12, 60)$, $p=0.95$). Detailed statistics for this figure can be found in the Appendix.

Observed values were similar for panAMPA and GluA2 labeling, consistent with previous reports which indicated presence of GluA2 subunit in all AMPAR in hippocampal pyramidal cells [58]. While labeling for GluA1 and GluA3 had similar values for synaptic

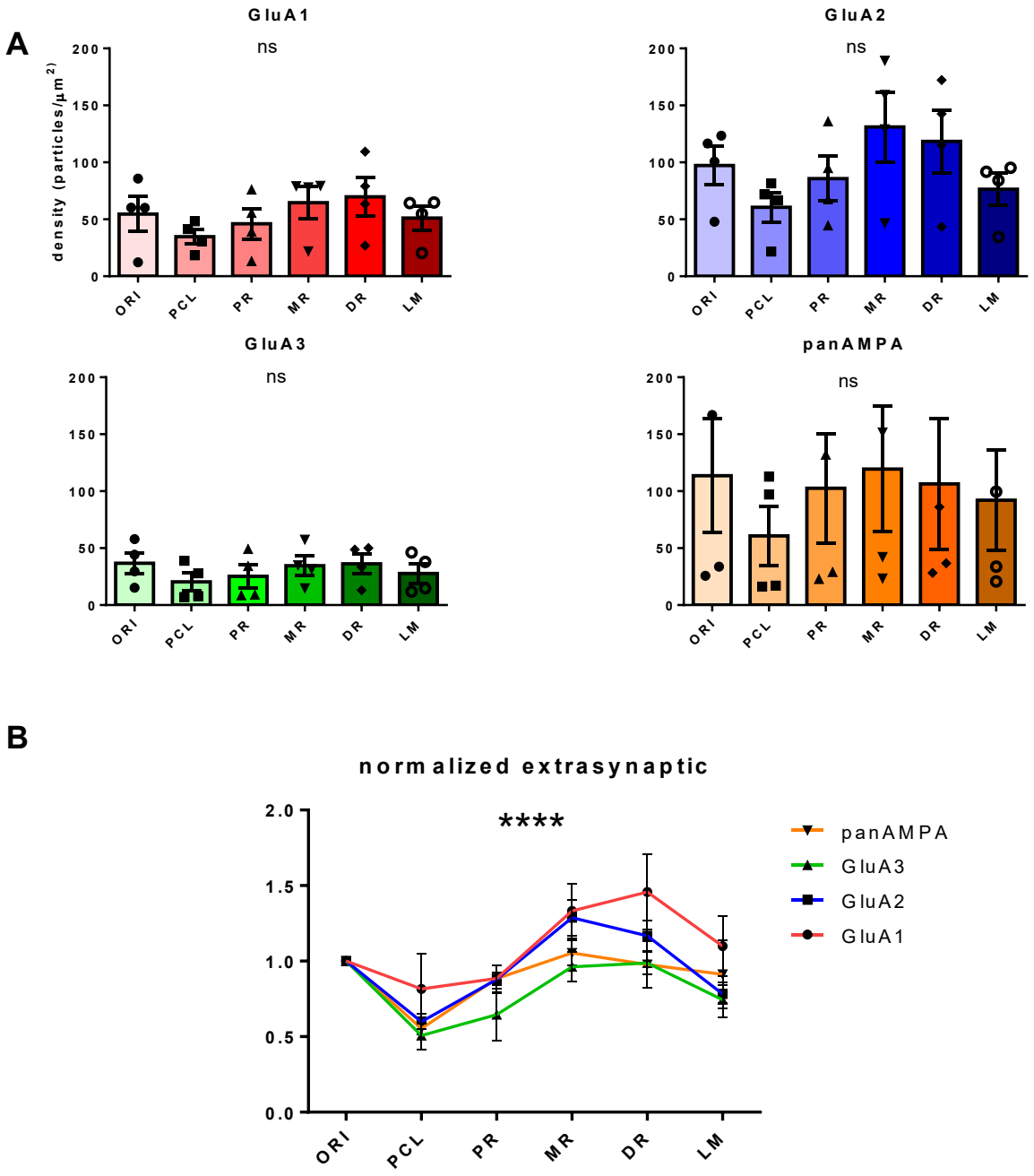

Figure 3.3. Labeling density for AMPAR subunits in extrasynaptic sites (soma and dendrites) (A) Absolute density values for each subunit in the extrasynaptic sites. (B) Normalized densities for each subunit in extrasynaptic areas (2-way ANOVA, layers $F(5, 72)=10.65$, $p<0.0001$;, subunits $F(3, 72)=5,52$, $p=0.0018$; interaction $F(15, 72)=0,64$, $p=0.83$). Detailed statistics for this figure can be found in the Appendix.

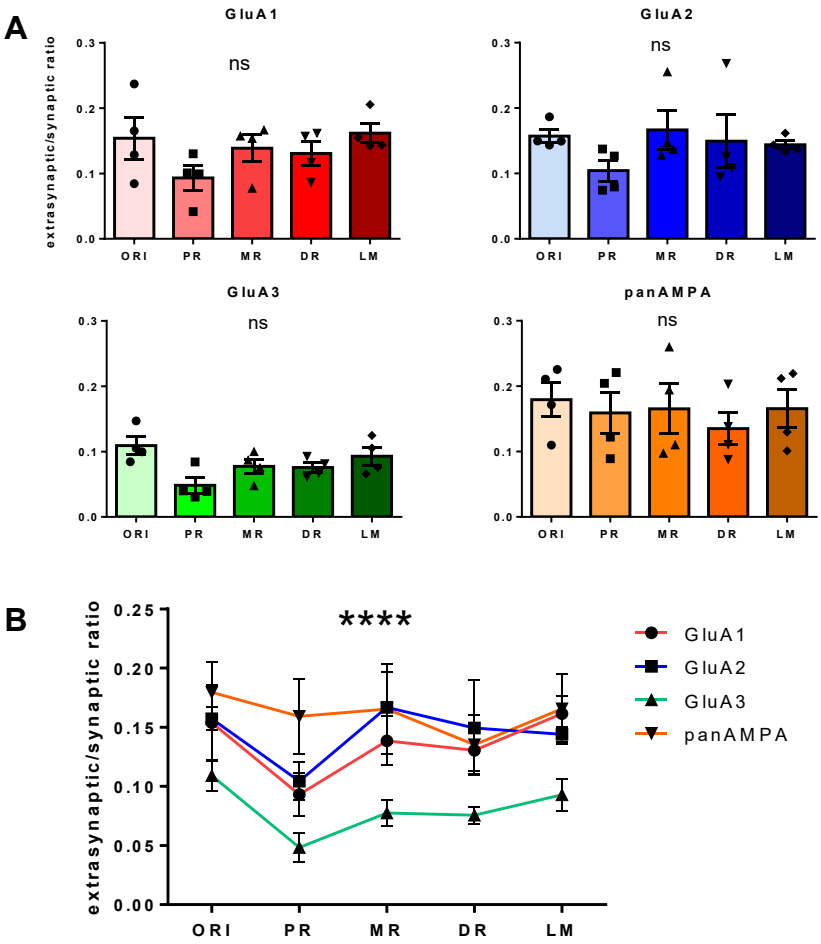

Figure 3.4. Extrasynaptic/synaptic labeling ratio(A) Individual values of extrasynaptic/synaptic density ratios in each substratum. (B) Comparison of E/S ratios for individual subunits and substrata (2-way ANOVA, layers $F(4,60)=2.73$, $p=0.036$; subunits $F(3,60)=11,45$, $p<0.0001$; interaction $F(12,60)=0.38$, $p=0.96$.) Detailed statistics can be found in the Appendix.

areas, labeling for GluA3 was much weaker in the extrasynaptic areas. To further investigate this point, ratio of labeling density (extrasynaptic/synaptic) was calculated and shown in Figure 3.4. In all layers except stratum oriens, GluA3 labeling has shown significantly lower density ratios compared to other subunits.

Altogether, highest labeling density for AMPAR subunits was found in the stratum radiatum in both synaptic and extrasynaptic sites. Density in extrasynaptic sites showed increasing gradient of density along apical dendrites from pyramidal cell bodies towards stratum lacunosum moleculare.

3.1.2 Association of AMPAR labeling with IMPs in the somatic membrane

Non-synaptic intramembrane particle (IMP) clusters frequently occur on somatic and dendritic membranes. Although it is considered that they represent accumulation of certain protein complexes, their actual identity and function is not yet clear [96]. In order to investigate whether these clusters are differentially involved in trafficking and accumulation of different AMPAR, I investigated association of gold particles with non-synaptic IMP clusters on somatic membranes by comparing ratios of IMP-associated and -unassociated particle density. IMP-associated particles were considered those which were found within IMP clusters and not more than 30nm away, while all others were considered IMP-unassociated. I found that GluA3 subunits were less associated with IMP clusters on somatic membrane (Figure 3.5).

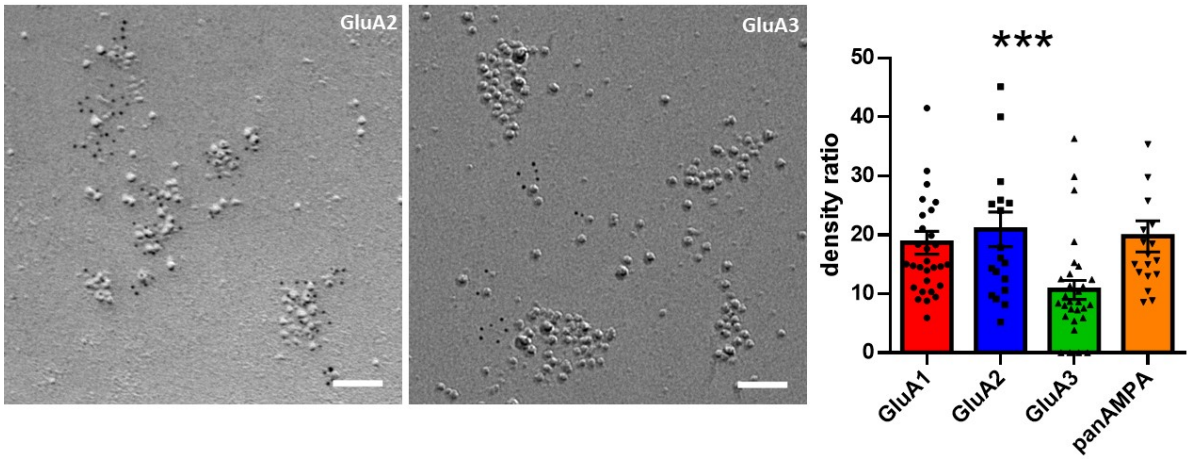

Figure 3.5. IMP cluster association of AMPAR subunit on somatic membrane Example images of labeling for GluA2 and GluA3 (left) in somatic membrane and ratio of densities of IMP cluster associated/unassociated particles (n=18-30, p=0.003, one-way ANOVA) Scalebar: 100nm. Detailed statistics for this figure can be found in the Appendix.

3.1.3 Intrasynaptic distribution of AMPAR subunit labeling

For the intrasynaptic distribution analysis I have prepared an additional set of samples using the "flattening" method which allows for more efficient sampling of synapses with complete PSD areas which were used in this part. Labeling was performed in the same way as in the previous paragraph, however, only synapses with complete PSDs and more than 4 gold particles were sampled and analyzed. Synapses were sampled only from middle part of stratum

radiatum. Number of sampled synapses was 15-25 per replica (one replica corresponding to one animal) and number of replicas (animals) was 3. Figure 3.6. shows mean area of sampled synapses and particle density for each subunit. No difference in PSD area was detected. Although higher density values of observed labeling were likely due to weaker fixation of samples and/or omission of synapses with less than 4 gold particles, the relative density between different subunits was consistent. Random placement of gold particles using the same shape, size and density values for each synapse was simulated using DAREA software and compared to the real data to detect if there is significant center-periphery preference and clustering in intrasynaptic distribution.

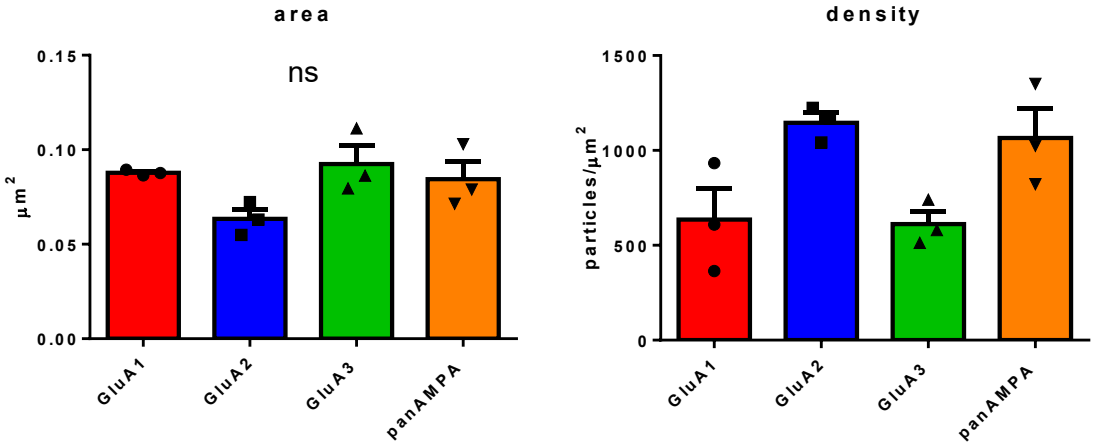

Figure 3.6. Average PSD size and labeling density of synapses sampled for intrasynaptic analysis (one-way ANOVA, ns).

3.1.3.1 Center periphery preference of AMPAR labeling

For each gold particle, center periphery index (CPI) was determined using the DAREA software and the mean was calculated for each synapse. Center periphery index is calculated using the formula:

$$CPI = \left(\frac{c}{c+e}\right)^2$$

where *c* indicates distance from the gold particle to the center of gravity of the synapse, while *e* indicates distance to the nearest edge of the demarcated synapse.

Labeling for GluA1, GluA2 and panAMPA has shown periphery preference compared to that of GluA3. Distribution of GluA1 labeling has shown significantly peripheral preference compared to the random simulation. Distribution of GluA3 labeling has shown tendency towards center compared to the simulation (Figure 3.7A). In addition to that, labeling for GluA3 had a significantly smaller percentage of particles in the outer rim of synapses compared to those for other subunits. (Figure 3.7B).

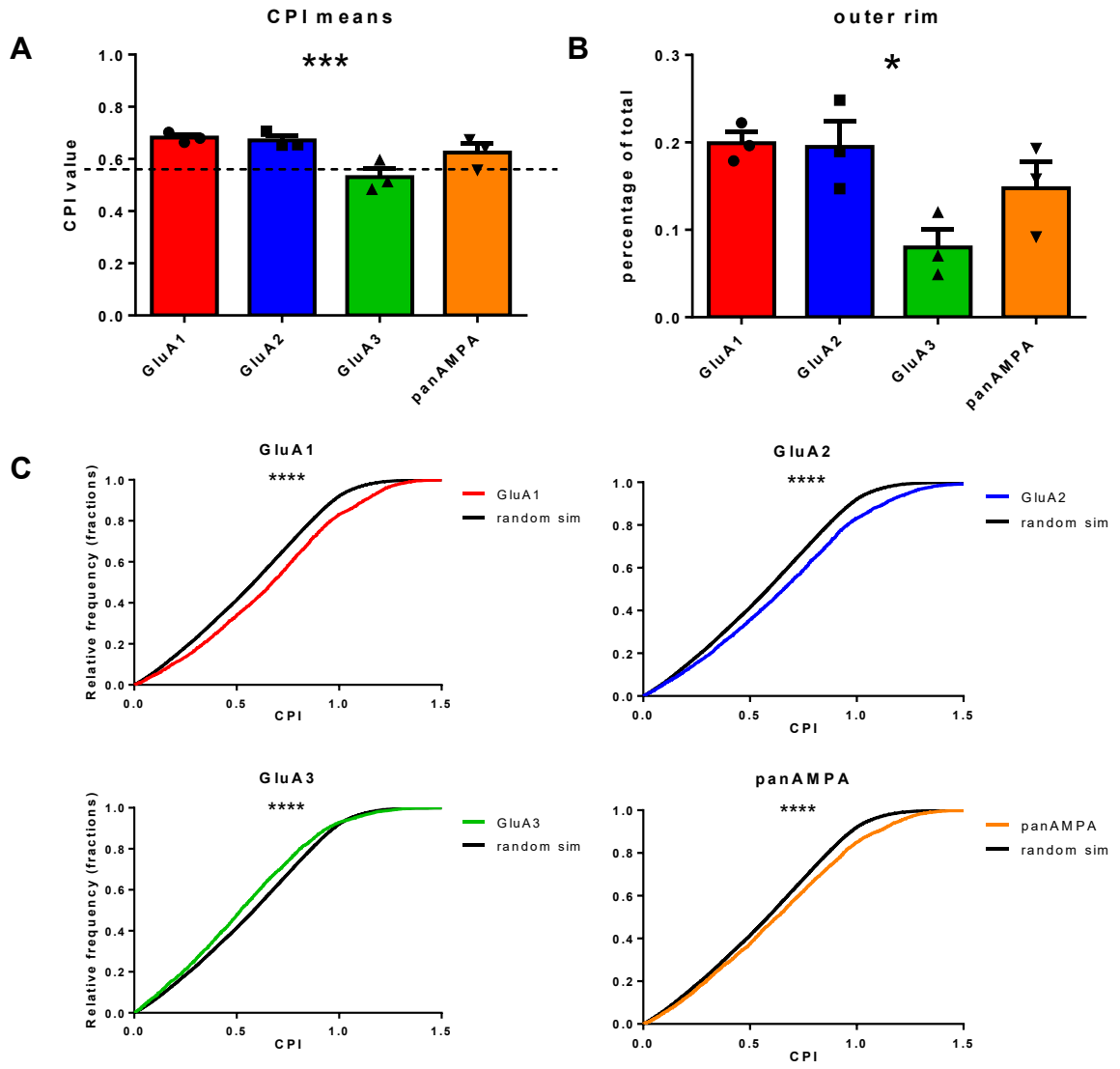

Figure 3.7. Center periphery preference of AMPAR labeling. (A) CPI means comparison. Horizontal line indicates average CPI value of random simulation for synapses with circular PSD (~0.57). CPI values were compared between each other (one-way ANOVA, p=0.0003) and with simulation (included in Appendix) (B) Percentage of particles found in outer rim (one-way ANOVA, p=0.02) (C) CPI cumulative distribution function comparison (Kolmogorov-Smirnov, detailed statistics included in the Appendix)

Cumulative distribution function of CPI values for all particles further indicated more central localization for GluA3 labeling and more peripheral for the GluA1, GluA2 and panAMPA labeling, compared to the simulation (Figure 3.7C).

3.1.3.2 Clustering of AMPAR labeling

Nearest neighbour distance (NND) has been shown to be the best indicator of possible clustering of gold particles [105]. To investigate possible clustering of gold particles in this dataset, nearest neighbour distance (NND) was calculated and compared to the NND of random simulation. Results have shown no difference between NND of real data and simulated data for GluA2 and panAMPA labeling, so they have not been included in further analysis (Figure 3.8A). Results for GluA3 have shown significant difference in NND compared to the simulation, and GluA1 showed tendency for shorter NND small but insignificant difference compared to the simulation. GluA3 labeling showed significantly fewer number of clusters, with tendencies for more particles per cluster, larger cluster area and lower cluster CPI compared to both GluA1 and simulation (Fig 3.8B).

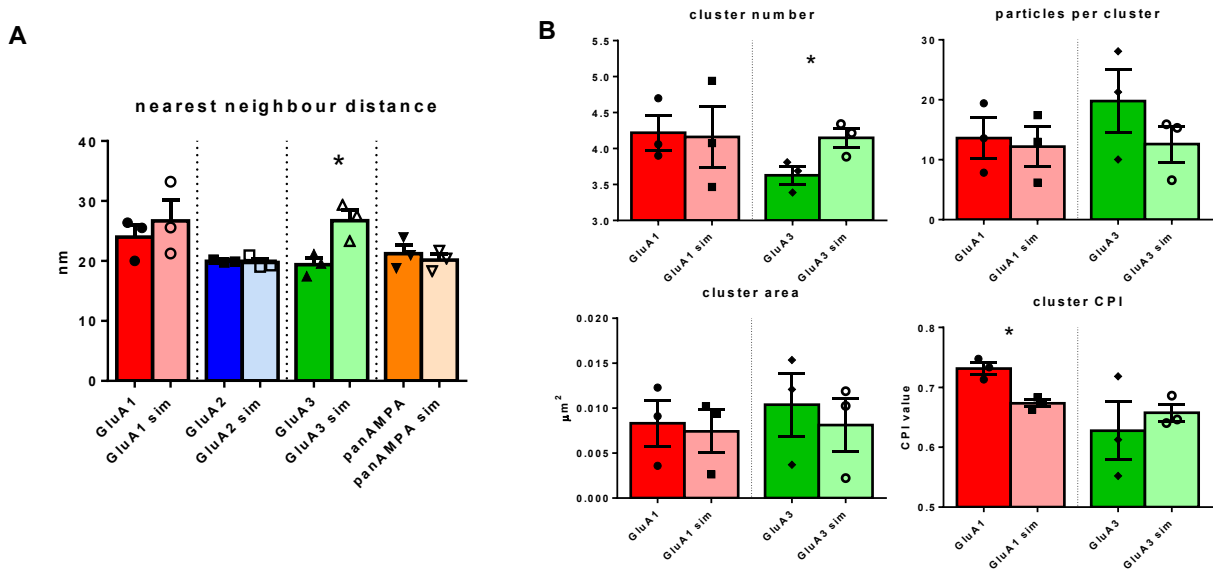

Figure 3.8. Clustering of AMPAR labeling. (A) Comparison of NND values with simulated random distribution of gold particles. (GluA3, p=0.01, paired t-test) (B) Comparison of individual cluster parameters for GluA1 and GluA3 with random simulations (detailed statistics included in Appendix)

Taken together, these results indicate possible arrangement of GluA3-containing receptors in one or more larger clusters, more centrally localized, while GluA1-containing clusters are more peripherally located in several smaller clusters. GluA2 and panAMPA labeling did not show any clustering according to NND analysis, but considering that GluA2 is included in all AMPA receptors at these synapses and panAMPA labeling also includes all AMPA receptors, more subtle rules of arrangement for GluA1- and GluA3-containing AMPAR could be masking the detection of clustering properties when labeling was performed for GluA2 or panAMPA.

3.2 *Learning induced changes in number and distribution of AMPAR subunits in CA1 synapses*

After determining the arrangement of synaptic receptors in the basal state, I wanted to investigate how this arrangement changes after induction of synaptic plasticity by physiological learning. Using the behaviour procedure described in Mitsushima et al. [72,73] with some modifications, I performed inhibitory avoidance (IA) training using male wild type (WT) adult C57BL/6 mice (Figure 3.9). Latency to enter the dark compartment of the IA apparatus before and after conditioning with foot shock is shown in Figure 3.10A. I tested some animals additionally after 24, 48 and 72 hours after training and these results (Fig 3.10B) indicate that memory is maintained over a longer period of time. For electron microscopy analysis, animals were perfused shortly after the memory retrieval (cca 10 min later), and fixed brains from animals with the latency longer than 100 seconds during second exposure were selected for further processing. Only replicas which contained a complete CA1 area where it was possible to determine part of CA1 proximal and distal to CA2 were included in the analysis. Since different mechanisms of LTP have been reported between synapses in stratum radiatum and stratum oriens [99,127,128,129,130,131,132], I examined these two layers. Replicas were labeled with single labeling with either GluA1, GluA2, GluA3 or panAMPA (GluA1-3) antibodies. From each of the regions of interest in the same replica (proximal CA1 radiatum, proximal CA1 oriens, distal CA1 radiatum, and distal CA1 oriens) (Fig 3.11) 20-30 synapses were sampled and analyzed further. Same as previously stated, each analyzed replica corresponded to individual animal and in total I analyzed 3-6 animals per dataset.

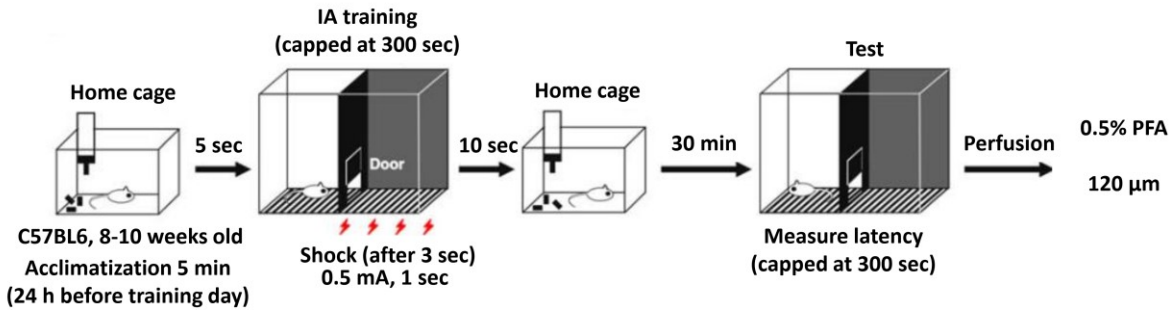

Figure 3.9. Inhibitory avoidance experimental setup used in this study (adapted from [73])

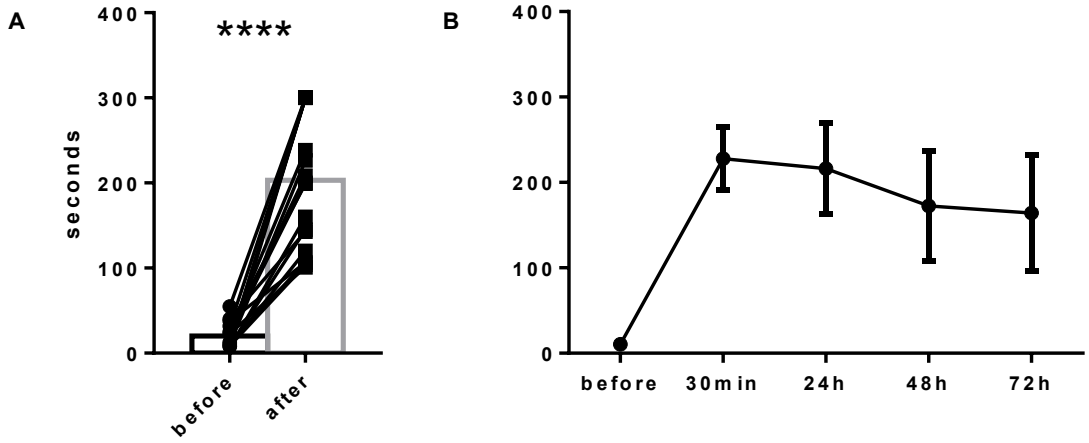

Figure 3.10. Inhibitory avoidance results. (A) Comparison of latencies before and after foot shock in animals which were selected for EM analysis (n=19, Wilcoxon, p<0.0001) (B) Latencies in animals exposed to IA apparatus several days after training

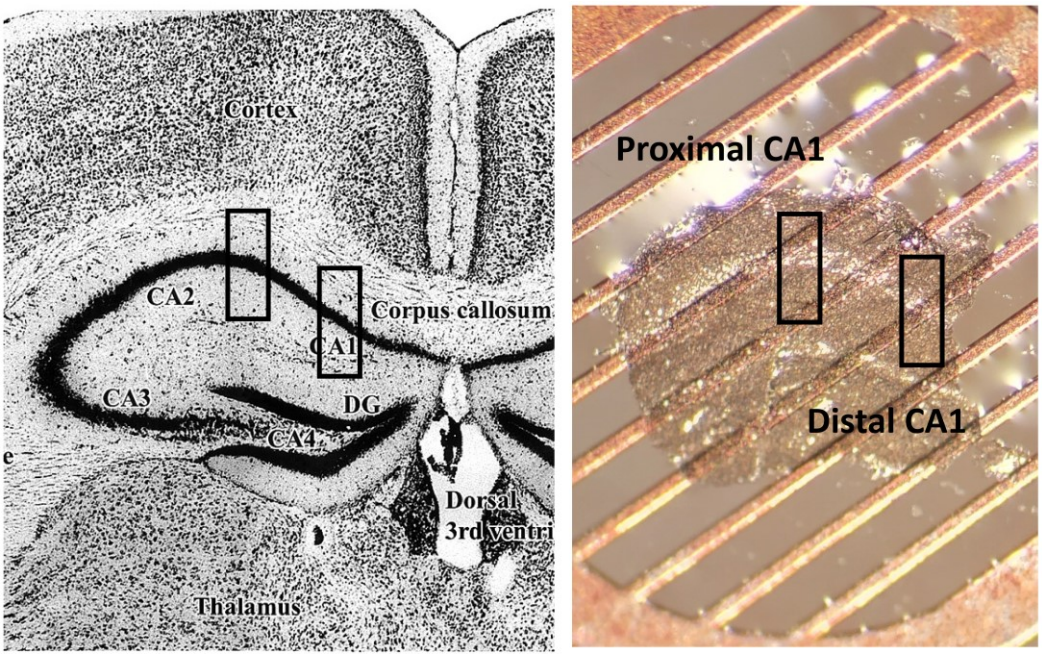

Figure 3.11. Proximal and distal regions of the CA1 area from which the images of synapses were sampled. Coronal mouse section (left) [104] and corresponding replica on the copper grid (right).

First, I compared labeling density for 4 different types of labeling (GluA1, GluA2, GluA3 and panAMPA) between proximal and distal stratum radiatum of CA1 area in control (untrained) and IA trained animals (Figure 3.12A and Table 3). Two-way analysis of variance (ANOVA) indicated significant difference in labeling density for GluA1 between proximal and distal stratum radiatum in trained animals. (p=0.04, detailed statistics in the Appendix). This

significance was further confirmed by direct comparison between these two groups only (p=0.002, paired t-test). ANOVA analysis of other datasets (GluA2, GluA3 and panAMPA did not reveal any significant difference between proximal and distal radiatum in control and trained animals. However, additional comparison of labeling densities between proximal and distal radiatum for GluA2 indicated significant difference (p=0.026, paired t-test)

To further investigate this point, I calculated the ratio of labeling between proximal and distal radiatum (P/D ratio) and compared those ratios between control and trained animals (Figure 3.12B. The value of P/D ratio was around 1 for control animals but showed a highly significant difference for GluA1 (p=0.001, unpaired t-test). This comparison also indicated a subtle decrease in labeling density for GluA2 (P/D ratio around 0.8 for trained animals) but did not show statistically significant difference, possibly due to high variability in control samples. Other labeling datasets (GluA3 and panAMPA) did not show any difference in P/D ratio

Next, I investigated whether the effect of IA training caused any differences in size of the synaptic area (Figure 3.13). I compared the PSD area of control and trained animals in proximal and distal radiatum and only samples labeled for GluA1 indicated some difference in PSD size (p=0.04, one-way ANOVA). No difference was detected in the other three datasets.

Table 3. Absolute labeling density of for AMPAR subunits in proximal and distal stratum radiatum in control and trained animals (mean±sem).

Region (density)	GluA1	GluA2	GluA3	panAMPA
Control – distal s.r.	221.6±47.1	434±230	471±68.2	1014±68.2
Control – proximal s.r.	218.6±53.4	373.1±160	421.6±77.1	1101±61.3
Trained – distal s.r.	111.4±14.5	531.6±136.4	296.9±73.3	864.4±143.3
Trained – proximal s.r.	239.4±27.2	436.7±115.4	228.7±7.3	926.6±210.8

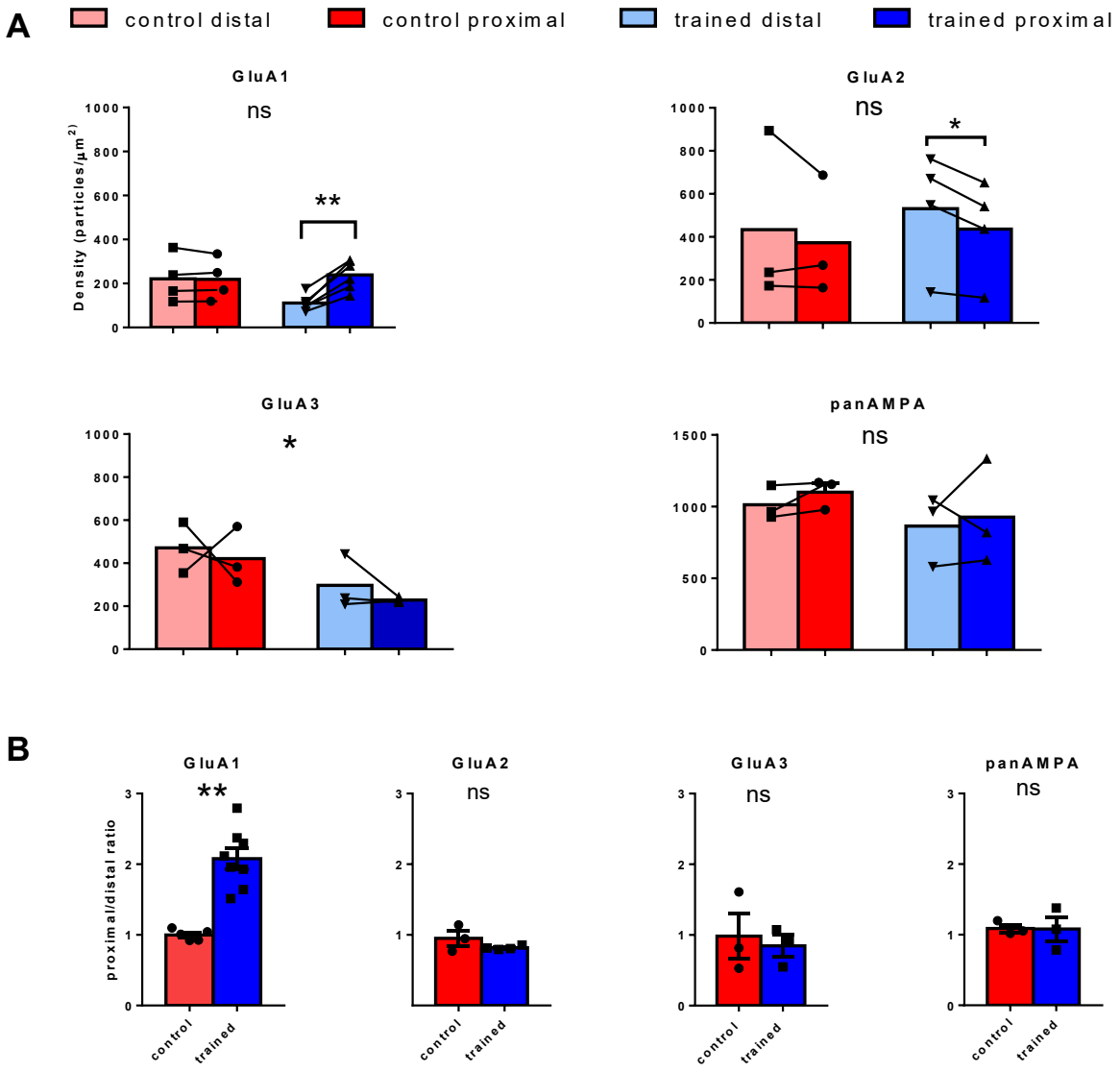

Figure 3.12. Labeling density for AMPAR subunits in stratum radiatum after IA learning (A) Comparison of observed labeling densities between control and trained animals in proximal and distal areas of CA1 radiatum. (two-way ANOVA, GluA1, ns; GluA2; ns; GluA3, proximal-distal $F(1,8)=0.86$, $p=0.83$; control-trained $F(1,8)=8.4$, $p=0.01$, interaction $F(1,8)=0.022$, $p=0.88$; panAMPA, ns.) Detailed statistics can be found in the Appendix) (B) Comparison of ratios of labeling density in proximal and distal area (P/D ratio) of CA1 stratum radiatum between control and trained animals (unpaired t-test, $p=0.002$ (GluA1)

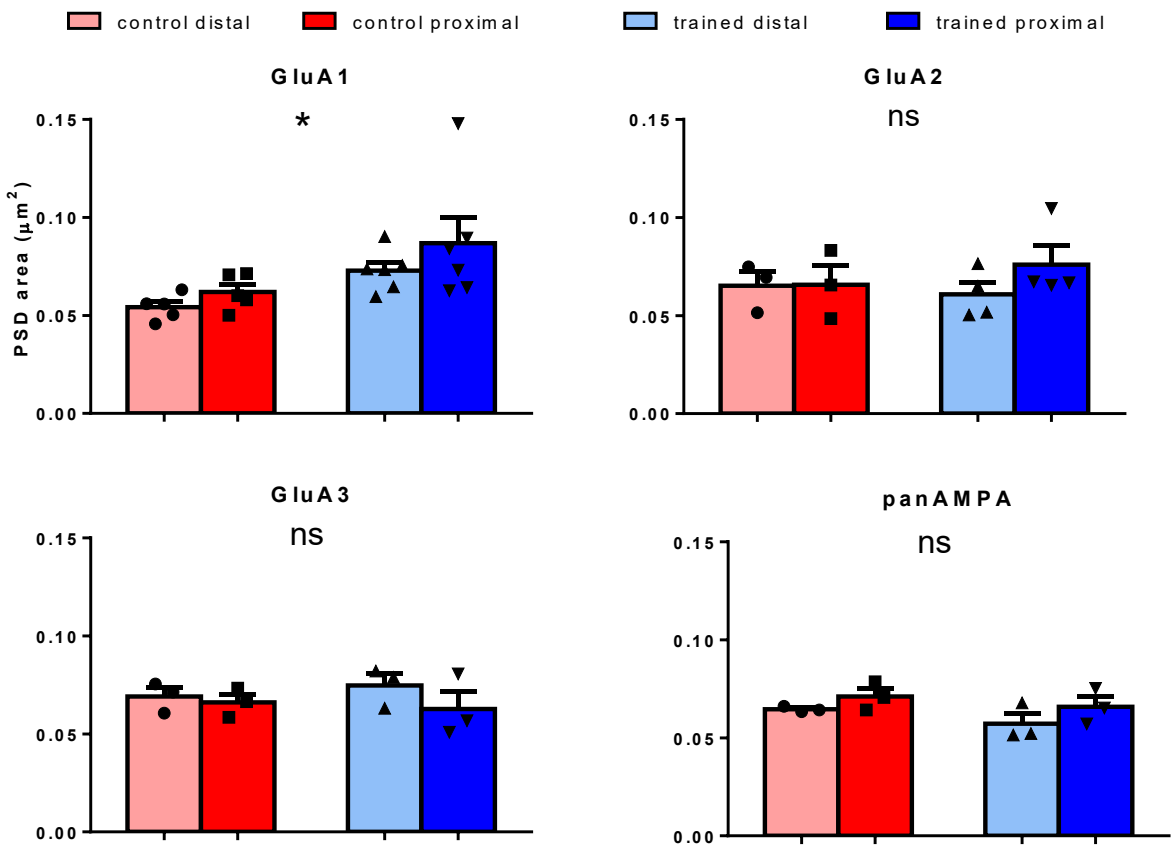

Figure 3.13. Comparison of sampled PSD area in CA1 stratum radiatum (GluA1, one-way ANOVA, p=0.044, detailed statistics in the Appendix)

3.2.1 Intrasynaptic analysis of AMPAR subunit labeling after IA training in CA1 stratum radiatum

I performed the same center-periphery analysis on samples obtained after IA training as described in section 3.1 of results. First, CPI value was determined for every particle in every image using DAREA software and then means for each synapse and for each animal were calculated. Comparison of CPI means indicated significant difference in center periphery arrangement for GluA1 labeling (p=0.027, one-way ANOVA, detailed statistics can be found in the Appendix). Results for GluA2 indicated lower CPI values in both proximal and distal CA1 radiatum in trained animals but this difference was not statistically significant. Results for GluA3 and panAMPA did not show any difference between control and trained animals or between proximal and distal CA1 radiatum (Figure 3.14A).

To further investigate center periphery arrangement, I plotted a cumulative distribution curve function using all CPI values and compared different distributions between each other and with random distribution of gold particles simulated by DAREA (Figure 3.14B).

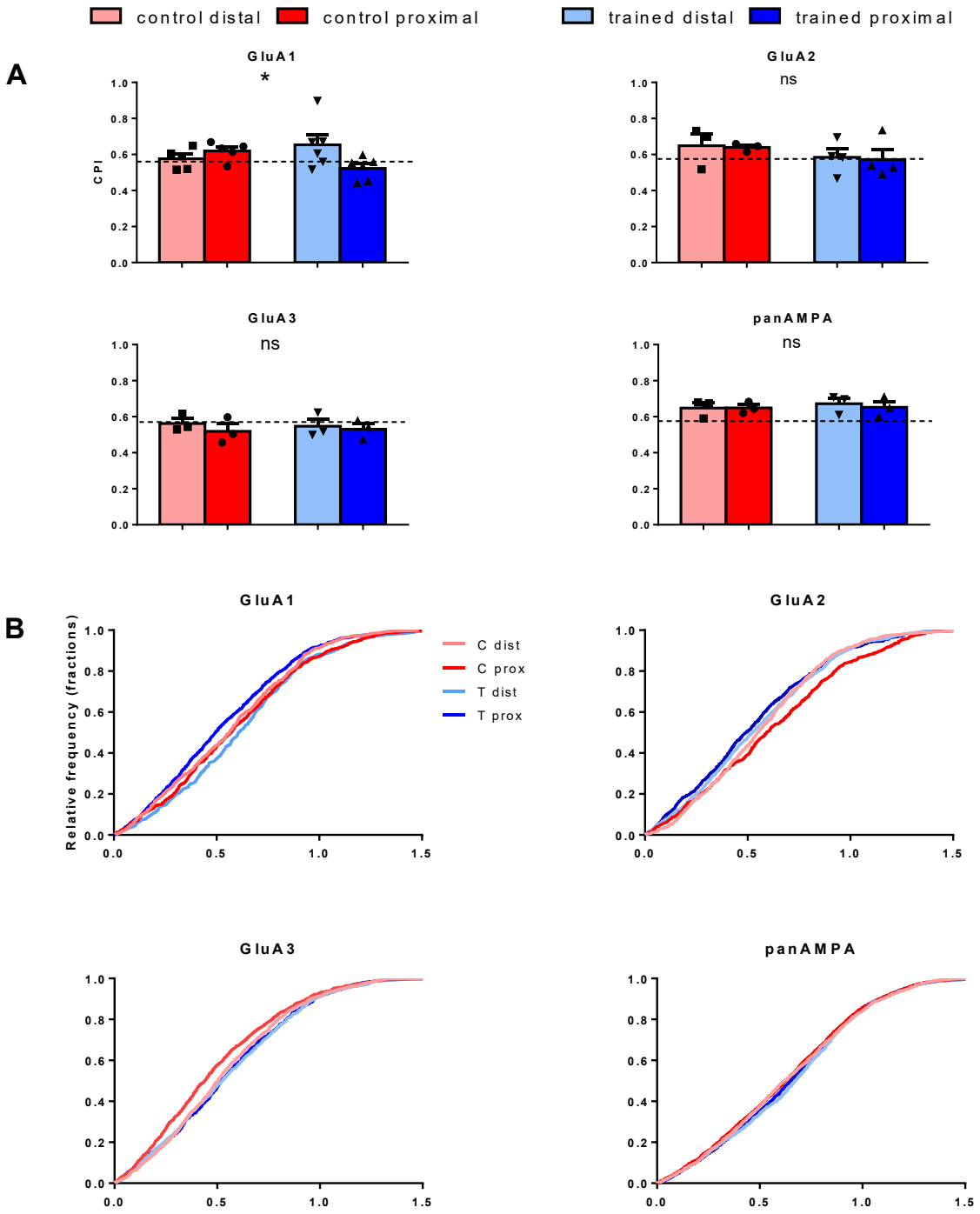

Figure 3.14. Center-periphery index analysis – stratum radiatum. (A) Comparison of CPI means (GluA1, p=0.027, one-way ANOVA) (B) comparison of CPI distribution between AMPAR subunits and random distribution simulated by DAREA. Detailed statistics can be found in the Appendix.

Similar to analysis of CPI means (Figure 3.14A), cumulative distribution analysis revealed significant difference in distribution of GluA1 labeling between proximal and distal radiatum in trained animals ($p<0.0001$, Kolmogorov-Smirnov test) and between proximal radiatum in trained animals and proximal radiatum in control animals ($p=0.004$, Kolmogorov-

Smirnov test). Labeling for GluA2 showed similar distribution between proximal and distal in trained animals but significantly different distribution in proximal radiatum between control and trained animals. Detailed statistics for CPI distribution can be found in Appendix.

One additional aspect of center periphery arrangement is the number of particles found in the outer rim of the area which belongs to the individual synapse (30 nm). I expressed this number as a percentage of total number of particles found in the particular synapse and compared it between control and trained animals and between distal and proximal area of CA1 stratum radiatum (Figure 3.15). Once again, the strongest difference was observed for GluA1 labeling (p=0.006, one-way ANOVA) and subsequent post-hoc analysis indicated the strongest difference for trained proximal, compared to control proximal and trained distal. Direct comparison between distal and proximal in trained animals also showed significant difference (p=0.01, paired t-test).

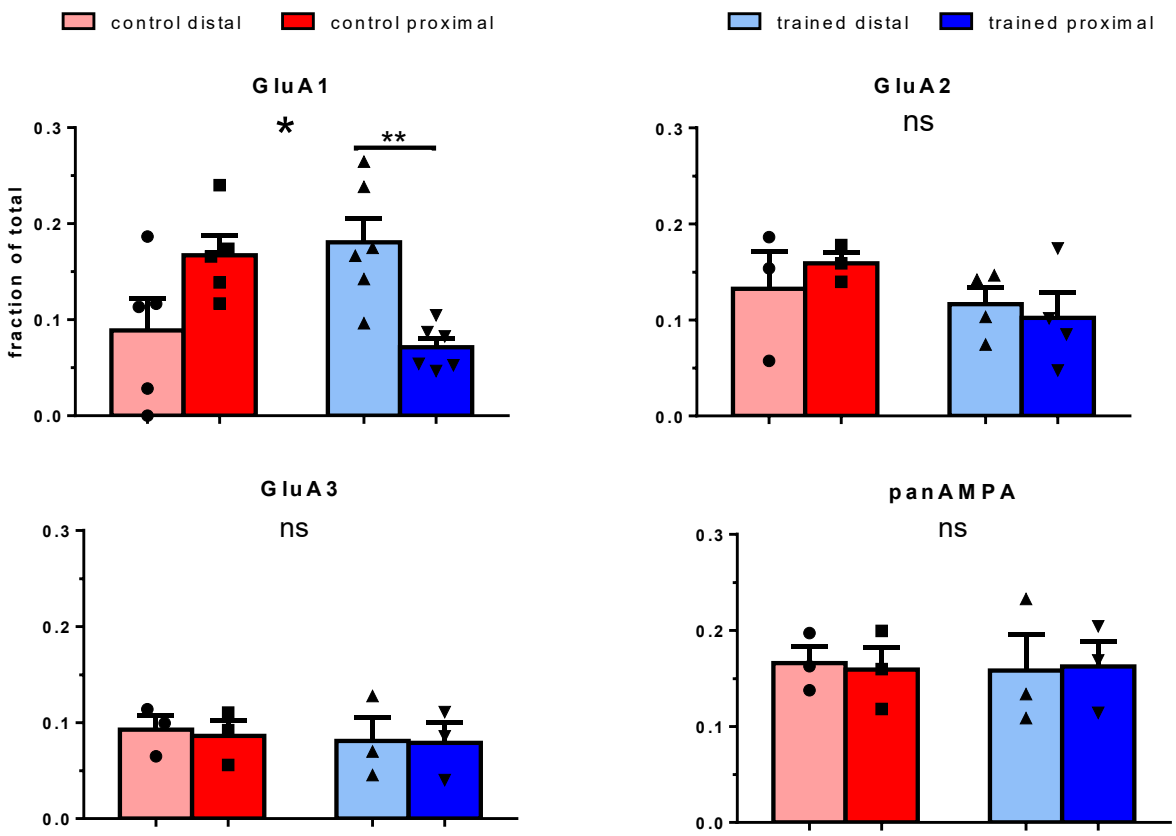

Figure 3.15. Fraction of gold particle number observed in outer rim of PSD (GluA1, p=0.006, one-way ANOVA)

3.2.2 Clustering of synaptic AMPAR labeling after IA training in CA1 stratum radiatum

I first determined and compared the nearest neighbour distance for gold particles in each dataset and compared it with random distribution of gold particles simulated by DAREA software. Again, the strongest difference from the random distribution was observed for GluA1 and GluA3 labeling (Figure 3.16. Detailed statistical analysis in the Appendix), which is consistent with results from 3.1, but still necessitates further clustering analysis to investigate possible changes

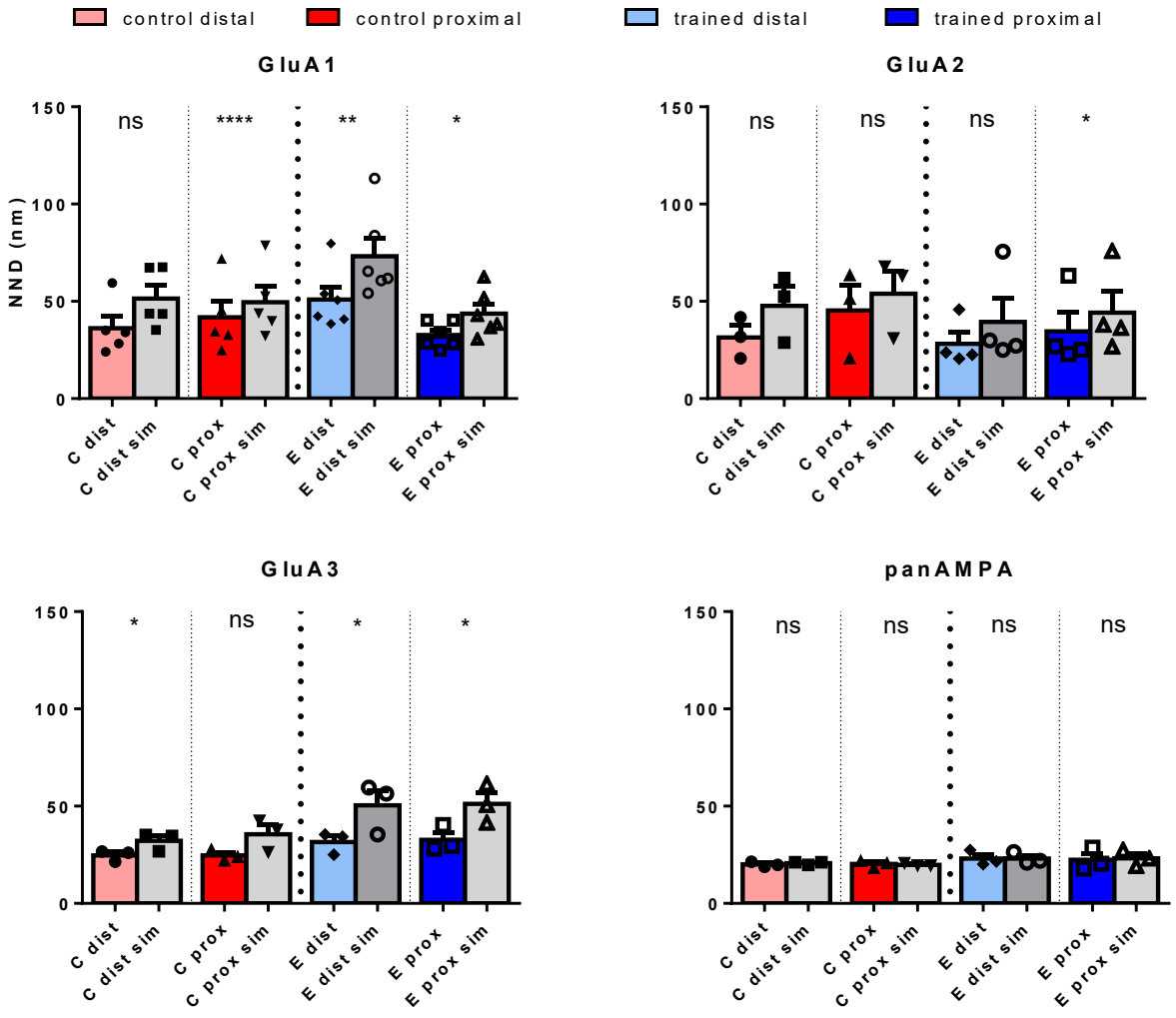

Figure 3.16. Nearest neighbour distance of particles in stratum radiatum. Detailed statistics can be found in Appendix.

caused by IA learning. Clusters were defined same as in 3.1., minimum number of particles to be included in the cluster was 3 and maximum distance was calculated as mean NND+ 2

standard deviations. I compared number of clusters, number of particles per cluster, cluster area and cluster CPI between control and trained animals and between distal and proximal stratum radiatum in CA1 area. Statistical analysis (one-way ANOVA) did not indicate any significant differences in any of the datasets, except GluA3. However, direct comparison of GluA1 labeling in proximal and distal radiatum in trained animals showed higher number of clusters ($p=0.008$, unpaired t-test), number of particles per cluster ($p=0.026$, unpaired t-test), cluster area ($p=0.049$, unpaired t-test) and lower cluster CPI ($p=0.045$, unpaired t-test) in proximal stratum radiatum in trained animals compared to distal stratum

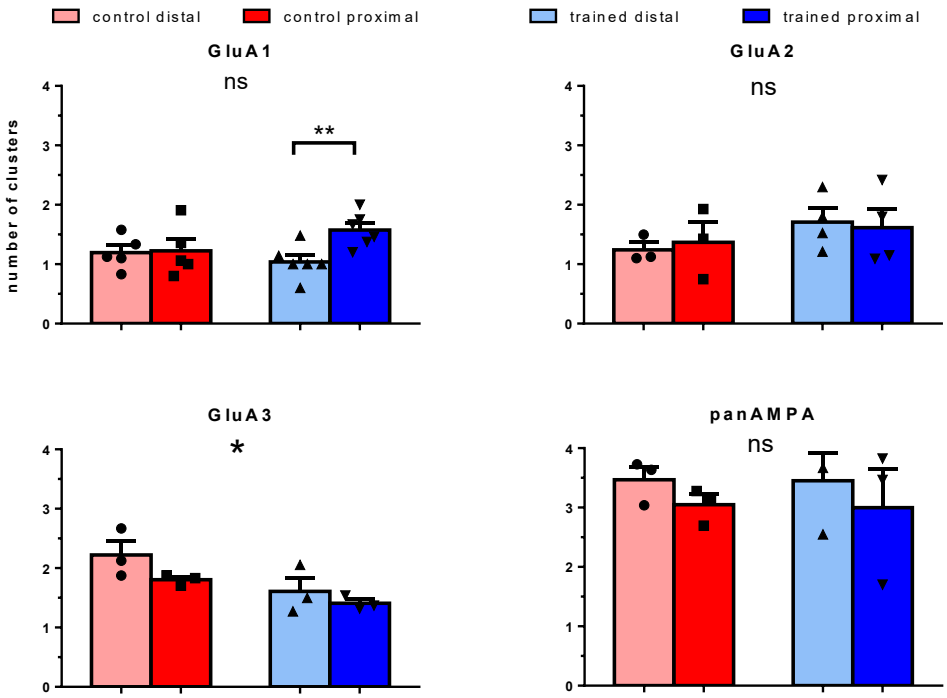

Figure 3.17. Number of clusters – stratum radiatum

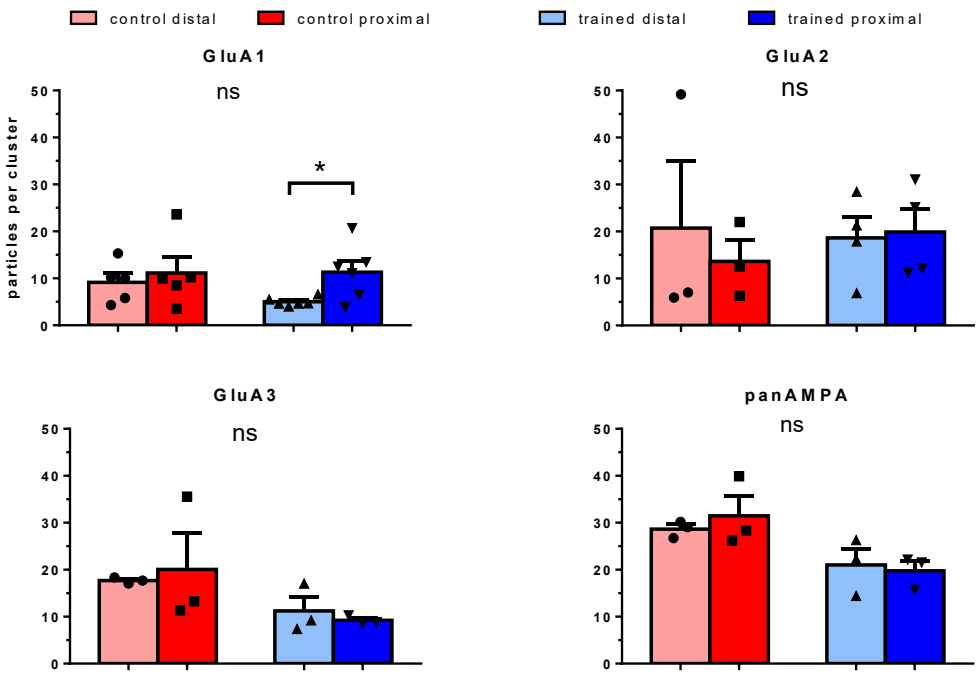

Figure 3.18. Number of particles per cluster – stratum radiatum

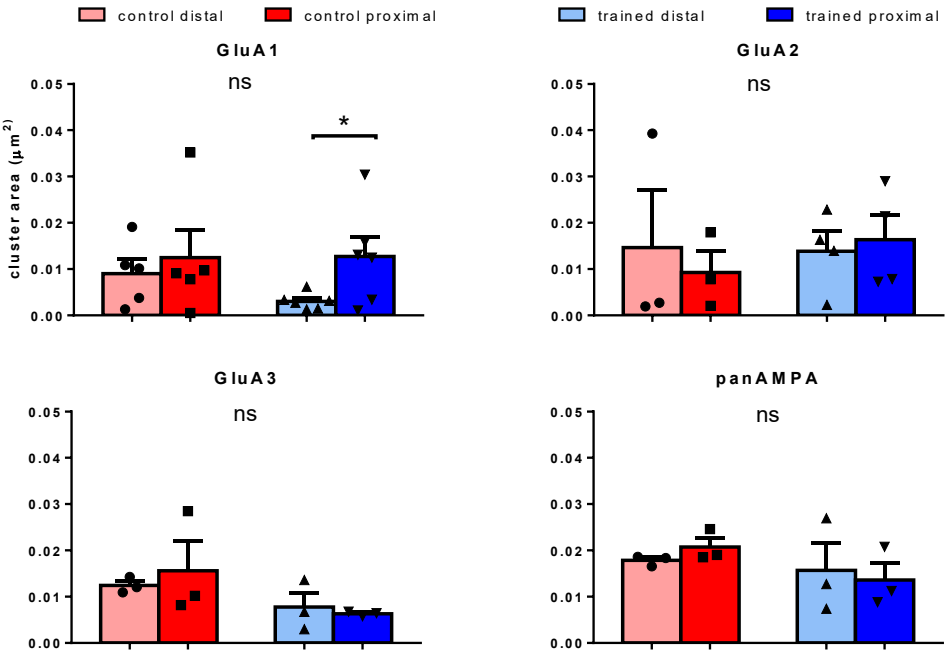

Figure 3.19. Cluster area – stratum radiatum

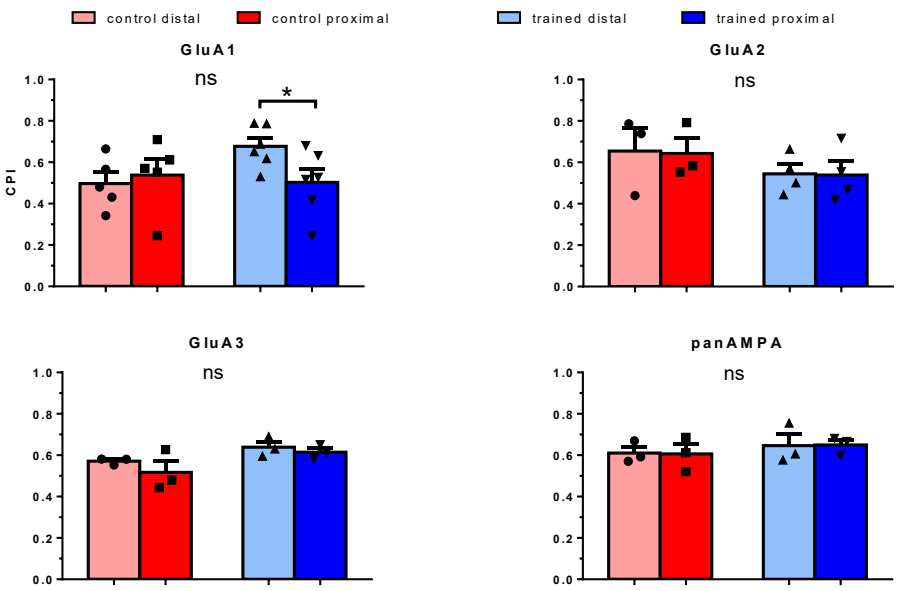

Figure 3.20. Cluster CPI – stratum radiatum

radiatum. Such difference could not be observed in control samples for GluA1 and both the control and trained samples for GluA2, GluA3 and panAMPA labeling.

3.2.3 AMPAR subunit changes after inhibitory avoidance training in stratum oriens of CA1

I also performed the same analysis on the images obtained from the stratum oriens in the CA1 area of the same samples. Analysis of labeling density did not show significant difference for any type of labeling between control and trained animals and between proximal and distal oriens. When directly comparing the proximal and distal oriens for the GluA1 labeling, there was a slight but significant increase in labeling density (Figure 3.21A, $p=0.046$, unpaired t-test) but this was not reflected in the analysis of P/D ratio (Figure 3.21B). Analysis of PSD area indicated a difference for GluA1 ($p=0.007$, one-way ANOVA) and GluA3 labeling ($p<0.0001$, one-way ANOVA, detailed statistics in the Appendix), however because of smaller sample size in oriens analysis, these results should be approached with caution.

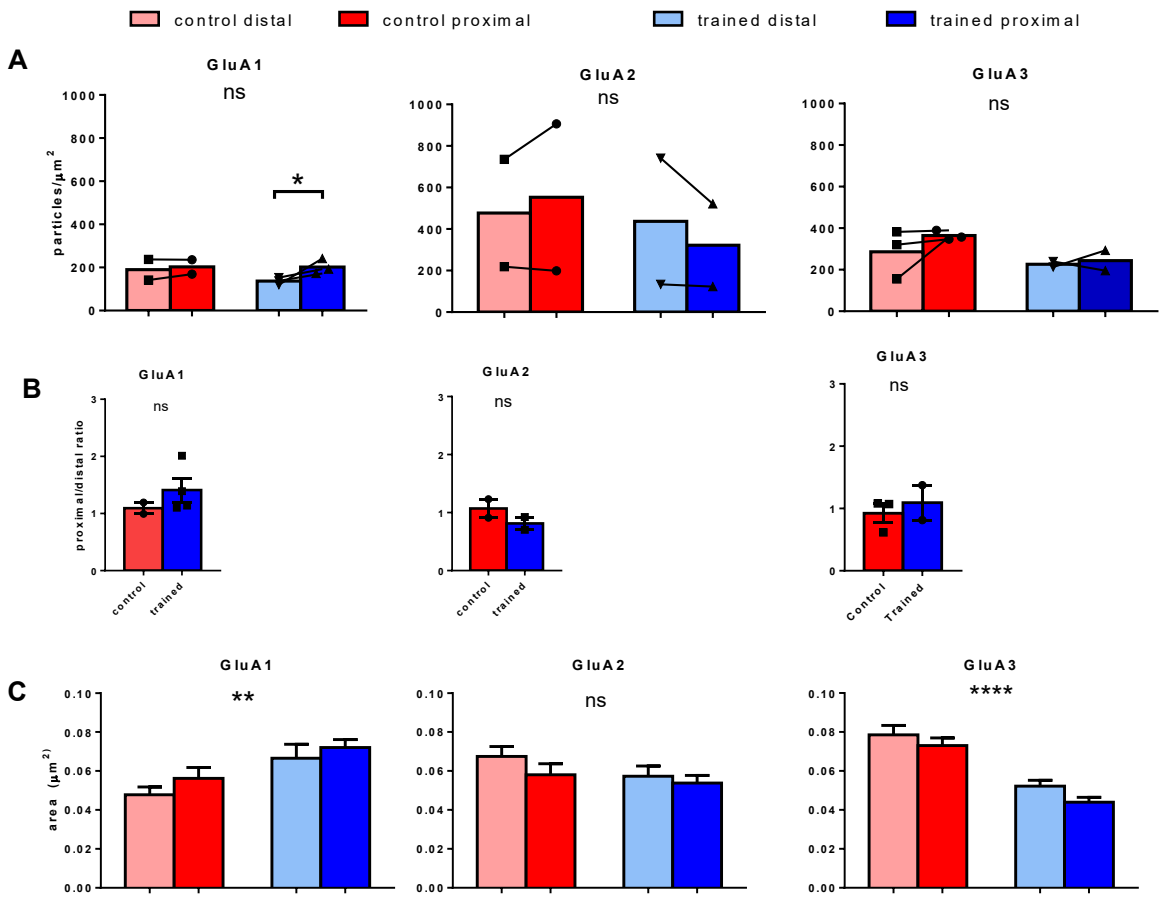

Figure 3.21.Labeling density and PSD area for AMPAR subunits in stratum oriens after IA learning (A) Comparison of observed labeling densities between control and trained animals in proximal and distal areas of CA1 oriens. (one-way ANOVA, ns) (B) Comparison of ratios of labeling density in proximal and distal area (P/D ratio) of CA1 stratum oriens between control and trained animals (C) Comparison of sampled PSD area in CA1 stratum radiatum (detailed statistics in the Appendix)

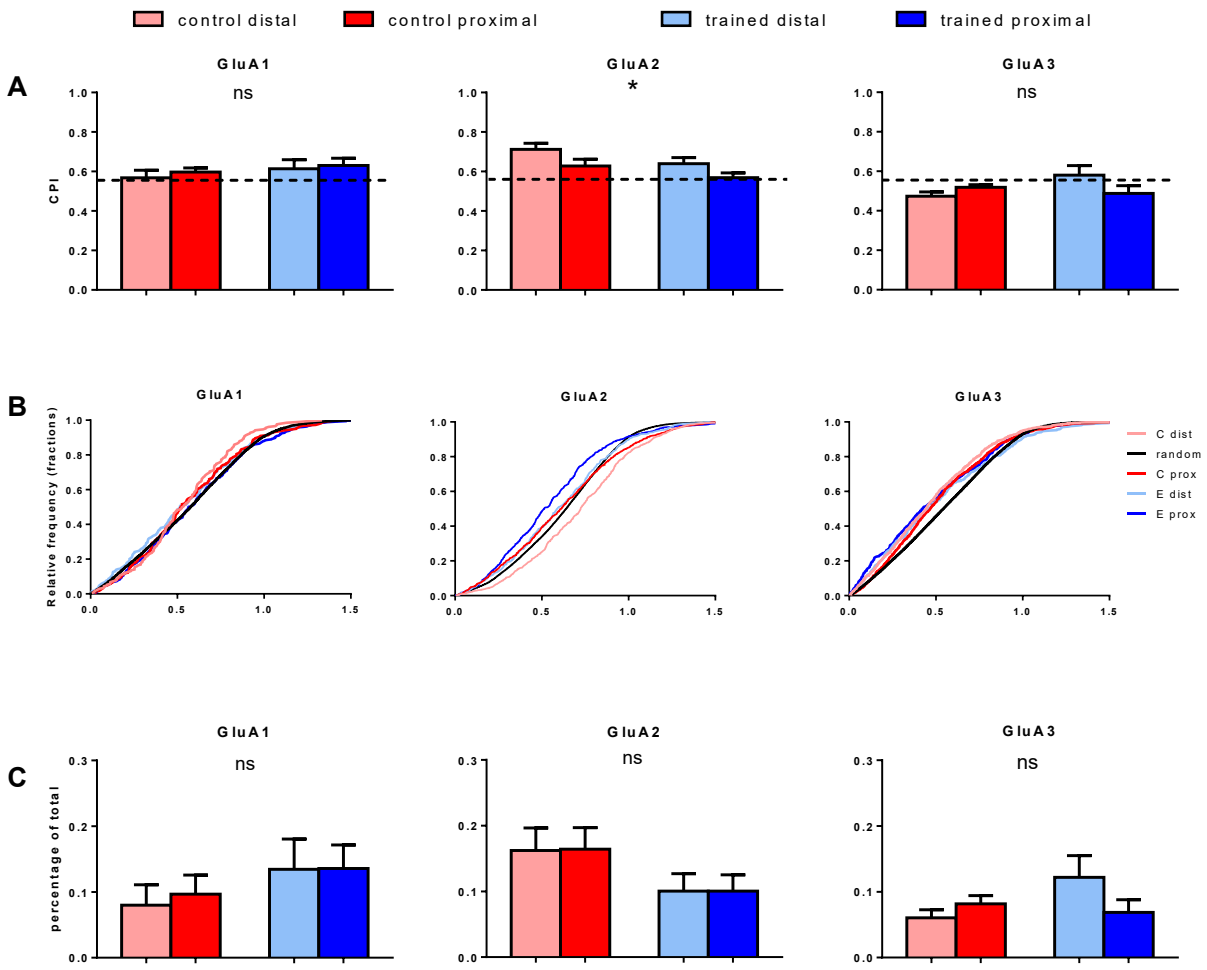

Figure 3.22. Center-periphery index analysis – stratum oriens. (A) Comparison of CPI means (GluA2, p=0.01, one-way ANOVA) (B) Comparison of CPI distribution between AMPAR subunits and random distribution simulated by DAREA. (C) Fraction of gold particle number observed in outer rim of PSD (one-way ANOVA, ns)

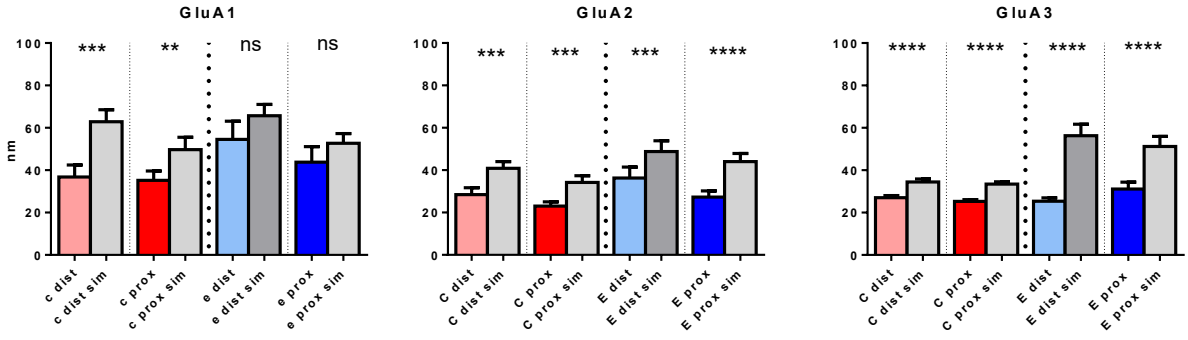

Figure 3.23. Nearest neighbour distance of particles in stratum oriens

Center-periphery analysis in stratum oriens did not indicate any changes caused by IA training in CPI means, CPI distribution and percentage of particles in the outer rim of synapses, except for CPI means for GluA2 ($p=0.01$, one-way ANOVA) (Figure 3.21)

I also analyzed possible clustering of AMPAR labeling in stratum oriens following IA training. Comparison of NND with random distribution of gold particles indicated strong difference in NND for all three AMPAR subunits (Figure 3.23, detailed statistics can be found in the Appendix), however subsequent clustering analysis indicated differences only in case of GluA3 (Figure 3.23), and suggested lower number of clusters ($p<0.0001$, one-way ANOVA), particles per cluster ($p=0.009$, one-way ANOVA) and cluster area ($p=0.013$, one-way ANOVA) in trained animals compared to the control. However, these results should be approached with caution due to smaller sample size compared to radiatum.

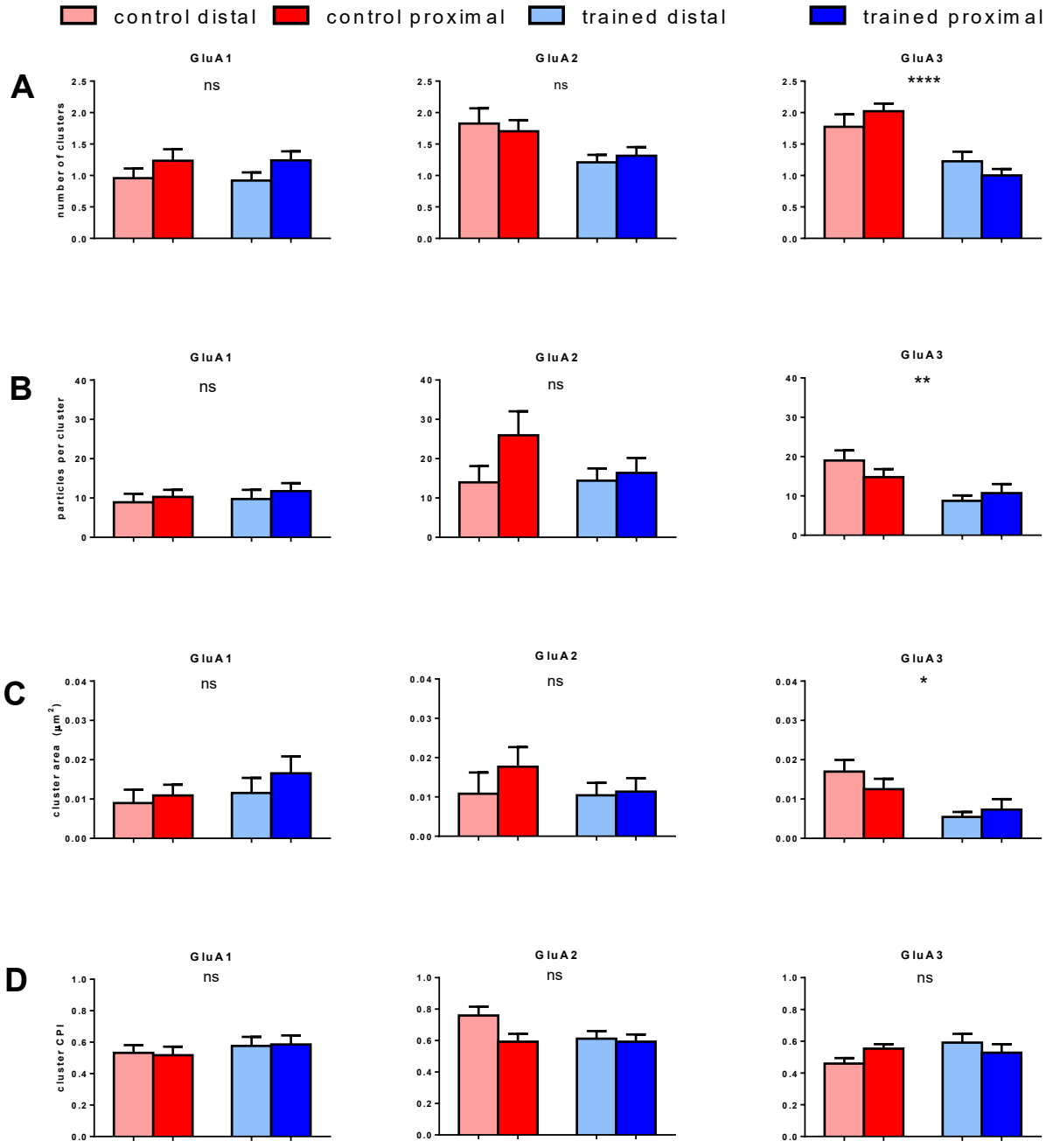

Figure 3.24.Clustering parameters – stratum oriens. Detailed statistics can be found in the Appendix.

3.3 Development of novel high resolution EM techniques for application on AMPA receptors

Results featured in part 3.3.1 were published under [77] and features contributions from Shigekazu Tabata, Nobutaka Kurashige, Hirokazu Fuchida, Munetsugu Kido, Kazushi Tani, Naoki Zenmyo, Shohei Uchinomiya, Harumi Harada, Makoto Itakura, Itaru Hamachi, Ryuichi Shigemoto and Akio Ojida.

3.3.1 Electron Microscopic Detection of Single Membrane Proteins by a Specific Chemical Labeling

We applied chemical labeling to EM detection in combination with sodium dodecyl sulfate (SDS)-digested freeze-fracture replica labeling (SDS-FRL) technique [95]. This technique is widely used to detect the two-dimensional distribution of membrane proteins on protoplasmic (P-) and exoplasmic (E) leaflet of lipid bilayer in freeze-fracture replicas [106]. We used chemical probe, which possesses a directly conjugated 1.4-nm nanogold particle to label helixD2-B2R-EGFP, and anti-FLAG antibody to label FLAG tag, which was inserted just next to the helixD2 tag in the extracellular domain of B2R (Figure 3.25A). Chemical probe was obtained by conjugation reaction of the amine probe with mono-sulfo-N-hydroxy-succinimide nanogold particles in HEPES buffer (pH 8.0), which was followed by dialysis to remove the excess of unconjugated probe**.** The labeling reaction of nanogold-conjugated chemical probe was conducted for an extended time (2 h, 37C) to fully label helixD2-B2R-EGFP expressed on HEK293 cells. To facilitate searching for E-face labeled with 1.4-nm gold particles by 200kV scanning transmission electron microscope (dark field mode), GluA2 subunit of AMPA glutamate receptor was co-expressed with helixD2-B2R-EGFP in HEK cells and labeled with 10-nm gold particles by an antibody for an extracellular epitope of GluA2 combined with anti-rabbit 10-nm gold particle-conjugated secondary antibody. On GluA2-labeled E-face, we found numerous 1.4-nm gold particles, often making high-density clusters of particles (3.25B and 5C). The specificity of the labeling was confirmed using HEK cells transfected with GluA2 but not with helixD2-B2R-EGFP (3.25B). The density of background labeling (5.9 particles/μm2) was 1.7% of the specific labeling (353 particles/μm2) (Figure 3.25H). In the immunogold labeling, the specific labeling by anti-FLAG tag antibody was observed on the E-

face with 5-nm particles (125 particles/μm2, n = 7 cells, Figure 3.25H), also showing clusters of particles (arrowheads in figure). The average density of B2R labeled with nanogold-conjugated chemical probe was 2.8 times higher than that with anti-FLAG antibody (Figure 3.25H, $p < 0.05$).

To compare the clusters of particles obtained with the chemical labeling and anti-FLAG immunolabeling, we first examined nearest neighbor distance (NND) distributions of particles and found sharper peak at smaller NND for the chemical labeling (8.6 G 10.8 nm, mean G SD, n = 1748 particles) than immunolabeling (47.4 G 56.1 nm, mean G SD, n = 998 particles, $p < 0.001$, Mann-Whitney U test) (Figure 3.25I). For defining the clusters, we fitted these peaks with Gaussian distribution and used mean + 2 SD as maximum distances allowed and three particles per cluster as a minimum number of particles per cluster [107]. In case we use definition of clusters with different mean + 2 SD values for chemical labeling (12 nm) and immunolabeling (42 nm), the numbers of particles per cluster were similar (Figure 3.25J) but the cluster area was much smaller for chemical labeling (70 nm2) than for immunolabeling (950 nm2, Figure 3.25K), indicating that the clusters detected by chemical labeling represent subclusters consisting single clusters detected by immunolabeling. In case we use the same definition of clusters obtained by immunolabeling for both (42 nm as a maximum distance allowed), the cluster areas became similar and the number of particles per cluster was twice higher for chemical labeling than for immunolabeling (9.4 G 1.4 particles, n = 10 cells for chemical labeling, 4.5 G 0.3 particles, n = 7 cells for immunolabeling, mean G SE, $p < 0.01$, Mann-Whitney U test, Figures 3.25J and 3.25K). Altogether, these results indicate higher labeling efficiency and detectability of high-density nanoclusters of proteins for chemical labeling with the probe directly conjugated with 1.4-nm nanogold particle than the immunolabeling with 5-nm gold-particle-conjugated secondary antibody.

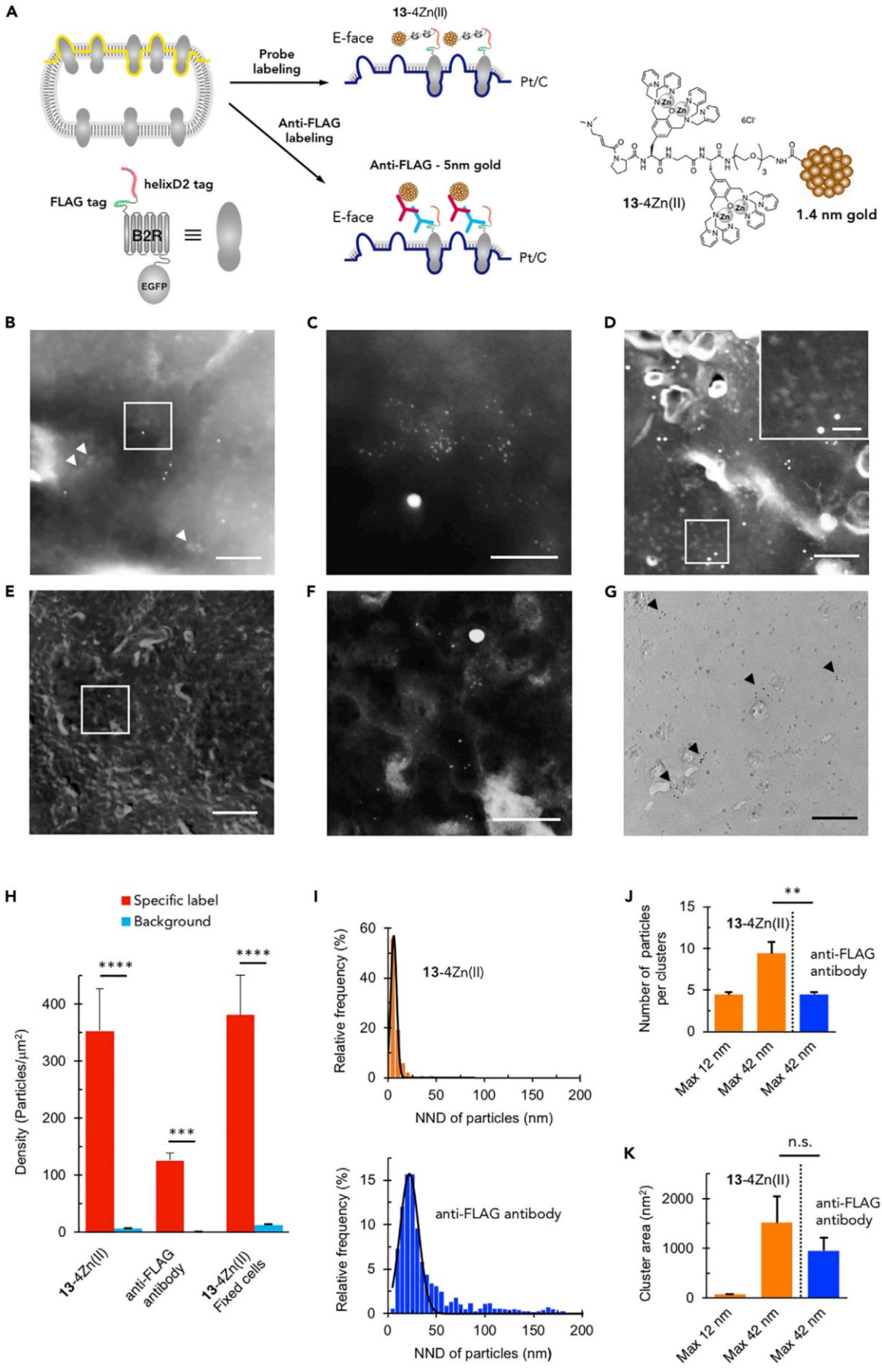
A
13-4Zn(II)
E-face
Probe labeling
Pt/C
Anti-FLAG labeling
Anti-FLAG - 5nm gold
E-face
Pt/C
FLAG tag
helixD2 tag
B2R
EGFP
13-4Zn(II)
1.4 nm gold
B
C
D
E
F
G
H
Specific label
Background
Density (Particles/μm²)
****
***
****
13-4Zn(II)
anti-FLAG antibody
13-4Zn(II) Fixed cells
I
Relative frequency (%)
13-4Zn(II)
NND of particles (nm)
Relative frequency (%)
anti-FLAG antibody
NND of particles (nm)
J
**
Number of particles per clusters
13-4Zn(II)
anti-FLAG antibody
Max 12 nm
Max 42 nm
Max 42 nm
K
n.s.
Cluster area (nm²)
13-4Zn(II)
anti-FLAG antibody
Max 12 nm
Max 42 nm
Max 42 nm

Figure 3.25. EM Detection of helixD2-Tag-Fused B2R Protein on HEK Cells Using the Probe Conjugated with a1.4-nm Gold Particle.

(A) Schematic illustration of labeling states of replicas
(B–D) Dark-field scanning transmission electron microscopy images of E-face replicas made from transfected (B and C) or non-transfected (D) HEK cells labeled with 13-4Zn(II) before aldehyde fixation.
(C) and the inset on (D) are magnified images of the area framed in (B) and (D), respectively. White arrowheads indicate B2R clusters labeled with 13-4Zn(II). Scale bar: 200 nm in (B) and the main picture of (D) and 50 nm in (C) and the inset on (D).
(E and F) Dark-field images of replicas made from transfected HEK cells labeled with 13-4Zn(II) after aldehyde fixation.
(F) A magnified image of the area framed in (E). Scale bar: 200 nm in (E) and 50 nm in (F).
(G) Bright-field TEM image of E-face replica labeled with anti-FLAG antibody combined with 5-nm gold-particle conjugated secondary antibody. Black arrowheads indicate B2R clusters labeled with 5-nm gold particles. Scale bar, 200 nm.
(H) Comparison of the specific and background labeling density with 13-4Zn(II) and anti-FLAG antibody. ‘‘13-4Zn(II)’’ and ‘‘13-4Zn(II), fixed cells’’ indicate results from HEK cells labeled before and after aldehyde fixation, respectively (13-4Zn(II), ****$p < 0.001$, Mann-Whitney U test; specific labeling, n = 9 cells; background labeling, n = 13 cells; mean G SE, anti-FLAG, ***$p < 0.005$, Mann-Whitney U test; specific labeling, n = 7 cells; background labeling, n = 7 cells; mean G SE, 13-4Zn(II), fixed cells, ****$p < 0.001$, Mann-Whitney U test; specific labeling, n = 11 cells; background labeling, n = 15 cells; mean G SE).
(I) Distribution histograms of nearest neighbor distance (NND) of gold particles observed on replicas labeled with 13-Zn(II) (upper, n = 1748 particles) and anti-FLAG antibody (bottom, n = 998 particles). Fitted lines show Gaussian distribution fitting for the peaks.
(J) Comparison of the number of particles per B2R cluster labeled with 13-4Zn(II) and anti-FLAG antibody. ‘‘Max 12 nm’’ and ‘‘Max 42 nm’’ mean the maximum NND of gold particles used for the definition of clusters labeled with 13-4Zn(II) and anti-FLAG antibody (13-4Zn(II) Max 12 nm; n = 10 cells, 13-4Zn(II) Max 42 nm, n = 10 cells; anti-FLAG Max 42 nm, n = 7 cells, mean ± SE, **$p < 0.01$, Mann-Whitney U test).
(K) Comparison of the B2R cluster area evaluated by chemical labeling with 13-4Zn(II) and immunolabeling with anti-FLAG antibody (13-4Zn(II) Max 12 nm; n = 10 cells; 13-4Zn(II) Max 42 nm, n = 10 cells; anti-FLAG 42 nm, n = 7 cells; mean G SE, n.s. $p > 0.05$, Mann-Whitney U test)

In typical SDS-FRL experiment, biological samples, such as sliced tissue, are initially fixed with aldehyde to maintain protein location by physical stabilization [96]. Therefore, we next applied the chemical labeling to the fixed cell samples. HEK293 cells expressing helixD2-B2R-EGFP were first fixed with 2% paraformaldehyde and then labeled with gold-conjugated chemical probe. We found specific labeling for helixD2-B2R-EGFP with the fixed cells comparable with that obtained with living cells (Figures 3.25E, 3.25F, and 3.25H). This was indicative of the compatibility of the developed chemical labeling with aldehyde fixation. Since the majority of the existing enzyme-mediated and ligand-directed protein labeling methods [109,108] are difficult to apply to denatured proteins by fixation, these results demonstrated the high utility of the chemical labeling method for SDS-FRL using fixed biological samples.

3.3.2 EM Detection of Tag-Fused Protein Using Nanogold-Conjugated Probes in Ultrathin Section

To further confirm higher resolution of the chemical labeling using gold-conjugated chemical probe, we performed EM analysis of ultrathin sections of resin-embedded HEK293 cells. We compared the distances from the silver-intensified 1.4-nm gold particles to cell membrane between the samples labeled by nanogold-conjugated chemical probe and those labeled by anti-FLAG antibody combined with 1.4-nm gold-particle-conjugated secondary antibody (Figures 3.26A and 3.26C). The background density of particles examined in non-transfected cells was 0.8% and 0.6% of the specific labeling by nanogold-conjugated chemical probe and anti-FLAG antibody, respectively. The silver-intensified gold particles appeared to be mostly attached to the cell membrane in the chemical labeling (Figure 3.26B), whereas those in the FLAG immunolabeling showed apparent gaps between the particles and the cell membrane (Figure 3.26D). Considering that silver intensification may occur in a non-isotropic/concentric manner around 1.4-nm gold particles, we used minimum time (3–6 min) for silver intensification and examined the correlation of the size of silver-intensified particles and the distance between the center of silver-intensified particles and the midpoint of lipid bilayer (Figure 3.26E). We found a significant positive correlation for both chemical labeling ($r_s = 0.24$, $p < 0.01$, $n = 147$ particles) and immunolabeling ($r_s = 0.26$, $p < 0.01$, $n = 228$ particles). By extrapolating linear fits, estimated distances of non-intensified 1.4-nm particles were calculated to be 5.4 nm and 9.9 nm for chemical labeling and immunolabeling, respectively. Since the half thickness of lipid bilayer was estimated to be 4 nm by EM analysis [110], the distance of 1.4-nm gold particles from the cell surface was deduced to be 1.4 and 5.9 nm for the chemical labeling and immunolabeling, respectively (Figure 3.26E). Although direct comparison of the distances from these labels to the respective tags is not possible because the exact tag positions are unknown, the variance of the measured distances is significantly smaller for nanogold-conjugated chemical probe than for anti-FLAG antibody ($F_{227, 146} = 2.0$, $p < 0.001$), indicating higher resolution of the chemical labeling method than the immunolabeling method (Figure 3.26F).

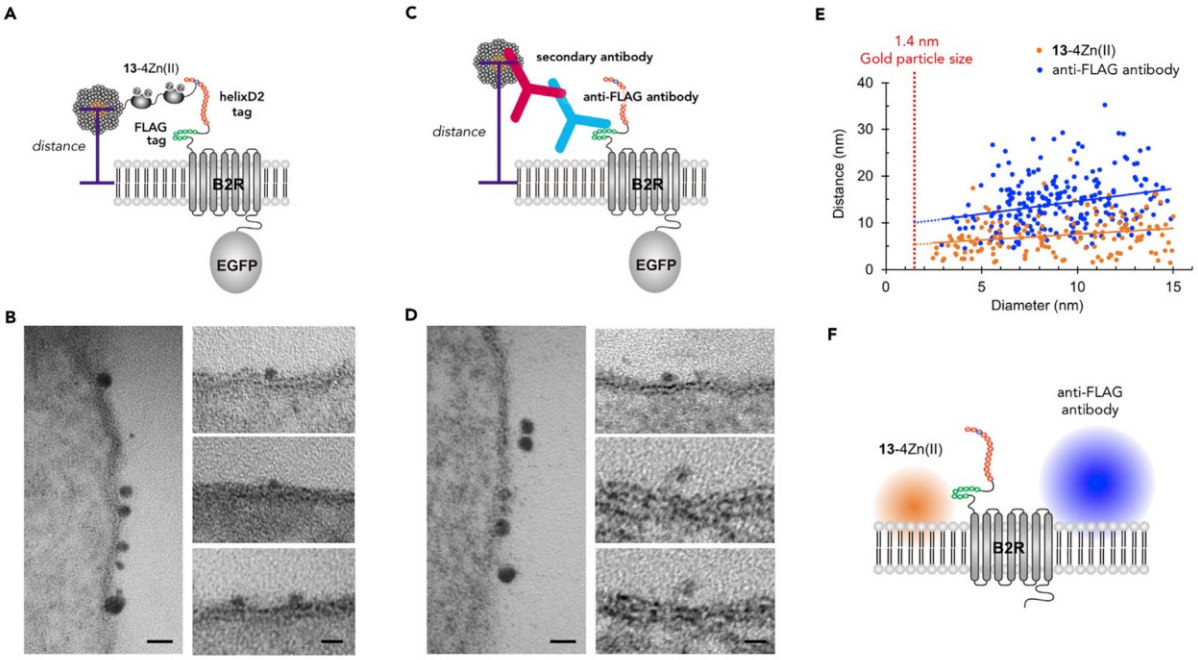

Figure 3.26. Comparison of Resolution between Chemical Labeling and Immunolabeling Methods

(A and C) Schematic illustration of labeling states of the tagged-B2R on HEK cells labeled with 13-4Zn(II) (A) and anti-FLAG antibody combined with 1.4-nm gold-particle-conjugated secondary antibody (C).
(B and D) EM images of ultrathin sections prepared from HEK cells labeled with 13-4Zn(II) (B) and anti-FLAG antibody (D), respectively. Gold particles were intensified by silver enhancement for 3–6 min. Distances between the particle center and the middle of the cell membrane were measured in sections tilted to obtain perpendicular views to the plasma membrane. Scale bars, 20 nm (left) and 10 nm (right).
(E) Correlation of the intensified particle size and distance between particle centers and the middle of the cell membrane (orange dots, 13-4Zn(II); blue dots,anti-FLAG antibody). Significant positive correlation was detected for both (correlation coefficient = 0.24, $p < 0.01$, $n = 147$ for 13-4Zn(II); correlation coefficient = 0.26, $p < 0.01$, $n = 228$ for anti-FLAG antibody, Pearson correlation analysis). The distances for non-intensified 1.4-nm particles were deduced from linear fits extrapolated (broken orange and blue lines) to 1.4 nm (red dotted line).
(F) Schematic illustration of positions of non-intensified 1.4-nm particles estimated by the two labeling methods in (E). The gradient circle indicates the deviation of the position.

3.3.3 Design of tagged AMPAR subunits for labeling with specific chemical and immunolabeling using nanobodies

I wanted to achieve higher labeling resolution in EM by utilizing some of the novel labeling approaches which use smaller labeling reagents than traditional antibody-based approaches. However, all of these novel labeling approaches are based on the interaction of a short peptide tag and labeling reagent (chemical probe or nanobody). So, in order to achieve this goal, it was necessary to genetically replace native AMPAR subunits with tagged ones. While doing this, it was necessary to verify that insertion of a short peptide tag at specific

location in the endogenous AMPAR subunit sequence is not going to interfere with natural expression, folding, trafficking and functionality of the AMPA receptors. Also, it was necessary to verify that the peptide tag is accessible enough to be labeled easily and with high efficiency.

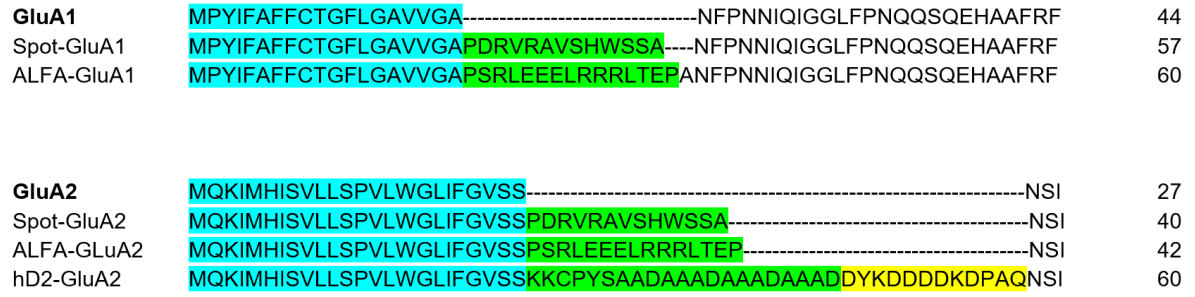

Figure 3.27. Amino acid sequence of the GluA1 and GluA2 proteins with peptide tags inserted in the N-Terminus, right after the signal peptide. Signal peptide is indicated with blue letters, peptide-tag sequence in green and linker sequence in yellow.

I attempted to insert hD2-tag (amino acid sequence as follows: KKCPYSAADAAADAAADAAAD), Spot-tag (PDRVRAVSHWSS) and ALFA-tag (SRLEEELRRRLTE) into several locations in the GRIA1 and GRIA2 genes in order to achieve above-described goal. Some of the initial attempts were not satisfactory because of low labeling efficiency or lethal phenotype of the transgenic animal. Thus, I performed further optimization of either tag-insertion location or linker sequence separating the tag from the rest of the sequence (not shown). Most successful tag insertion location proved to be in the N-termini of both GluA1 and GluA2 proteins, right after the signal peptide (signal peptide amino acid sequence for GluA1: MPYIFAFFCTGFLGAVVG, GluA2: MQKIMHISVLLSPVLWGLIFGVSS) (Figure 3.27). These constructs were initially designed in the plasmids suitable for expression in HEK cells culture but subsequently AAV viral vectors for application in neuronal cultures or stereotaxic injections into mouse brain were also made.

After successful verification of proper expression and labeling in the *in vitro* and *in vivo* systems (Figure 3.28), I proceeded to generate transgenic animals which would have tagged AMPAR subunits expressed endogenously. Transgenic lines with tagged subunits as indicated in Figure 3.27 are either ready for experiments or in various phases of completion, however, the final goal, which is to utilize these tagging systems for the electron microscopy to achieve higher labeling efficiency and spatial resolution, is still hindered, mainly due to lack

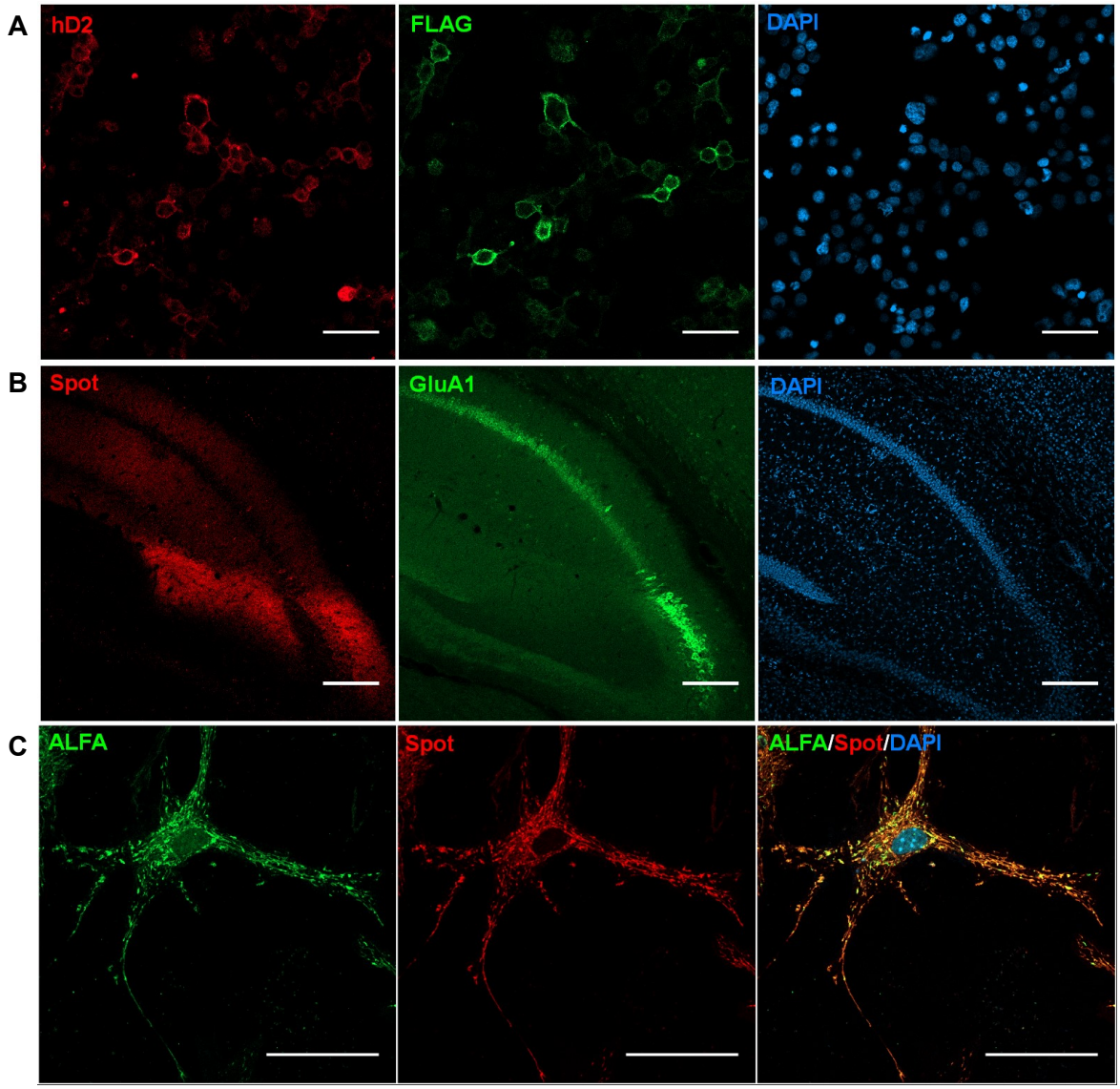

Figure 3.28. Expression and labeling of the tagged AMPAR subunits in different in vitro and in vivo conditions. (A) hD2-GluA2 expressed in HEK cells, labeled with biotinylated chemical probe followed by streptavidin AlexaFluor-647. Additional labeling with anti-Flag antibody coupled with AlexaFluor-488 revealed colocalization of immuno- and chemical labeling and proper membrane expression of the tagged GluA2 subunit. (B) Expression of AAV encoding Spot-GluA1 in vivo after stereotaxic injection and colocalization of Spot labeling (red) and GluA1 immunolabeling (green) (C) Coexpression of Spot-GluA1 and ALFA-GluA2 in the hippocampal neuron culture and first example of successful double labeling of tagged AMPAR subunits expressed in the same cells. (ALFA-GluA2 – green, Spot-GluA1 – red)

of EM-suitable nanobodies and chemical probes at this very moment. Conjugation of these labeling reagents with gold particles which is required for successful and meaningful EM utilization is also an ongoing work in progress, but it is beyond the scope of this thesis.

4 DISCUSSION

In this study I investigated detailed distribution of AMPA receptor subtypes (GluA1-, GluA2- and GluA3-containing) CA1 subregion of mouse hippocampus using SDS-FRL, the most sensitive imaging method to study high-resolution two-dimensional distribution of transmembrane proteins, in combination with highly specific antibodies for subunits for AMPA receptors. With this approach I aimed to reveal special rules of AMPA receptor distribution and synaptic organization along with its potential effect on basal synaptic transmission and synaptic plasticity.

First, I investigated the AMPAR distribution in different layers of the CA1 area of CA1 by labeling the endogenous AMPAR subunits and quantifying their densities in membranes of various extrasynaptic (somata, apical and basal dendrites) and synaptic sites, followed by detailed intrasynaptic distribution analysis performed specifically on CA3-CA1 synapses in stratum radiatum. Next thing was to investigate how AMPA receptor distribution and synaptic organization might change during learning-induced plasticity by combining inhibitory avoidance behavioral task with SDS-FRL. I investigated synaptic AMPAR labeling across the wider CA1 area, more precisely along the proximodistal axis and in strata radiatum and oriens.

Finally, even though I used AMPAR subunit antibodies which are highly specific and sensitive, direct observation of subunit composition of AMPA receptors at the single channel level is hampered by inherent limitation of using antibodies due to their large size. Therefore, I attempted to develop a novel approach for higher labeling resolution to label multiple subunits in single AMPA receptors.

4.1 Distribution of AMPAR labeling in pyramidal neurons of hippocampal CA1 area

I have found the highest density of AMPAR subunits in stratum radiatum, followed by stratum oriens and stratum lacunosum moleculare and lowest in stratum pyramidale (membrane on the cell bodies). This distribution was common for all subunits and it was similar for both synaptic and extrasynaptic densities (with exception of synaptic labeling on cell bodies). Labeling density for GluA2 and panAMPA (which labels all of GluA1-3) were similar which

would indicate presence of the GluA2 subunit in all of the labeled AMPAR. Labeling density for GluA1 and GluA3 were similar in the synapses and approximately half of the density observed for GluA2 and panAMPA. Assuming similar labeling efficiency of these antibodies, this result would indicate that the AMPAR in the synapses were composed of 50% GluA1-GluA2 and 50% GluA2-GluA3 heteromers. Previous reports based on proteomic and genetic analyses have indicated that GluA3-containing receptors represent only 20% of total AMPAR pool in the hippocampal membranes [115, 116]. In my study, GluA3-containing AMPAR had significantly lower density in the extrasynaptic areas (dendrites and soma), around 20-30% compared to GluA2 and panAMPA labeling density. These results are consistent with the previous studies, considering that extrasynaptic sites occupy ~99% of the plasma membrane ($\frac{99\times0.2+1\times0.5}{99\times0.8+1\times0.5} = 25.5\%$). This difference in the density of GluA3-containing receptors in synaptic and extrasynaptic compartments points toward different mechanisms and ways of delivering these receptors into the membranes. GluA3-containing receptors were also less associated with the IMP clusters on cell bodies of CA1 pyramidal neurons. Although precise role and protein content of these IMP clusters is not yet clear [96], it is possible that these clusters harbor some of the proteins that interact with c-termini of AMPAR receptors and serve as extrasynaptic pools of AMPAR receptors, sites of AMPAR exocytosis or both. GluA3 subunit of AMPAR indeed has a short intracellular c-tail which is different from the GluA1 subunit and possibly does not interact with the proteins contained in the observed IMP clusters [115,11]. That would mean that GluA3-containing receptors would go through some different pathway for delivery into the synapses than GluA1-containing receptors. Higher content of overall AMPAR in stratum radiatum compared to stratum oriens and lacunosum moleculare may indicate higher number of exocytosis sites and/or extracellular pools of AMPAR for insertion into the synapses following plasticity events. It would be interesting to check whether the density of IMP clusters follows the gradient of extrasynaptic AMPAR subunit density along the apical dendrites in the stratum radiatum of CA1. Discrepancy between numbers of GluA3-containing receptors in synapses and extrasynaptic membranes compared to GluA1- and GluA2-containing receptors raises question of subunit composition of AMPAR receptors in extrasynaptic membranes. One recent publication indicated that the AMPAR in the extrasynaptic membranes do not exist as fully formed tetramers, and that the extrasynaptic pool of AMPAR could be composed of subunit monomers, dimers and trimers in addition to tetramers, [117], however best and direct proof for this point would be direct visualization by novel approaches of subunit composition high resolution labeling, as one of my aims was.

I then investigated intrasynaptic distribution of AMPAR subunits, in particular center-periphery preference of AMPAR subunit labeling and clustering. I simulated the same number of particles randomly distributed in the same PSD areas and compared the real data with the simulation. GluA1, GluA2 and panAMPA distribution showed stronger preference towards periphery of the synapse, together with higher number of particles in outer rim. This was consistent with previous reports on the periphery preference of AMPA receptors [118]. In contrast, GluA3 was concentrated more centrally, with fewer particles in the outer rim. However, outer rim analysis results should be approached carefully because it refers to the area 30 nm away from the synapse, which is primarily searched for the existence of intrasynaptic receptors that are detected outside of the PSD area due to limitations of antibody labeling. It's possible that this area contains not only gold particles associated with receptors located inside of PSD area but also some receptors which are actually contained in this area and serve as perisynaptic pool of reserve receptors to be inserted into the synapse upon plasticity induction. However, this cannot be directly shown or proven with the current methodology and requires the higher labeling resolution so it could be pursued additionally in the future. In any case, GluA1, GluA2 and panAMPA labeling has shown higher presence of particles in this area compared to GluA3. This further supports the possibility for GluA3-containing receptors to have different pathways of synapse delivery which does not necessarily require lateral diffusion, but direct insertion into the synaptic sites [120]. Overall, I couldn't detect clustering of AMPA receptors when looking at panAMPA or GluA2 labeling but there were some tendencies in clustering of GluA1- and GluA3-containing receptors. GluA3 labeling showed fewer number of clusters, more particles per cluster, larger cluster area and lower cluster CPI compared to both GluA1 results and simulation. These results indicate possible arrangement of GluA3-containing receptors in one or more larger clusters which are more centrally localized, while GluA1-containing clusters are more peripherally located in several smaller clusters. GluA2 and panAMPA labeling did not show any clustering but it is possible that the high labeling density and deviation of gold particle detection sites from the epitopes merges clusters, making them more difficult to properly detect and quantify clustering. Since GluA2 is present in all AMPA receptors, this might be additionally masking the detection of clustering properties when labeling was performed for GluA2 or panAMPA.

Physiologically, higher peripheral GluA1 density would indicate involvement of GluA1-containing receptors in the synaptic plasticity via lateral diffusion, whereas higher central GluA3-containing receptors would be more involved in the basal neurotransmission, as suggested in previous literature [115]. I could not detect clusters of GluA2 which would

indicate the existence of transsynaptic nanocolumns, as suggested previously [44]. This difference could be explained by different preparations of samples (*in vitro* vs *in vivo*), AMPAR labeling method (different antibodies and EM vs LM) or cluster detection method used to detect such structures. It is possible that only GluA1-GluA2 AMPAR are organized in nanocolumns but high labeling efficiency of SDS-FRL approach and high labeling density of GluA2 labeling is making it difficult to detect such structures, when intermixed with GluA2-GluA3 heteromers.

4.2 Learning induced changes in number and distribution of AMPAR subunit labeling in CA1 synapses

I was also interested to see how synaptic plasticity affects the above-described molecular distribution of AMPA receptors; i.e., whether any changes occur, what kind of changes and where those changes are located. With all this in mind, I induced physiological learning in a form of inhibitory avoidance training on wild type adult mice because of its simplicity of the learning induction protocol, strong memory formation and previous evidence of AMPAR receptor changes in the specific subregions of hippocampus induced by this protocol [62,72,73]. I combined this with the same EM approach described above to analyze changes along the proximo-distal axis of the CA1 region of hippocampus (proximal refering to proximity to CA2), and in stratum oriens and stratum radiatum. Observed differences in labeling density for GluA1 and GluA2 indicated an increase of GluA1-containing receptors after learning in the proximal part of CA1 stratum radiatum together with subtle decrease in GluA2-containing receptors, also localized in proximal radiatum in trained animals only. Because such differences could not be observed for GluA3 and panAMPA, overall density of AMPA receptors does not seem to be influenced by the learning, at least in the initial stages. This seems inconsistent with the recent electrophysiological study which reported an increased ratio of AMPA/NMDA currents in the proximal CA1 stratum radiatum after IA training [72]. However, the reported increase in the AMPA/NMDA ratio does not necessarily indicate increased overall number of synaptic AMPA receptors. Increased conductance of AMPA receptors (which was reported to be the main contributor of the increased AMPA/NMDA ratio) due to changes in subunit composition of AMPAR, rearrangement of synaptic AMPAR distribution, or both could also be the reasons for the increased AMPA/NMDA ratio. It is known that the homomeric GluA1-containing AMPAR have larger single channel conductance

compared to the GluA2-containing AMPAR [126]. The observed differences in the ratios of labeling densities between proximal and distal stratum radiatum for GluA1, GluA2 and panAMPA might indicate change in subunit composition of AMPA receptors in the initial stages of learning induced synaptic plasticity in CA3-CA1 synapses in proximal stratum radiatum. This may be driven by an influx of homomeric GluA1-containing receptors and possible decrease in the number of GluA1-GluA2 heterotetramers. Although never investigated at nanoscale after the physiological learning, such change has been demonstrated previously using electrical stimulation on acute slice preparation and it presents the current consensus about the timeline of LTP in its initial phases [11,48,121]. Total density of panAMPA labeling is expected to be higher in trained animals compared to control or at least in the proximal stratum radiatum compared to distal stratum radiatum in trained animals only, but this was not the case. Perhaps the difference was too subtle to successfully be detected with our approach. Such difference was not noticed in untrained animals or in trained animal for the GluA3 labeling, which further confirms absence of the GluA3-containing AMPA receptor involvement in synaptic plasticity, at least at CA3-CA1 synapses after physiological learning [115]. Differences in sampled PSD size could be explained in several ways: either the sampling of the synapses was not uniform and representative or there are some different population of synapses which are differently enriched with GluA1-containing receptors. We did not perform double labeling for different AMPAR subunits simultanously due to lack of suitable antibodies (all used antibodies were produced in same animal) but it would be interesting to explore this point further.

Intrasynaptic analysis has shown additionally some rearrangement in the localization of AMPA receptors after learning, in the form of decreased center-periphery index (CPI) of GluA1-containing receptors compared with untrained control only in proximal radiatum of trained animals. It is possible that in the initial stages of learning-induced LTP some rearrangement of the existing receptors takes place in order to enhance the response to the increased firing of the presynaptic neurons, rather than simply adding the new receptors into the postsynaptic membrane. This is consistent with the studies that suggest that more precise alignment of the AMPA receptors with vesicle release machinery can influence glutamate response more than increased number of AMPA receptors, due to their low affinity for the glutamate [45]. It has been demonstrated earlier that AMPAR overexpression does not lead to increased EPSC [21] and that preventing exocytosis of AMPAR does not block the first phase of synaptic potentiation, which also indicated reorganization [40]. The idea that the subunit composition is also changed (from GluA1-GluA2 heteromers to GluA1 homomers, which have

higher conductance) also fits this interpretation. This effect could not be observed for the panAMPA, possibly due to high labeling density and mixture with GluA3 labeling which could mask the detection of such rearrangement if it is only confined to the GluA1- and GluA2-containing receptors. Absence of any detectable effect of learning on the arrangement of the GluA3-containing receptors indicates lesser involvement of these receptors in the synaptic plasticity, as suggested before [115].

Clustering analysis has further confirmed the possible rearrangement of the AMPA receptors within the synapse as a possible effect of learning-induced plasticity, even though this effect was only detected for GluA1 labeling. Increased number of detected clusters, particles per cluster and cluster area only for GluA1-containing receptors might indicate that the newly inserted GluA1 homomers accumulate in the areas more precisely aligned to the presynaptic vesicle release sites and not randomly within the synapse. Such effect could not be detected for the GluA2 labeling which might indicate that either only GluA1-containing receptors are involved in these clustering changes or that such changes are too subtle to be detected on the level of GluA2 labeling. Once again, GluA3-containing receptors did not show any changes as an effect of IA training induced plasticity in the proximal stratum radiatum of CA1 area in mouse hippocampus.

I also investigated the changes of AMPAR subunit labeling in stratum oriens following the IA-training induced plasticity and the results from stratum oriens did not replicate the findings from the stratum radiatum regarding GluA1 and GluA2 labeling. However, I did find some difference in the samples labeled for GluA3 which were reflected in the fewer number of clusters, less particles per cluster and smaller cluster area which were detected only in trained animals (both proximal and distal oriens) and not in untrained animals. It has been shown previously that LTP in cerebellar Purkinje neurons [124] and hippocampal pyramidal cells [125] can be mediated by GluA3-containing AMPAR by increasing the open probability of these receptors through a cAMP-dependent pathway. Due to smaller sample size in analysis of stratum oriens these results should be approached carefully but it may be interesting to inspect this point further by increasing the number of animals analyzed.

Taken together, results for stratum radiatum may point out to a model in which learning-induced plasticity in the hippocampal CA3-CA1 synapses is mediated by a subunit composition change in those synapses by decreasing number of GluA1-GluA2 heteromers while increasing number of the GluA1 homomers, as reflected in the increase of the GluA1, decrease of GluA2, and no changes in panAMPA labeling density. This fits previously described models which were obtained from acute slice preparation and high frequency electrical stimulations [11, 47,

48, 121]. The rearrangement of the existing receptors to better align with the presynaptic release machinery may be a result of the rearrangement in the underlying synaptic scaffolding proteins, also previously labeled as immobilization "slots" [57]. It is known that AMPA receptors do not directly interact with the synaptic scaffolding proteins but that this is achieved through interaction of intracellular c-tail of AMPAR subunits with some of the AMPAR associated auxiliary subunits such as, for example transmembrane AMPAR regulatory proteins (TARPs), which in turn interact with some of the scaffolding proteins such as PSD-95 [11]. It would be interesting to perform similar synaptic distribution analysis on one of the TARPs which are present in the hippocampus, such as TARP γ-8, and PSD-95 to see if they follow similar rules of distribution before and after the learning induced plasticity. This would fit with the previously published idea that the LTP can be induced by any type of AMPAR, in absence of GluA1 homomers, simply by filling the synaptic slots with any glutamate receptors that are available at that moment, even kainate receptors [57]. Of course, I could not directly observe and determine the subunit composition of existing receptors in current work but that remains one of the goals for the future. In figure 4.1 I proposed the model of AMPAR synaptic distribution in basal and potentiated state which fits most of the results observed in this study.

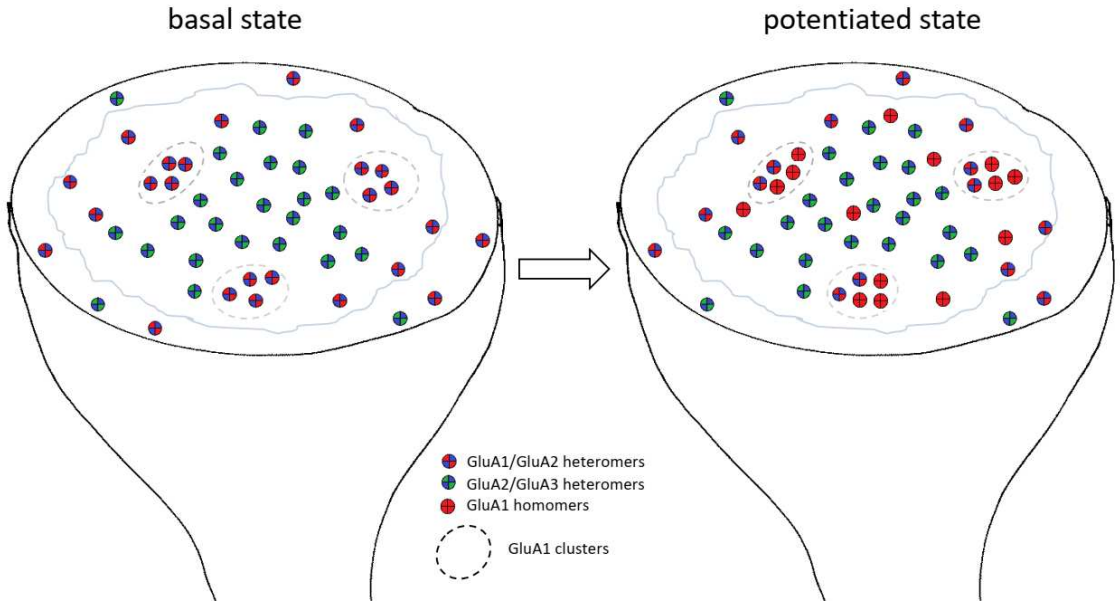

Figure 4.1. Proposed model of AMPAR synaptic distribution in basal and potentiated state.

In this study I analyzed nanoscale distribution of AMPA receptors after the learning-induced plasticity in the mouse hippocampus. Big advantage of this study is the fact that I used natural learning combined with the SDS-FRL, highest resolution imaging method available. Powerful DAREA software additionally enabled us to decipher the subtle rules of intrasynaptic

distribution of different AMPAR subunits and subtypes which was not an easy task before the existence of this software. Most of the findings are consistent with the current view of the plasticity of the AMPA receptors, and the possible contradictions might be caused by differences in animals used, type of preparation, types of antibodies used, labeling and imaging method, etc. Biggest drawback of the currently used approach is the technical variability of replica labeling, which can vary substantially among samples even from the same animal. Another potential problem is the low number of samples used in this study, due to long times for sample preparation and laborious collecting and processing images from these samples, which is very time consuming and limited us to having 3-6 animals per data set in the current study. Possible solution for both drawbacks is the automatization of imaging process by recently developed DarEM software [122], which will save time on image collection while the researchers can focus on increasing the number of samples which would definitely benefit this and all future studies.

Functionally, the hippocampal CA1 region can be subdivided into distal, intermediate and proximal CA1. It has been previously reported that proximal CA1 cells have higher spatial specificity and play a crucial role in spatial memory formation. In contrast, distal CA1 cells process non-spatial, object-related information, such as odor-based memory [68]. The integration of object-related information with spatial and temporal contexts induces sequence coding activity, which is highest in the intermediate CA1 region [70]. Although studies have shown that there are functional differences along the proximodistal axis of the CA1 region [68,70], synaptic plasticity along the proximo-distal axis is not well studied. Consistent with the previous report [72], I found proximodistal heterogeneity in plasticity at CA3-CA1 synapses. The CA3-CA1 inputs showed postsynaptic plasticity in the proximal, but not the distal region, where object-related information is mostly processed. These results suggested that the proximal/intermediate CA1 regions played a role in processing integrated information for IA learning.

4.3 Electron Microscopic Detection of Single Membrane Proteins by a Specific Chemical Labeling

In summary, we have achieved EM detection of GPCR by chemical labeling using a reactive peptide tag-probe pair. Rational design of the highly reactive α-helical peptide tag and the fine-tuning of probe reactivity enabled the specific cysteine conjugation of the tag-fused B2R protein on cell surface. EM detection using the tag-probe pair was successfully applied to determine the localization of B2R receptor on cell surface with a high labeling specificity. Furthermore, the probe directly conjugated with a 1.4-nm gold particle enabled the detection of the membrane proteins with a few times higher labeling efficiency and significantly higher spatial resolution than that of the antibody-mediated labeling, revealing high-density nanoclusters of proteins. EM detection methods for in-cell proteins using genetically encoded peroxidases have been developed in recent years [111,112,113]. Despite their usefulness, these methods are hardly applicable to single-protein detection since they have been devised for EM contrast imaging based on OsO_4 staining in combination with oxidative diaminobenzidine (DAB) polymerization. To the best of our knowledge, the research presented herein is the first example of high-resolution single-protein detection by EM utilizing a chemical labeling. The use of our labeling method is currently limited to cell surface proteins. Nevertheless, this method can be widely used for EM analysis of membrane proteins on replicas in combination with SDS-FRL. We envision further application of the chemical labeling approach to reveal subunit composition of single-protein complexes on cell surface in combination with other tag-probe pairs [114, 123].

In our study, we demonstrate higher efficiency and resolution of the newly developed chemical labeling method compared with the common immunolabeling methods at the EM level using HEK cells expressing tagged B2R. Accurate evaluation of labeling resolution, however, requires understanding of the exact molecular structure of the tagged receptor. Since background and labeling conditions can be different between cell culture and various tissue environments, usefulness of the reported reactive peptide tag-probe pair needs further verification in more complex sample preparations.

4.4 *Development of novel high resolution EM techniques for application on AMPA receptors*

Because of the limitations of immunolabeling with regards to spatial resolution and labeling efficiency and cannot be used to investigate exact AMPAR subunit composition *in situ*, ultimate goal of this study was to develop novel EM labeling approach by utilizing short peptide tag and chemical probe/nanobody approach and obtain the final full picture of how the AMPAR distribution, arrangement and subunit composition changes during learning-induced plasticity.

In order to fully utilize above-described novel chemical labeling for membrane proteins, apply it on AMPA receptor subunits to obtain higher labeling resolution and be able to investigate subunit composition of these receptors and inspect the clustering parameters in more details, it was necessary to design AMPAR subunits modified to carry a short peptide tag for successful interaction with small probe and labeling of the protein. Same goes for the peptide tags designed for recognition using the nanobodies. I managed to design several constructs of these tagged AMPAR subunits (GluA1 and GluA2) with hd2, ALFA and Spot tag and test their successful expression, membrane trafficking and labeling in variety of biological systems of various complexity, such as in vitro cell and neuron cultures, as well as in vivo stereotaxic injection of viral vectors encoding for the tagged subunits. I also proceeded to generate the transgenic animals with endogenously expressed tagged AMPAR subunits. It is still necessary to verify the proper assembly and function of the full tetrameric receptors in the living animals and look for negative effects these modified receptors might have on the viability and behaviour of the transgenic animals.

I managed to successfully label the tagged AMPA receptor subunits in both living and fixed cells and tissue but only at the level of light microscopy. Further development and labeling were hindered by the lack of suitable nanobodies and probes for electron microscopy. Conjugation of these molecules with suitable gold nanoparticles for electron microscopy is another ongoing area of work which is beyond the scope of this thesis. One significant advantage of the nanobody based labeling approach is the cost and simplicity of production of large quantities of unconjugated nanobodies compared to the traditional antibodies. Even with carefully designed transgenic animal lines with tagged AMPAR subunits and successfully gold-conjugated nanobodies/chemical probes, several possible technical difficulties may arise before subunit composition of single channels *in situ* could be directly observed and quantified.

Nanobodies have not previously been used in combination with SDS-FRL and one possible problem include denaturation of tag sequence by SDS during tissue digestion which may eliminate or reduce the labeling efficiency.

Despite several presently existing limitations and drawbacks, work performed so far hopefully presents a good foundation for future achievement of my main goal in the study of AMPA receptors

5 CONCLUSIONS

Over the course of my PhD project, I managed to investigate in great detail the rules of synaptic localization and distribution of AMPA receptor subunits in the basal and potentiated state. In the basal state, GluA1 and GluA2 subunits mostly followed general distribution of AMPA receptor (revealed by panAMPA labeling), while GluA3-containing receptors were found to be sparsely present in the dendrites and somata of CA1 pyramidal neurons and mostly located in the synapses, occupying more central position, possibly in one big cluster located in the center of the synapse. GluA1-containing receptors were located more peripherally, possibly in several smaller cluster. GluA2-containing receptors did show more peripheral localization similar to GluA1-containing receptors, but no indication of clustering.

Investigation of synaptic AMPAR receptor in potentiated state induced by inhibitory avoidance revealed strong involvement of GluA1- and GluA2-containing receptors in the early phases of learning-induced LTP. Changes in numbers and distribution of these receptors indicated: 1. Possible influx of GluA1-homomeric AMPAR in the synapse (20% of receptors, indicated by decrease in GluA2 labeling) and 2. Rearrangement of existing and newly incorporated receptors within synapse to take more central localization, possibly to be incorporated in the existing clusters (potentially aligned with the neurotransmitter release sites). No changes in number or distribution of GluA3-containing receptors indicate no involvement of these receptors in the process of learning-induced LTP, at least in its early phases.

We successfully utilized novel chemical labeling for electron microscopy to visualize and detect membrane proteins and compared it with current immunolabeling methods. This comparison revealed higher labeling efficiency, better spatial resolution and more sensitive cluster detection of our novel approach compared to standard labeling using antibodies. I attempted to utilize this approach for the AMPA receptor subunits in order to achieve similar goals – which would give us even more insight into the distribution and subunit composition of these receptors in the synapses in the basal and potentiated state. By combining this approach with peptide tag/nanobody based approach, I made substantial progress in designing the tagged AMPAR subunits and creating the transgenic animals which endogenously express tagged AMPAR subunits. However, utilization of these animals for the EM analysis of AMPAR is still ahead of us.

References

1. Williams RW, Herrup K (1988). "The control of neuron number". Annual Review of Neuroscience. 11 (1): 423–53. doi:10.1146/annurev.ne.11.030188.002231. PMID 3284447.
2. Breitenfeld, T.; Jurasic, M. J.; Breitenfeld, D. (September 2014). "Hippocrates: the forefather of neurology". Neurological Sciences. 35 (9): 1349–1352.
3. Freemon, F. R. (23 Sep 2009). "Galen's ideas on neurological function". Journal of the History of the Neurosciences. 3 (4): 263–271. doi:10.1080/09647049409525619.
4. Santiago Ry (1894). "The Croonian Lecture: La Fine Structure des Centres Nerveux". Proceedings of the Royal Society of London. 55 (331–335): 444–468. Bibcode:1894RSPS...55..444C. doi:10.1098/rspl.1894.0063.
5. Mehta, Arpan R.; Mehta, Puja R.; Anderson, Stephen P.; MacKinnon, Barbara L. H.; Compston, Alastair (2020-01-01). "Etymology and the neuron(e)". Brain. 143 (1): 374–379. doi:10.1093/brain/awz367. ISSN 0006-8950. PMC 6935745. PMID 31844876.
6. Hebb D (1949). The Organization of Behavior: A NEUROPSYCHOLOGICAL THEORY. New York: JOHN WILEY if SONS, Inc. ISBN 978-0805843002.
7. Bliss TV, Lomo T. Long-lasting potentiation of synaptic transmission in the dentate area of the anaesthetized rabbit following stimulation of the perforant path. J Physiol. 1973 Jul;232(2):331-56. doi: 10.1113/jphysiol.1973.sp010273. PMID: 4727084; PMCID: PMC1350458.
8. Honoré T, Lauridsen J, Krogsgaard-Larsen P (January 1982). "The binding of [3H]AMPA, a structural analogue of glutamic acid, to rat brain membranes". Journal of Neurochemistry. 38 (1): 173–8. doi:10.1111/j.1471-4159.1982.tb10868.x. PMID 6125564. S2CID 42753770.
9. Watkins JC, Jane DE. The glutamate story. Br J Pharmacol. 2006 Jan;147 Suppl 1(Suppl 1):S100-8. doi: 10.1038/sj.bjp.0706444. PMID: 16402093; PMCID: PMC1760733.
10. Meyer D, Bonhoeffer T, Scheuss V. Balance and stability of synaptic structures during synaptic plasticity. Neuron. 2014 Apr 16;82(2):430-43. doi: 10.1016/j.neuron.2014.02.031. Erratum in: Neuron. Jun 4;82(5):1188. PMID: 24742464.

11. Chater T.E. and Goda Y. The role of AMPA receptors in postsynaptic mechanisms of synaptic plasticity. Front. Cell. Neurosci (2014). 8:401. doi: 10.3389/fncel.2014.00401
12. Henley, J.M. and Wilkinson K.A. Synaptic AMPA receptor composition in development, plasticity and disease Nature Reviews Neuroscience 17,337–350 (2016) doi:10.1038/nrn.2016.37
13. Cull-Candy S., Kelly L., Farrant M.: Regulation of Ca2+-permeable AMPA receptors: synaptic plasticity and beyond. Curr Opin Neurobiol, 16:288-297 (2006)
14. Collingridge GL, Isaac JT, Wang YT. Receptor trafficking and synaptic plasticity. Nat Rev Neurosci. 2004 Dec;5(12):952-62. doi: 10.1038/nrn1556. PMID: 15550950.
15. Lambolez B, Ropert N, Perrais D, Rossier J, Hestrin S. Correlation between kinetics and RNA splicing of alpha-amino-3-hydroxy-5-methylisoxazole-4-propionic acid receptors in neocortical neurons. Proc Natl Acad Sci U S A. 1996 Mar 5;93(5):1797-802. doi: 10.1073/pnas.93.5.1797. PMID: 8700838; PMCID: PMC39861.
16. Zhu JJ, Esteban JA, Hayashi Y, Malinow R. Postnatal synaptic potentiation: delivery of GluR4-containing AMPA receptors by spontaneous activity. Nat Neurosci. 2000 Nov;3(11):1098-106. doi: 10.1038/80614. PMID: 11036266.
17. Wenthold RJ, Petralia RS, Blahos J II, Niedzielski AS. Evidence for multiple AMPA receptor complexes in hippocampal CA1/CA2 neurons. J Neurosci. 1996 Mar 15;16(6):1982-9. doi: 10.1523/JNEUROSCI.16-06-01982.1996. PMID: 8604042; PMCID: PMC6578515.
18. Kauer, J.A. & Malenka, R.C. Synaptic plasticity and addiction. Nat. Rev. Neurosci. 8, 844–858 (2007).
19. Kessels, H.W. & Malinow, R. Synaptic AMPA receptor plasticity and behavior. Neuron 61, 340–350 (2009).
20. Liu, S.Q. & Cull-Candy, S.G. Synaptic activity at calcium-permeable AMPA receptors induces a switch in receptor subtype. Nature 405, 454–458 (2000).
21. Shi, S., Hayashi, Y., Esteban, J.A. & Malinow, R. Subunit-specific rules governing AMPA receptor trafficking to synapses in hippocampal pyramidal neurons. Cell 105, 331–343 (2001)
22. R.A. Nicoll, S. Tomita, D.S. Bredt. Auxiliary subunits assist AMPA-type glutamate receptors, Science, 311 (2006), pp. 1253–1256
23. E.B. Ziff, TARPs and the AMPA receptor trafficking paradox Neuron, 53, pp. 627–633 (2007)

24. Bredt DS, Nicoll RA. AMPA receptor trafficking at excitatory synapses. Neuron. 2003 Oct 9;40(2):361-79. doi: 10.1016/s0896-6273(03)00640-8. PMID: 14556714.
25. Song I, Huganir RL. Regulation of AMPA receptors during synaptic plasticity. Trends Neurosci. 2002 Nov;25(11):578-88. doi: 10.1016/s0166-2236(02)02270-1. PMID: 12392933.
26. Jonas P, Sakmann B. Glutamate receptor channels in isolated patches from CA1 and CA3 pyramidal cells of rat hippocampal slices. J Physiol. 1992 Sep;455:143-71. doi: 10.1113/jphysiol.1992.sp019294. PMID: 1282929; PMCID: PMC1175637.
27. Nusser Z, Lujan R, Laube G, Roberts JD, Molnar E, Somogyi P. Cell type and pathway dependence of synaptic AMPA receptor number and variability in the hippocampus. Neuron. 1998 Sep;21(3):545-59. doi: 10.1016/s0896-6273(00)80565-6. PMID: 9768841.
28. Masugi-Tokita M, Shigemoto R. High-resolution quantitative visualization of glutamate and GABA receptors at central synapses. Curr Opin Neurobiol. 2007 Jun;17(3):387-93. doi: 10.1016/j.conb.2007.04.012. Epub 2007 May 11. PMID: 17499496.
29. Matsuzaki, M., Ellis-Davies, G. C., Nemoto, T., Miyashita, Y., Iino, M., and Kasai, H. Dendritic spine geometry is critical for AMPA receptor expression in hippocampal CA1 pyramidal neurons. Nat. Neurosci. 4, 1086–1092 (2001). doi: 10.1038/nn736
30. Baude A, Nusser Z, Molnár E, McIlhinney RA, Somogyi P. High-resolution immunogold localization of AMPA type glutamate receptor subunits at synaptic and non-synaptic sites in rat hippocampus. Neuroscience. 1995 Dec;69(4):1031-55. doi: 10.1016/0306-4522(95)00350-r. PMID: 8848093.
31. Kharazia VN, Weinberg RJ. Tangential synaptic distribution of NMDA and AMPA receptors in rat neocortex. Neurosci Lett. 1997 Nov 28;238(1-2):41-4. doi: 10.1016/s0304-3940(97)00846-x. PMID: 9464650.
32. Takumi Y, Ramírez-León V, Laake P, Rinvik E, Ottersen OP. Different modes of expression of AMPA and NMDA receptors in hippocampal synapses. Nat Neurosci. 1999 Jul;2(7):618-24. doi: 10.1038/10172. PMID: 10409387.
33. Nair D, Hosy E, Petersen JD, et al. Super-resolution imaging reveals that AMPA receptors inside synapses are dynamically organized in nanodomains regulated by PSD95. J Neurosci. 2013;33(32):13204-13224. doi:10.1523/JNEUROSCI.2381-12.2013

34. Lisman JE, Raghavachari S, Tsien RW. The sequence of events that underlie quantal transmission at central glutamatergic synapses. Nat Rev Neurosci. 2007 Aug;8(8):597-609. doi: 10.1038/nrn2191. PMID: 17637801.
35. Liu G, Choi S, Tsien RW. Variability of neurotransmitter concentration and nonsaturation of postsynaptic AMPA receptors at synapses in hippocampal cultures and slices. Neuron. 1999 Feb;22(2):395-409. doi: 10.1016/s0896-6273(00)81099-5. PMID: 10069344.
36. Helassa N, Dürst CD, Coates C, Kerruth S, Arif U, Schulze C, Wiegert JS, Geeves M, Oertner TG, Török K. Ultrafast glutamate sensors resolve high-frequency release at Schaffer collateral synapses. Proc Natl Acad Sci U S A. 2018 May 22;115(21):5594-5599. doi: 10.1073/pnas.1720648115. Epub 2018 May 7. PMID: 29735711; PMCID: PMC6003469.
37. Wu XS, Xue L, Mohan R, Paradiso K, Gillis KD, Wu LG. The origin of quantal size variation: vesicular glutamate concentration plays a significant role. J Neurosci. 2007 Mar 14;27(11):3046-56. doi: 10.1523/JNEUROSCI.4415-06.2007. PMID: 17360928; PMCID: PMC6672571.
38. Budisantoso T, Matsui K, Kamasawa N, Fukazawa Y, Shigemoto R. Mechanisms underlying signal filtering at a multisynapse contact. J Neurosci. 2012 Feb 15;32(7):2357-76. doi: 10.1523/JNEUROSCI.5243-11.2012. PMID: 22396411; PMCID: PMC6621803.
39. Tarusawa E, Matsui K, Budisantoso T, Molnár E, Watanabe M, Matsui M, Fukazawa Y, Shigemoto R. Input-specific intrasynaptic arrangements of ionotropic glutamate receptors and their impact on postsynaptic responses. J Neurosci. 2009 Oct 14;29(41):12896-908. doi: 10.1523/JNEUROSCI.6160-08.2009. PMID: 19828804; PMCID: PMC6665298.
40. Choquet D, Hosy E. AMPA receptor nanoscale dynamic organization and synaptic plasticities. Curr Opin Neurobiol. 2020 Aug;63:137-145. doi: 10.1016/j.conb.2020.04.003. Epub 2020 May 13. PMID: 32416471.
41. Sinnen BL, Bowen AB, Forte JS, Hiester BG, Crosby KC, Gibson ES, Dell'Acqua ML, Kennedy MJ. Optogenetic Control of Synaptic Composition and Function. Neuron. 2017 Feb 8;93(3):646-660.e5. doi: 10.1016/j.neuron.2016.12.037. Epub 2017 Jan 26. PMID: 28132827; PMCID: PMC5300939.

42. Takumi Y, Matsubara A, Rinvik E, Ottersen OP. The arrangement of glutamate receptors in excitatory synapses. Ann N Y Acad Sci. 1999 Apr 30;868:474-82. doi: 10.1111/j.1749-6632.1999.tb11316.x. PMID: 10414324.
43. MacGillavry HD, Song Y, Raghavachari S, Blanpied TA. Nanoscale scaffolding domains within the postsynaptic density concentrate synaptic AMPA receptors. Neuron. 2013 May 22;78(4):615-22. doi: 10.1016/j.neuron.2013.03.009. PMID: 23719161; PMCID: PMC3668352.
44. Tang, AH., Chen, H., Li, T. et al. A trans-synaptic nanocolumn aligns neurotransmitter release to receptors. Nature 536, 210–214 (2016). https://doi.org/10.1038/nature19058
45. Savtchenko LP, Rusakov DA. Moderate AMPA receptor clustering on the nanoscale can efficiently potentiate synaptic current. Philos Trans R Soc Lond B Biol Sci. 2013 Dec 2;369(1633):20130167. doi: 10.1098/rstb.2013.0167. PMID: 24298165; PMCID: PMC3843895.
46. Bliss TV, Collingridge GL. A synaptic model of memory: long-term potentiation in the hippocampus. Nature. 1993 Jan 7;361(6407):31-9. doi: 10.1038/361031a0. PMID: 8421494.
47. Nicoll RA, Roche KW. Long-term potentiation: peeling the onion. Neuropharmacology. 2013 Nov;74:18-22. doi: 10.1016/j.neuropharm.2013.02.010. Epub 2013 Feb 21. PMID: 23439383; PMCID: PMC3718856.
48. Nicoll RA. A Brief History of Long-Term Potentiation. Neuron. 2017 Jan 18;93(2):281-290. doi: 10.1016/j.neuron.2016.12.015. PMID: 28103477.
49. Malenka RC, Kauer JA, Perkel DJ, Mauk MD, Kelly PT, Nicoll RA, Waxham MN. An essential role for postsynaptic calmodulin and protein kinase activity in long-term potentiation. Nature. 1989 Aug 17;340(6234):554-7. doi: 10.1038/340554a0. PMID: 2549423.
50. Meyer D, Bonhoeffer T, Scheuss V. Balance and stability of synaptic structures during synaptic plasticity. Neuron. 2014 Apr 16;82(2):430-43. doi: 10.1016/j.neuron.2014.02.031. Erratum in: Neuron. Jun 4;82(5):1188. PMID: 24742464.
51. Schuman EM, Dynes JL, Steward O. Synaptic regulation of translation of dendritic mRNAs. J Neurosci. 2006 Jul 5;26(27):7143-6. doi: 10.1523/JNEUROSCI.1796-06.2006. PMID: 16822969; PMCID: PMC6673937.
52. Reymann KG, Frey JU. The late maintenance of hippocampal LTP: requirements, phases, 'synaptic tagging', 'late-associativity' and implications. Neuropharmacology.

2007 Jan;52(1):24-40. doi: 10.1016/j.neuropharm.2006.07.026. Epub 2006 Aug 21. PMID: 16919684.

53. Choquet D. Linking Nanoscale Dynamics of AMPA Receptor Organization to Plasticity of Excitatory Synapses and Learning. J Neurosci. 2018 Oct 31;38(44):9318-9329. doi: 10.1523/JNEUROSCI.2119-18.2018. PMID: 30381423; PMCID: PMC6705996.
54. Hayashi Y, Shi SH, Esteban JA, Piccini A, Poncer JC, Malinow R. Driving AMPA receptors into synapses by LTP and CaMKII: requirement for GluR1 and PDZ domain interaction. Science. 2000 Mar 24;287(5461):2262-7. doi: 10.1126/science.287.5461.2262. PMID: 10731148.
55. Díaz-Alonso J, Sun YJ, Granger AJ, Levy JM, Blankenship SM, Nicoll RA. Subunit-specific role for the amino-terminal domain of AMPA receptors in synaptic targeting. Proc Natl Acad Sci U S A. 2017 Jul 3;114(27):7136-7141. doi: 10.1073/pnas.1707472114. Epub 2017 Jun 19. PMID: 28630296; PMCID: PMC5502653.
56. Park P, Kang H, Sanderson TM, Bortolotto ZA, Georgiou J, Zhuo M, Kaang BK, Collingridge GL. The Role of Calcium-Permeable AMPARs in Long-Term Potentiation at Principal Neurons in the Rodent Hippocampus. Front Synaptic Neurosci. 2018 Nov 22;10:42. doi: 10.3389/fnsyn.2018.00042. PMID: 30524263; PMCID: PMC6262052.
57. Granger AJ, Shi Y, Lu W, Cerpas M, Nicoll RA. LTP requires a reserve pool of glutamate receptors independent of subunit type. Nature. 2013 Jan 24;493(7433):495-500. doi: 10.1038/nature11775. Epub 2012 Dec 12. PMID: 23235828; PMCID: PMC3998843.
58. Adesnik H, Nicoll RA. Conservation of glutamate receptor 2-containing AMPA receptors during long-term potentiation. J Neurosci. 2007 Apr 25;27(17):4598-602. doi: 10.1523/JNEUROSCI.0325-07.2007. PMID: 17460072; PMCID: PMC6672988.
59. Gray, E. E., Fink, A. E., Sarinaña, J., Vissel, B., and O'Dell, T. J. Long-term potentiation

    in the hippocampal CA1 region does not require insertion and activation of GluR2-20

    lacking AMPA receptors. J. Neurophysiol. 98, 2488–2492 (2007). doi: 10.1152/jn.00473.2007

60. Watson JF, Ho H, Greger IH. Synaptic transmission and plasticity require AMPA receptor anchoring via its N-terminal domain. Elife. 2017 Mar 14;6:e23024. doi: 10.7554/eLife.23024. PMID: 28290985; PMCID: PMC5370185.
61. Squire LR. The legacy of patient H.M. for neuroscience. Neuron. 2009;61(1):6-9. doi:10.1016/j.neuron.2008.12.023
62. Whitlock JR, Heynen AJ, Shuler MG, Bear MF. Learning induces long-term potentiation in the hippocampus. Science. 2006 Aug 25;313(5790):1093-7. doi: 10.1126/science.1128134. PMID: 16931756.
63. Martin SJ, Grimwood PD, Morris RG. Synaptic plasticity and memory: an evaluation of the hypothesis. Annu Rev Neurosci. 2000;23:649-711. doi: 10.1146/annurev.neuro.23.1.649. PMID: 10845078.
64. Taubenfeld SM, Wiig KA, Bear MF, Alberini CM. A molecular correlate of memory and amnesia in the hippocampus. Nat Neurosci. 1999 Apr;2(4):309-10. doi: 10.1038/7217. PMID: 10204535.
65. Liu, X. et al. Optogenetic stimulation of a hippocampal engram activates fear memory recall. Nature 484, 381–385 (2012)
66. Takemoto, K. et al. Optical inactivation of synaptic AMPA receptors erases fear memory. Nat. Biotechnol. 35, 38–47 (2017)
67. Henriksen et al., 2010 E. Henriksen, L. Colgin, C. Barnes, M. Witter, M. Moser, E. Moser Spatial representation along the proximodistal axis of CA1 Neuron, 68 (1) (2010), pp. 127-137, 10.1016/j.neuron.2010.08.042
68. Igarashi KM, Ito HT, Moser EI, Moser MB. Functional diversity along the transverse axis of hippocampal area CA1. FEBS Lett. 2014 Aug 1;588(15):2470-6. doi: 10.1016/j.febslet.2014.06.004. Epub 2014 Jun 6. PMID: 24911200.
69. Nakazawa Y, Pevzner A, Tanaka KZ, Wiltgen BJ. Memory retrieval along the proximodistal axis of CA1. Hippocampus. 2016 Sep;26(9):1140-8. doi: 10.1002/hipo.22596. Epub 2016 May 6. PMID: 27068122; PMCID: PMC4996732.
70. Ng CW, Elias GA, Asem JSA, Allen TA, Fortin NJ. Nonspatial sequence coding varies along the CA1 transverse axis. Behav Brain Res. 2018 Nov 15;354:39-47. doi: 10.1016/j.bbr.2017.10.015. Epub 2017 Oct 28. PMID: 29107714; PMCID: PMC7567427.
71. Oliva A, Fernández-Ruiz A, Buzsáki G, Berényi A. Spatial coding and physiological properties of hippocampal neurons in the Cornu Ammonis subregions. Hippocampus.

2016 Dec;26(12):1593-1607. doi: 10.1002/hipo.22659. Epub 2016 Sep 27. PMID: 27650887.

72. Paw-Min-Thein-Oo, Sakimoto Y, Kida H, Mitsushima D. Proximodistal Heterogeneity in Learning-promoted Pathway-specific Plasticity at Dorsal CA1 Synapses. Neuroscience. 2020 Jun 15;437:184-195. doi: 10.1016/j.neuroscience.2020.04.040. Epub 2020 Apr 30. PMID: 32360699.
73. Mitsushima D, Ishihara K, Sano A, Kessels HW, Takahashi T. Contextual learning requires synaptic AMPA receptor delivery in the hippocampus. Proc Natl Acad Sci U S A. 2011 Jul 26;108(30):12503-8. doi: 10.1073/pnas.1104558108. Epub 2011 Jul 11. PMID: 21746893; PMCID: PMC3145714.
74. Kida H, Mitsushima D. Mechanisms of motor learning mediated by synaptic plasticity in rat primary motor cortex. Neurosci Res. 2018 Mar;128:14-18. doi: 10.1016/j.neures.2017.09.008. Epub 2017 Sep 23. PMID: 28951322.
75. Fujita A, Cheng J, Hirakawa M, Furukawa K, Kusunoki S, Fujimoto T. Gangliosides GM1 and GM3 in the living cell membrane form clusters susceptible to cholesterol depletion and chilling. Mol Biol Cell. 2007 Jun;18(6):2112-22. doi: 10.1091/mbc.e07-01-0071. Epub 2007 Mar 28. PMID: 17392511; PMCID: PMC1877094.
76. Griffin BA, Adams SR, Tsien RY. Specific covalent labeling of recombinant protein molecules inside live cells. Science. 1998 Jul 10;281(5374):269-72. doi: 10.1126/science.281.5374.269. PMID: 9657724.
77. Tabata S, Jevtic M, Kurashige N, et al. Electron Microscopic Detection of Single Membrane Proteins by a Specific Chemical Labeling. iScience. 2019;22:256-268. doi:10.1016/j.isci.2019.11.025
78. Lotze J, Reinhardt U, Seitz O, Beck-Sickinger AG. Peptide-tags for site-specific protein labelling in vitro and in vivo. Mol Biosyst. 2016 May 24;12(6):1731-45. doi: 10.1039/c6mb00023a. PMID: 26960991.
79. Nonaka H, Fujishima SH, Uchinomiya SH, Ojida A, Hamachi I. Selective covalent labeling of tag-fused GPCR proteins on live cell surface with a synthetic probe for their functional analysis. J Am Chem Soc. 2010 Jul 14;132(27):9301-9. doi: 10.1021/ja910703v. PMID: 20568758.
80. Götzke H, Kilisch M, Martínez-Carranza M, Sograte-Idrissi S, Rajavel A, Schlichthaerle T, Engels N, Jungmann R, Stenmark P, Opazo F, Frey S. The ALFA-tag is a highly versatile tool for nanobody-based bioscience applications. Nat Commun.

2019 Sep 27;10(1):4403. doi: 10.1038/s41467-019-12301-7. PMID: 31562305; PMCID: PMC6764986.

81. Virant D, Traenkle B, Maier J, Kaiser PD, Bodenhöfer M, Schmees C, Vojnovic I, Pisak-Lukáts B, Endesfelder U, Rothbauer U. A peptide tag-specific nanobody enables high-quality labeling for dSTORM imaging. Nat Commun. 2018 Mar 2;9(1):930. doi: 10.1038/s41467-018-03191-2. PMID: 29500346; PMCID: PMC5834503.
82. AMPA receptors:Dynamics and targets of disease Eduardo E. Benarroch Neurology Sep 2016, 87 (12) 1281-1288; DOI: 10.1212/WNL.0000000000003138
83. Sobolevsky AI, Rosconi MP, Gouaux E. X-ray structure, symmetry and mechanism of an AMPA-subtype glutamate receptor. Nature. 2009;462(7274):745-756. doi:10.1038/nature08624
84. Henley, J.M., & Wilkinson, K.A. (2013). AMPA receptor trafficking and the mechanisms underlying synaptic plasticity and cognitive aging. Dialogues in Clinical Neuroscience, 15, 11 - 27.
85. Sheng M, Lee SH. AMPA receptor trafficking and the control of synaptic transmission. Cell. 2001 Jun 29;105(7):825-8. doi: 10.1016/s0092-8674(01)00406-8. PMID: 11439178.
86. Jacobi E, von Engelhardt J. Modulation of information processing by AMPA receptor auxiliary subunits. J Physiol. 2021 Jan;599(2):471-483. doi: 10.1113/JP276698. Epub 2020 Jul 24. PMID: 32628275.
87. Antal M, Fukazawa Y, Eördögh M, Muszil D, Molnár E, Itakura M, Takahashi M, Shigemoto R. Numbers, densities, and colocalization of AMPA- and NMDA-type glutamate receptors at individual synapses in the superficial spinal dorsal horn of rats. J Neurosci. 2008 Sep 24;28(39):9692-701. doi: 10.1523/JNEUROSCI.1551-08.2008. PMID: 18815255; PMCID: PMC3844880.
88. Rubio ME, Matsui K, Fukazawa Y, Kamasawa N, Harada H, Itakura M, Molnár E, Abe M, Sakimura K, Shigemoto R. The number and distribution of AMPA receptor channels containing fast kinetic GluA3 and GluA4 subunits at auditory nerve synapses depend on the target cells. Brain Struct Funct. 2017 Nov;222(8):3375-3393. doi: 10.1007/s00429-017-1408-0. Epub 2017 Apr 10. PMID: 28397107; PMCID: PMC5676837
89. Eguchi K, Velicky P, Hollergschwandtner E, Itakura M, Fukazawa Y, Danzl JG, Shigemoto R. Advantages of Acute Brain Slices Prepared at Physiological Temperature

in the Characterization of Synaptic Functions. Front Cell Neurosci. 2020 Mar 19;14:63. doi: 10.3389/fncel.2020.00063. PMID: 32265664; PMCID: PMC7096554.

90. Bhandari P, Vandael D, Fernández-Fernández D, Fritzius T, Kleindienst D, Önal C, Montanaro J, Gassmann M, Jonas P, Kulik A, Bettler B, Shigemoto R, Koppensteiner P. $GABA_B$ receptor auxiliary subunits modulate Cav2.3-mediated release from medial habenula terminals. Elife. 2021 Apr 29;10:e68274. doi: 10.7554/eLife.68274. PMID: 33913808; PMCID: PMC8121548.

91. Gold PE. The use of avoidance training in studies of modulation of memory storage. Behav Neural Biol. 1986 Jul;46(1):87-98. doi: 10.1016/s0163-1047(86)90927-1. PMID: 3015121.
92. McGaugh JL, Roozendaal B. Drug enhancement of memory consolidation: historical perspective and neurobiological implications. Psychopharmacology (Berl). 2009 Jan;202(1-3):3-14. doi: 10.1007/s00213-008-1285-6. Epub 2008 Aug 15. PMID: 18704369.
93. Mitsushima D, Ishihara K, Sano A, Kessels HW, Takahashi T. Contextual learning requires synaptic AMPA receptor delivery in the hippocampus. Proc Natl Acad Sci U S A. 2011 Jul 26;108(30):12503-8. doi: 10.1073/pnas.1104558108. Epub 2011 Jul 11. PMID: 21746893; PMCID: PMC3145714.
94. Paw-Min-Thein-Oo, Sakimoto Y, Kida H, Mitsushima D. Proximodistal Heterogeneity in Learning-promoted Pathway-specific Plasticity at Dorsal CA1 Synapses. Neuroscience. 2020 Jun 15;437:184-195. doi: 10.1016/j.neuroscience.2020.04.040. Epub 2020 Apr 30. PMID: 32360699.
95. Fujimoto K. SDS-digested freeze-fracture replica labeling electron microscopy to study the two-dimensional distribution of integral membrane proteins and phospholipids in biomembranes: practical procedure, interpretation and application. Histochem Cell Biol. 1997 Feb;107(2):87-96. doi: 10.1007/s004180050092. PMID: 9062793.
96. Masugi-Tokita M, Shigemoto R. High-resolution quantitative visualization of glutamate and GABA receptors at central synapses. Curr Opin Neurobiol. 2007 Jun;17(3):387-93. doi: 10.1016/j.conb.2007.04.012. Epub 2007 May 11. PMID: 17499496.
97. Dauncey MJ, Bicknell RJ. Nutrition and neurodevelopment: mechanisms of developmental dysfunction and disease in later life. Nutr Res Rev. 1999 Dec;12(2):231-53. doi: 10.1079/095442299108728947. PMID: 19087453.

98. Luján R, Aguado C, Ciruela F, Cózar J, Kleindienst D, de la Ossa L, Bettler B, Wickman K, Watanabe M, Shigemoto R, Fukazawa Y. Differential association of $GABA_B$ receptors with their effector ion channels in Purkinje cells. Brain Struct Funct. 2018 Apr;223(3):1565-1587. doi: 10.1007/s00429-017-1568-y. Epub 2017 Nov 25. PMID: 29177691; PMCID: PMC5869904.

99. Kleindienst D, Montanaro J, Bhandari P, Case MJ, Fukazawa Y, Shigemoto R. Deep Learning-Assisted High-Throughput Analysis of Freeze-Fracture Replica Images Applied to Glutamate Receptors and Calcium Channels at Hippocampal Synapses. Int J Mol Sci. 2020 Sep 14;21(18):6737. doi: 10.3390/ijms21186737. PMID: 32937911; PMCID: PMC7555218.

100. Penn, A., Zhang, C., Georges, F. *et al.* Hippocampal LTP and contextual learning require surface diffusion of AMPA receptors. *Nature* **549,** 384–388 (2017). https://doi.org/10.1038/nature23658

101. Nonaka H, Fujishima SH, Uchinomiya SH, Ojida A, Hamachi I. Selective covalent labeling of tag-fused GPCR proteins on live cell surface with a synthetic probe for their functional analysis. J Am Chem Soc. 2010 Jul 14;132(27):9301-9. doi: 10.1021/ja910703v. PMID: 20568758.

102. Gibson, D., Young, L., Chuang, RY. *et al.* Enzymatic assembly of DNA molecules up to several hundred kilobases. *Nat Methods* **6,** 343–345 (2009). https://doi.org/10.1038/nmeth.1318

103. Kaech, S., Banker, G. Culturing hippocampal neurons. *Nat Protoc* **1,** 2406–2415 (2006). https://doi.org/10.1038/nprot.2006.356

104. Dauncey MJ, Bicknell RJ. Nutrition and neurodevelopment: mechanisms of developmental dysfunction and disease in later life. Nutr Res Rev. 1999 Dec;12(2):231-53. doi: 10.1079/095442299108728947. PMID: 19087453.

105. Szoboszlay M, Kirizs T, Nusser Z. Objective quantification of nanoscale protein distributions. Sci Rep. 2017 Nov 10;7(1):15240. doi: 10.1038/s41598-017-15695-w. PMID: 29127366; PMCID: PMC5681686.

106. Meier C, Beckmann A. Freeze fracture: new avenues for the ultrastructural analysis of cells in vitro. Histochem Cell Biol. 2018 Jan;149(1):3-13. doi: 10.1007/s00418-017-1617-x. Epub 2017 Nov 13. PMID: 29134300.

107. Miki T, Kaufmann WA, Malagon G, Gomez L, Tabuchi K, Watanabe M, Shigemoto R, Marty A. Numbers of presynaptic Ca^{2+} channel clusters match those of functionally defined vesicular docking sites in single central synapses. Proc Natl Acad

Sci U S A. 2017 Jun 27;114(26):E5246-E5255. doi: 10.1073/pnas.1704470114. Epub 2017 Jun 12. PMID: 28607047; PMCID: PMC5495264.

108. Matsuo K., Hamachi I. Ligand-directed tosyl and acyl imidazole chemistry. In: Algar W.R., Dawson P., Medintz I.L., editors. Vol. 1. Wiley-VCH Verlag GmbH; 2017. pp. 147–163. (Chemoselective and Bioorthogonal Ligation Reactions: Concepts and Applications).

109. Walper S.A., Turner K.B., Medintz I.L. Vol. 2. Wiley-VCH Verlag GmbH; 2017. Bioorthogonal labeling of cellular proteins by enzymatic and related mechanisms; pp. 165–230. (Chemoselective and Bioorthogonal Ligation Reactions: Concepts and Applications).

110. Robertson J.D. The cell membrane concept, J. Physiol. (London) 1958;140:58–59.

111. Shu X, Lev-Ram V, Deerinck TJ, Qi Y, Ramko EB, Davidson MW, Jin Y, Ellisman MH, Tsien RY. A genetically encoded tag for correlated light and electron microscopy of intact cells, tissues, and organisms. PLoS Biol. 2011 Apr;9(4):e1001041. doi: 10.1371/journal.pbio.1001041. Epub 2011 Apr 5. PMID: 21483721; PMCID: PMC3071375.

112. Martell JD, Deerinck TJ, Sancak Y, Poulos TL, Mootha VK, Sosinsky GE, Ellisman MH, Ting AY. Engineered ascorbate peroxidase as a genetically encoded reporter for electron microscopy. Nat Biotechnol. 2012 Nov;30(11):1143-8. doi: 10.1038/nbt.2375. Epub 2012 Oct 21. PMID: 23086203; PMCID: PMC3699407.

113. Hainfeld JF, Powell RD. New frontiers in gold labeling. J Histochem Cytochem. 2000 Apr;48(4):471-80. doi: 10.1177/002215540004800404. PMID: 10727288.

114. Uchinomiya S, Nonaka H, Wakayama S, Ojida A, Hamachi I. In-cell covalent labeling of reactive His-tag fused proteins. Chem Commun (Camb). 2013 Jun 4;49(44):5022-4. doi: 10.1039/c3cc41979g. Epub 2013 Apr 24. PMID: 23612601.

115. Italia M, Ferrari E, Di Luca M, Gardoni F. GluA3-containing AMPA receptors: From physiology to synaptic dysfunction in brain disorders. Neurobiol Dis. 2021 Dec;161:105539. doi: 10.1016/j.nbd.2021.105539. Epub 2021 Oct 29. PMID: 34743951.

116. Schwenk J, Baehrens D, Haupt A, Bildl W, Boudkkazi S, Roeper J, Fakler B, Schulte U. Regional diversity and developmental dynamics of the AMPA-receptor proteome in the mammalian brain. Neuron. 2014 Oct 1;84(1):41-54. doi: 10.1016/j.neuron.2014.08.044. Epub 2014 Sep 18. PMID: 25242221.

117. Morise J, Suzuki KGN, Kitagawa A, Wakazono Y, Takamiya K, Tsunoyama TA, Nemoto YL, Takematsu H, Kusumi A, Oka S. AMPA receptors in the synapse turnover by monomer diffusion. Nat Commun. 2019 Nov 20;10(1):5245. doi: 10.1038/s41467-019-13229-8. PMID: 31748519; PMCID: PMC6868016.

118. Jacob AL, Weinberg RJ. The organization of AMPA receptor subunits at the postsynaptic membrane. *Hippocampus*. 2015;25(7):798-812. doi:10.1002/hipo.22404

119. Staubli, U. & Lynch, G. 1987 Stable hippocampal long-term potentiation elicited by 'theta' pattern stimulation. Brain Res. 435, 227–234.

120. Gerges NZ, Backos DS, Rupasinghe CN, Spaller MR, Esteban JA. Dual role of the exocyst in AMPA receptor targeting and insertion into the postsynaptic membrane. EMBO J. 2006 Apr 19;25(8):1623-34. doi: 10.1038/sj.emboj.7601065. Epub 2006 Apr 6. PMID: 16601687; PMCID: PMC1440842.

121. Plant K, Pelkey KA, Bortolotto ZA, Morita D, Terashima A, McBain CJ, Collingridge GL, Isaac JT. Transient incorporation of native GluR2-lacking AMPA receptors during hippocampal long-term potentiation. Nat Neurosci. 2006 May;9(5):602-4. doi: 10.1038/nn1678. Epub 2006 Apr 2. PMID: 16582904.

122. Kleindienst D, Constanzo T, Shigemoto R, Automated Imaging and Analysis of Synapses in Freeze-Fracture Replica Samples with Deep Learning, submitted, 2022.

123. Shigemoto R. Electron microscopic visualization of single molecules by tag-mediated metal particle labeling. Microscopy (Oxf). 2022 Feb 18;71(Supplement_1):i72-i80. doi: 10.1093/jmicro/dfab048. Erratum in: Microscopy (Oxf). 2022 Mar 22;: PMID: 35275179.

124. Gutierrez-Castellanos N, Da Silva-Matos CM, Zhou K, Canto CB, Renner MC, Koene LMC, Ozyildirim O, Sprengel R, Kessels HW, De Zeeuw CI. Motor Learning Requires Purkinje Cell Synaptic Potentiation through Activation of AMPA-Receptor Subunit GluA3. Neuron. 2017 Jan 18;93(2):409-424. doi: 10.1016/j.neuron.2016.11.046. PMID: 28103481; PMCID: PMC5263704.

125. Renner MC, Albers EH, Gutierrez-Castellanos N, et al. Synaptic plasticity through activation of GluA3-containing AMPA-receptors. *Elife*. 2017;6:e25462. Published 2017 Aug 1. doi:10.7554/eLife.25462

126. Clem RL, Huganir RL. Calcium-permeable AMPA receptor dynamics mediate fear memory erasure. Science. 2010 Nov 19;330(6007):1108-12. doi:

10.1126/science.1195298. Epub 2010 Oct 28. PMID: 21030604; PMCID: PMC3001394.

127. Haley, J. E.; Schaible, E.; Pavlidis, P.; Murdock, A.; Madison, D. V. Basal and apical synapses of CA1 pyramidal cells employ different LTP induction mechanisms. *Learning & Memory* **1996**, 3, 289–295.

128. Brzdak, P.; Wójcicka, O.; Zareba-Koziol, M.; Minge, D.; Henneberger, C.; Wlodarczyk, J.; Mozrzymas, J. W.; Wójtowicz, T. Synaptic Potentiation at Basal and Apical Dendrites of Hippocampal Pyramidal Neurons Involves Activation of a Distinct Set of Extracellular and Intracellular Molecular Cues. *Cerebral Cortex* **2019**, 29, 283–304.

129. Leung, L. S.; Shen, B. Long-term potentiation at the apical and basal dendritic synapses of CA1 after local stimulation in behaving rats. *Journal of Neurophysiology* **1995**, 73, 1938–1946.

130. Li, S.-B.; Du, D.; Hasan, M. T.; Köhr, G. D4 Receptor Activation Differentially Modulates Hippocampal Basal and Apical Dendritic Synapses in Freely Moving Mice. *Cerebral Cortex* **2014**, bhu229.

131. Herwerth, M.; Jensen, V.; Novak, M.; Konopka, W.; Hvalby, O.; Kohr, G. D4 Dopamine Receptors Modulate NR2B NMDA Receptors and LTP in Stratum Oriens of Hippocampal CA1. *Cerebral Cortex* **2012**, 22, 1786–1798.

132. Leung, L. S.; Peloquin, P. Cholinergic Modulation Differs between Basal and Apical Dendritic Excitation of Hippocampal CA1 Pyramidal Cells. *Cerebral Cortex* **2010**, 20, 1865–1877.

133. Witter, M. P. (2010). Connectivity of the Hippocampus. Hippocampal Microcircuits, 5–26. doi:10.1007/978-1-4419-0996-1_1

A. Appendix 1

Figure 3.2A	p=0.20 (GluA1), p=0.49 (GluA2), p=0.48 (GluA3), p=0.98 (panAMPA)
Figure 3.2B synaptic	Tukey's multiple comparisons test / Significant? / Summary ORI vs. PR / Yes / * ORI vs. MR / Yes / * ORI vs. DR / Yes / ** PR vs. LM / Yes / ** MR vs. LM / Yes / ** DR vs. LM / Yes / ***
Figure 3.3A	p=0.49 (GluA1), p=0.23 (GluA2), p=0.71 (GluA3), p=0.96 (panAMPA)
Figure 3.3. extrasynaptic	Tukey's multiple comparisons test / Significant? / Summary GluA1 vs. GluA3 / Yes / *** GluA1 vs. panAMPA / Yes / * ORI vs. PCL / Yes / *** PCL vs. MR / Yes / **** PCL vs. DR / Yes / **** PCL vs. LM / Yes / * PR vs. MR / Yes / ** PR vs. DR / Yes / ** MR vs. LM / Yes / *
Figure 3.4B	Tukey's multiple comparisons test / Significant? / Summary ORI vs. PR / Yes / * GluA1 vs. GluA3 / Yes / ** GluA2 vs. GluA3 / Yes / *** GluA3 vs. panAMPA / Yes / ****
Figure 3.5.	Tukey's multiple comparisons test / Significant? / Summary GluA1 vs. GluA3 / Yes / * GluA2 vs. GluA3 / Yes / ** GluA3 vs. panAMPA / Yes / *
Figure 3.7A	Tukey's multiple comparisons test / Significant? / Summary GluA1 vs. GluA1 sim / Yes / * GluA1 vs. GluA3 / Yes / *** GluA2 vs. GluA3 / Yes / ** GluA3 vs. panAMPA / Yes / *
Figure 3.7B	Tukey's multiple comparisons test / Significant? / Summary GluA1 vs. GluA3 / Yes / * GluA2 vs. GluA3 / Yes / *
Figure 3.7C	GluA1 vs random simulation, p<0.0001; GluA2 vs random simulation, p<0.0001 GluA3 vs random simulation, p<0.0001; panAMPA vs random simulation, p<0.0001; Kolmogorov-Smirnov test
Figure 3.8B	cluster number, GluA3 vs GluA3 sim, p=0.018, paired t-test cluster CPI, GluA1 vs GluA1 sim, p=0.017, paired t-test
Figure 3.12A	Tukey's multiple comparisons test / Significant? / Summary trained proximal vs. trained distal / Yes / *
Figure 3.13.	Tukey's multiple comparisons test / Significant? / Summary

	Control DIST vs. trained PROX — Yes — *
Figure 3.14A	Tukey's multiple comparisons test — Significant? — Summary E dist vs. E prox — Yes — *
Figure 3.14B	GluA1 (t dist vs t prox, p<0.0001, c prox vs t prox, p=0.004); GluA2 (c prox vs t prox, p<0.0001, c prox vs t dist, p=0.0005); GluA3 (c prox vs t prox, p<0.0001, t prox vs t dist, p=0.97); panAMPA, ns; Kolmogorov-Smirnov test
Figure 3.15	Tukey's multiple comparisons test — Significant? — Summary control proximal vs. trained proximal — Yes — * trained distal vs. trained proximal — Yes — *
Figure 3.16	Comparison with random simulation, paired t-test. GluA1 — GluA2 — GluA3 — panAMPA c dist — p=0.004 — ns — p=0.02 — ns c prox — p<0.0001 — ns — ns — ns t dist — p=0.001 — ns — p=0.04 — ns t prox — p=0.01 — p=0.02 — p=0.03 — ns
Figure 3.21C GluA1	Tukey's multiple comparisons test — Significant? — Summary control distal vs. trained proximal — Yes — **
Figure 3.21C GluA3	Tukey's multiple comparisons test — Significant? — Summary c dist vs. e dist — **** c dist vs. e prox — **** c prox vs. e dist — *** c prox vs. e prox — ****
Figure 3.22A	Tukey's multiple comparisons test — Significant? — Summary C dist vs. E prox — Yes — **
Figure 3.23	Comparison with random simulation, paired t-test GluA1 — GluA2 — GluA3 c dist — p=0.0005 — p=0.0007 — p<0.00001 c prox — p=0.001 — p<0.0001 — p<0.00001 t dist — p=0.05 — p=0.0002 — p<0.00001 t prox — p=0.13 — p=0.0005 — p<0.00001
Figure 3.23A	Tukey's multiple comparisons test — Significant? — Summary c dist vs. e prox — Yes — ** c prox vs. e dist — Yes — ** c prox vs. e prox — Yes — ****
Figure 3.23B	Tukey's multiple comparisons test — Significant? — Summary c dist vs. e dist — Yes — *
Figure 3.23C	Tukey's multiple comparisons test — Significant? — Summary c dist vs. e dist — Yes — *